

Aus dem Institut für Physiologie
der Medizinischen Fakultät Charité – Universitätsmedizin Berlin

DISSERTATION

Microrheology in skeletal muscle vessels of erythrocytic mice

zur Erlangung des akademischen Grades
Doctor medicinae dentariae (Dr. med. dent.)

vorgelegt der Medizinischen Fakultät
Charité – Universitätsmedizin Berlin

von

Vincent Richter

aus Hoyerswerda

Gutachter/in: 1. Prof. Dr. med. A. R. Pries
 2. Prof. Dr. med. M. Sperandio
 3. Prof. Dr. H. Lipowsky

Datum der Promotion: 18.11.2011

CONTENTS

1.	Introduction	1
1.1.	Scope	1
1.2.	The Fåhræus-Lindqvist effect and the Fåhræus effect	3
1.3.	Effective viscosity and dynamic hematocrit <i>in vivo</i> and the effect of the endothelial surface layer.....	7
1.4.	Mouse model with systemic hematocrit of up to 0.90	12
1.5.	Objectives of the study	14
2.	Material and Methods.....	16
2.1.	Summary of methods	16
2.2.	Preliminary remarks	17
2.3.	Experimental groups	18
2.4.	Anesthesia and animal preparation	19
2.5.	Optical and electronic set-up for intravital microscopy	21
2.6.	Intravital microscopy.....	22
2.7.	Hemodilution.....	24
2.8.	Off-line generation of data	25
2.9.	Image analysis	25
2.10.	Collection of μ -PIV data and raw data plot.....	26
2.11.	Selection and analysis of μ -PIV data	27
2.12.	Estimation of ESL thickness	31
2.13.	Hemodynamic flow model	34
2.14.	Statistical analysis	35
2.15.	Error sources	35
3.	Results.....	37
3.1.	Systemic hemodynamic parameters	37
3.1.1.	Hematocrit	37
3.1.2.	Mean arterial pressure and heart rate	38
3.2.	Microrheological parameters.....	40
3.2.1.	Blood flow velocity	40
3.2.2.	Flow rate.....	42

3.2.3.	Velocity profiles	44
3.2.4.	Shear rate and shear stress	48
3.2.5.	Relative apparent viscosity	51
3.2.6.	Microvascular hematocrit	54
3.2.7.	ESL thickness	56
4.	Discussion	58
4.1.	Key findings	58
4.2.	Endothelial surface layer	59
4.3.	Hemodynamics	63
4.4.	Blood viscosity <i>in vivo</i>	72
4.5.	Implications and conclusions	75
5.	Summary	77
6.	Zusammenfassung	79
7.	References	81
7.1.	Literature	81
7.2.	Figures	91
7.3.	Tables	94
8.	Appendix	95
8.1.	List of Materials	95
8.2.	List of Abbreviations and Acronyms	96
8.3.	Acknowledgements	97
8.4.	Curriculum Vitae	98
8.5.	Publications and presentations	99
8.6.	Selbständigkeitserklärung	100

1. Introduction

1.1. Scope

The main functions of the blood circulation are to supply organs with oxygen and nutrients and to remove the waste products of metabolism such as carbon dioxide. The amount of blood volume perfusing a tissue of given angioarchitecture per unit of time depends on both the cardiac output and the rheological[#] properties of blood, most importantly the blood viscosity. Blood viscosity, in turn, most crucially depends on the level of hematocrit[¶].

Thus, it may be interesting to consider the clinical importance of the correlation between hematocrit and viscosity, especially in cases of an increased level of hematocrit. For instance, patients suffering from polycythemia vera [31,52,170], neonatal polycythemia [143,176] or chronic mountain sickness [91,114] are characterized by an elevated hematocrit. The concomitant exponential rise of viscosity poses a considerable challenge to the cardiovascular system. This may be due to:

- increased blood pressure [17,32,61,63,111,165],
- spontaneous platelet aggregation [67,83,97],
- impaired filling and hypertrophy of the left ventricle [146,147].

Many long-term studies on human subjects have found evidence that an elevated hematocrit generally predisposes the cardiovascular system to ischemic cardiovascular disease (CVD). Corresponding events such as myocardial infarction, angina pectoris, stroke and intermittent claudication indicate impaired cardiac, cerebral and peripheral perfusion, respectively [2,21,23,27,40,47,58,63,76,87,98,111,142,166,169,192,193,198]. The positive correlation between the hematocrit level and CVD-related events is significant in most studies even after adjustment for other risk factors, e.g. cigarette smoking, elevated blood pressure or increased levels of lipoprotein and cholesterol. The above mentioned relationship between CVD events and hematocrit can be roughly delineated by an U-shaped curve, indicating that both anemia and erythrocytosis increase the risk of CVD-related

[#] Rheology, (Greek: *rhei* 'flow', *logos* 'theory') is the science of the deformation and flow of matter [196].

[¶] Hematocrit, Hct, is defined as the volume ratio of red blood cells (rbc) relative to the volume of whole blood. Accordingly, hematocrit data is expressed as a decimal fraction in this study (except where otherwise noted).

events, whereas the risk is minimal at moderate hematocrit values, i.e. at ~0.42 and ~0.44 for women and men, respectively [58,115,193].

By contrast, permanent high-altitude dwellers, e.g. Tibetans and Andeans, do not display higher incidence of CVD events in spite of a significantly elevated hematocrit induced by chronic hypobaric hypoxia [10,11,57,185,200]. This gives rise to an attenuated relation between hematocrit and cardiovascular risk in such highlanders as compared to lowlanders, indicating the presence of adaptive and/or compensative mechanisms [57,77,80,184,200]. Respective adjustments of the cardio- and microvasculature and of the hemorheological properties in these populations, however, have not yet been completely identified [12-15,45,57,60,62,64,105,106,174,200].

In order to experimentally investigate feasible pathophysiological consequences of erythrocytic and, thus, highly viscous blood, a mouse line, termed tg6, has recently been generated. These animals being transgenic for the human EPO[#] gene reach extremely high levels of systemic hematocrit of 0.80 to 0.90 at 2-3 months of age [141]. Taking the above mentioned studies on sea-level residents into account, it is astonishing that these animals are viable [191]. Their cardiovascular and microvascular systems are seemingly able to adjust to the gradually increasing hematocrit within the first 2-3 months of life, e.g. by means of augmented synthesis of endothelial nitric oxide [68,141].

The present study shall examine the special rheological features of blood flow in the microvasculature of the cremaster muscle in tg6 mice. Consecutively, conceivable adaptive mechanisms of the microvascular system shall be deduced.

In the following, the scientific background of the present study is described in more detail.

[#] EPO, erythropoietin

1.2. The Fåhræus-Lindqvist effect and the Fåhræus effect

In addition to hematocrit, the viscosity of blood flowing through vessels or tubes is also influenced by their inner diameter, D (Fig. 1). This property of blood flow, named for its first discoverers ‘Fåhræus-Lindqvist effect’ [49,102], has been extensively investigated in glass tubes over a large range of diameter for shear rates above 50 s^{-1} . As the tube diameter is progressively reduced from about $1000 \mu\text{m}$ to capillary size, the viscosity of blood for a given hematocrit considerably declines. At $\sim 6\text{-}7 \mu\text{m}$ and physiological hematocrit, the viscosity yields a minimum value just 25 % higher than the viscosity of the suspending plasma. If the tube diameter falls below $\sim 5 \mu\text{m}$, a steep rise in apparent viscosity is observed. Blood viscosity must, therefore, not be considered as a fixed but rather as a variable material property which is strongly influenced by the present dimensions of the tube or vessel, respectively. Consequently, the terms ‘apparent viscosity’[#], η_{app} , and ‘effective viscosity’[¶], η_{eff} , respectively, have been introduced [34,123].

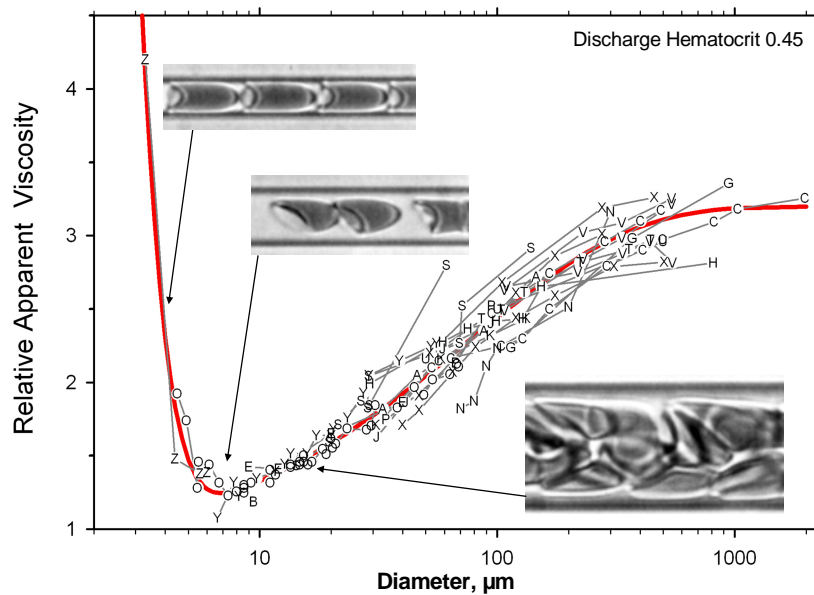


Figure 1. Relative apparent viscosity (normalized to plasma viscosity) as a function of tube diameter for flow of a rbc suspension with a discharge (or feed) hematocrit of 0.45; the red curve corresponds to best fit to data compiled from several *in vitro* studies [123]; insets show photomicrographs of red blood cells (discharge, or feed hematocrit 0.45) flowing through glass tubes of 3, 7 and 17 μm in diameter.

[#] ‘Apparent viscosity’ is the viscosity required to satisfy Hagen-Poiseuille’s law [$Q = \frac{\pi \cdot r^4}{8l \cdot \eta} \cdot \Delta P$] in a blood-

perfused glass tube, and, thus, refers to the rheological phenomenon of ‘complex’ fluids such as blood to change their viscosity with tube diameter at a given hematocrit, also referred to as the Fåhræus-Lindqvist effect [124]. This definition is distinct from that of other authors, who reserve this term to describe the influence of shear rate on blood viscosity (‘shear-thinning’ property), as measured in rotational viscometers [33,34,196]. As for viscosity data obtained in such viscometers, the term ‘bulk viscosity’ is used in the present study instead.

[¶] ‘Effective viscosity’ is the viscosity required to satisfy Poiseuille’s law in a living vessel of given inner diameter.

While flowing through small ($< 1000 \mu\text{m}$ in diameter) glass tubes, red cells exhibit the tendency to migrate towards the center and then to travel along the axis of the tube. This phenomenon, termed '*axial migration*', leads to a gradient in hematocrit with high red cell concentration near the center of the tube and with a virtually cell-depleted zone adjacent to the wall.

In addition, the velocity of any fluid perfusing a tube exhibits a radial distribution with high flow velocities in the center and progressively decreasing velocities towards the walls of the tube. Under standard conditions, established flow of Newtonian fluids is characterized by a parabolic velocity profile. In complex fluids, e.g. those with a heterogeneous cross-sectional viscosity distribution, the profile deviates from the parabolic shape. In the presence of inward migrated red blood cells the viscosity is higher in farther axial flow regions and the velocity profile becomes blunted [177,178]. Due to the velocity profile prevailing within vessels or tubes the central high-hematocrit core moves relatively faster than the 'sleeve of plasma' surrounding it.

As result of these gradients in hematocrit and velocity, the transit time of plasma or whole blood (t_{blood}), respectively, through a given tube segment is longer than that of red cells (t_{cell}). Thus, at any moment the concentration of cells being found in a section of the tube or vessel (volume of cells in the tube divided by the volume of whole blood in the tube, the so-called '*tube hematocrit*', H_T) is smaller than that in the blood entering or leaving the tube or vessel ('*discharge hematocrit*', H_D).

The dynamic reduction in hematocrit ($H_T/H_D < 1$) is also termed '*Fåhræus effect*' (Fig. 2), referring to the pioneering studies conducted by Robin Fåhræus [48]. He demonstrated that the ratio of H_T/H_D depends on the tube diameter: the ratio declines as the tube diameter is reduced below $\sim 1000 \mu\text{m}$. This behavior is qualitatively similar to the diameter-dependency of apparent viscosity, but H_T/H_D exhibits a minimum at tube diameters of $\sim 15 \mu\text{m}$. Thus, the '*Fåhræus effect*' may explain the dynamic reduction in apparent viscosity ('*Fåhræus-Lindqvist effect*') only for diameters down to this range [34,121]. For even smaller diameters, ranging from 15 to $6 \mu\text{m}$, both phenomena display discrepant behavior, with η_{app} continuing to decrease but H_T/H_D increasing again [1,6].

The increase in H_T/H_D observed at diameters below $15\ \mu\text{m}$ is explained by the fact that the spatial portion, which the marginal plasma zone takes up, relative to the whole tube cross-section gets progressively smaller with decreasing tube diameter. Below diameters of $\sim 5\ \mu\text{m}$, red cells occupy almost the entire tube section and the plasma is redistributed into the space between successive red cells. Thus, whole blood velocity approaches that of red cells giving rise to very similar or equal transit times of whole blood and red cells, and to the increase in the ratio of H_T/H_D (Fig. 2).

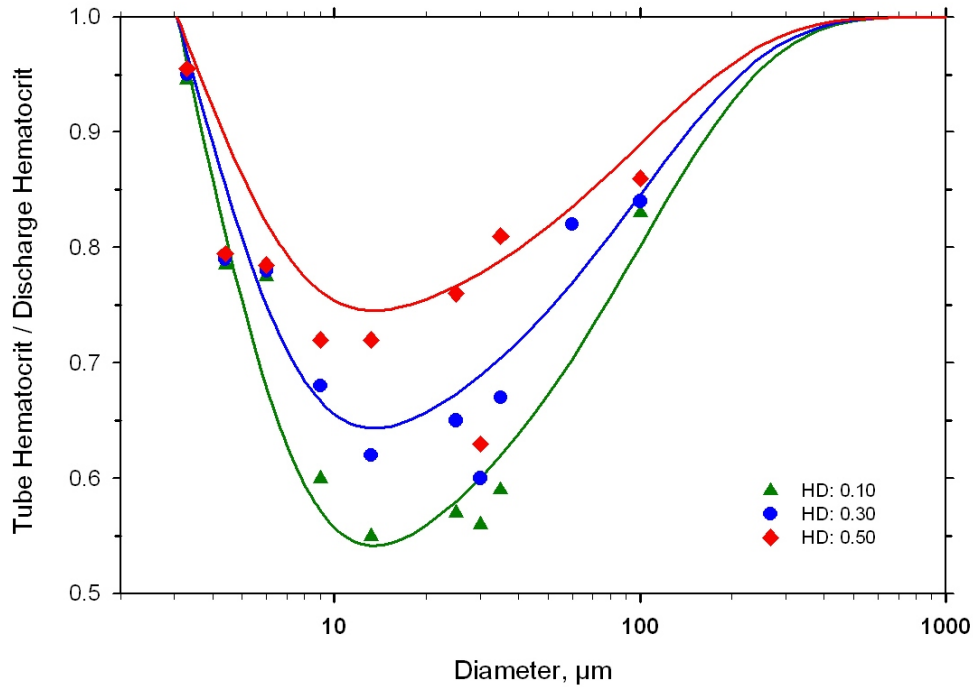


Figure 2. Tube hematocrit, H_T , normalized with respect to discharge hematocrit, H_D , as a function of tube diameter (*Fåhræus effect*) for different levels of H_D [121].

The continuing decline in apparent viscosity below $15\ \mu\text{m}$ (Fig. 1) might be explained by transitions of the prevailing flow pattern. With a reduction of tube diameter from $\sim 15\ \mu\text{m}$ to $6\ \mu\text{m}$, the flow pattern changes from a clearly ‘*multi-file*’ flow, in which at least two red cells are accommodated per tube cross-section, to a purely ‘*single-file*’ flow with only one red cell being found at any given cross-section (Fig. 1, insets). In 6 to 7- μm -diameter tubes, single-file flow regime leads to both minimal cell-to-cell interference and minimal cell-to-wall interference because red cells are optimally aligned within the lumen relative to each other and to the wall. This corresponds to minimal energy dissipation and minimal resistance to flow, or minimal η_{app} , respectively. Only for diameters below $\sim 4\ \mu\text{m}$ does the fixed surface-to-volume ratio of red cells [152,157] prohibit further cell deformation, thereby generating the steep increase in η_{app} (Fig. 1).

The transition between single-file and multi-file flow regime also influences the relation between η_{app} and discharge hematocrit at a given tube diameter, as shown in figure 3 for distinct diameters ranging from 3.3 to 40 μm [123].

- For pure single-file flow in tubes with diameters below $\sim 6 \mu\text{m}$, η_{app} and H_D are approximately linearly related with the line of smallest slope occurring at the diameter corresponding to lowest apparent viscosity, i.e. at $\sim 6 \mu\text{m}$. Each red cell adds a constant value to overall flow resistance (Fig. 3, upper panels).
- In somewhat larger-diameter tubes a similar behavior is seen for lower discharge hematocrits.
- Above a certain ‘threshold’ hematocrit, η_{app} starts rising exponentially with increasing H_D due to augmented cell-to-cell and cell-to-wall interaction, corresponding to the point where multi-file flow begins. A similar behavior is generally observed in large tubes ($>300 \mu\text{m}$) and in rotational viscometers.
- The ‘threshold’ hematocrit, where the linear relationship between apparent viscosity and discharge hematocrit turns into an exponential relationship, shifts towards progressively lower H_D as the tube or vessel diameter increases.

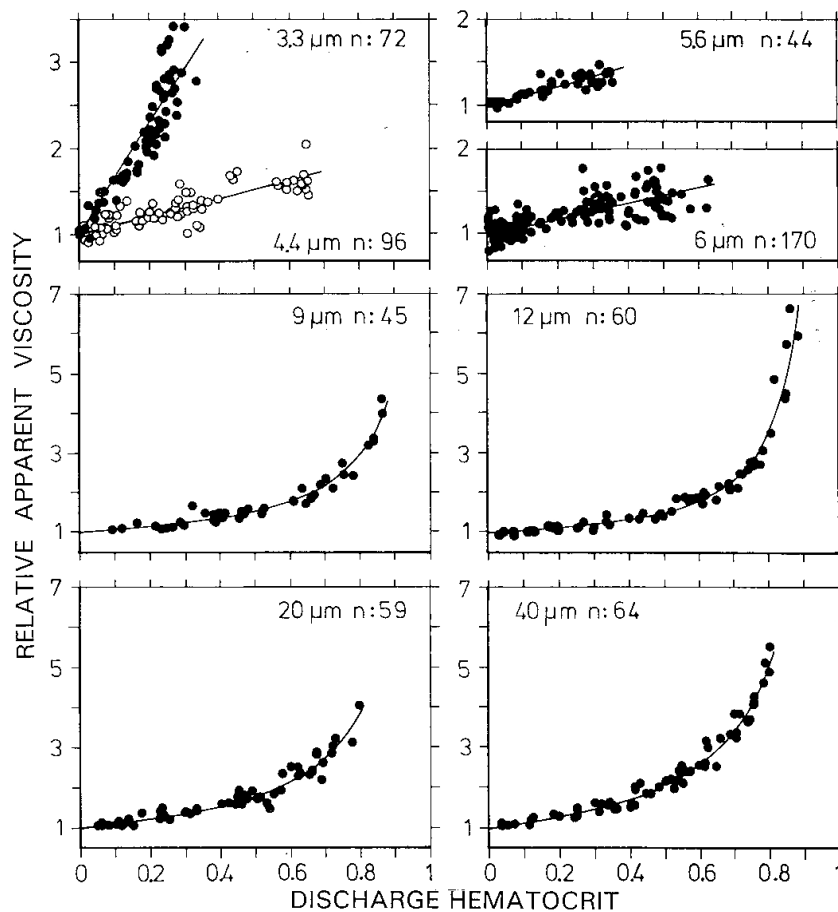


Figure 3. Relative apparent viscosity as a function of discharge hematocrit for distinct tube diameters *in vitro* [123].

1.3. Effective viscosity and dynamic hematocrit *in vivo* and the effect of the endothelial surface layer

In vessels, blood flow naturally faces a number of additional factors not present in tubes, e.g. varying vessel diameter in the direction of blood flow, irregularities of the inner vessel wall, vessel bifurcations or short vessel segments. In light of these and other factors, the aforementioned phenomena influencing effective viscosity and vessel hematocrit need to be reassessed:

Both *in vivo* measurements of viscosity in single unbranched microvessels [92,93] and mathematical simulations of blood flow through microvascular networks [121,122,124,132] indicate that, especially at vessel diameters smaller than 100 μm , the *in vivo* viscosity (effective viscosity) is significantly higher than that found *in vitro* (apparent viscosity) at comparable diameter (Fig. 4). Lowest values of η_{eff} for a given hematocrit are found in larger-diameter vessels than anticipated from tube flow experiments (30-40 μm vs. 6-7 μm). With regard to capillary-sized blood vessels, variations in hematocrit seem to have greater impact on the viscosity than *in vitro*. As a result, the *in vivo* flow resistance is about twice the *in vitro* resistance [124].

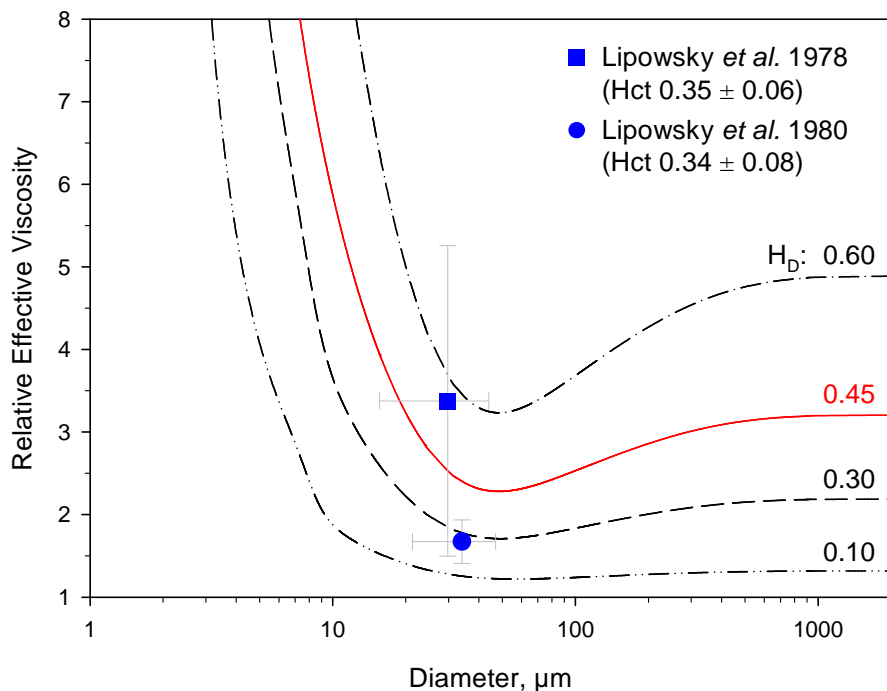


Figure 4. Relative effective viscosity as a function of vessel diameter for different levels of discharge hematocrit, H_D , as calculated with a parametric equation, known as the *in vivo* viscosity law [124]. Symbols represent data derived from *in vivo* measurements of intravascular pressure drop [92,93].

Several concepts attempting to explain the discrepancy between *in vivo* and *in vitro* viscosity have been considered in the past. Among those are:

- non-cylindrical vessel lumen and short vessel segments [84,127],
- non-proportional distribution of both hematocrit and blood flow at vessel bifurcations [51,119,120] and
- effects of rolling and adhering leukocytes impeding blood flow [20,194].

The main reason, however, seems to be the presence of an approximately 0.5 - 1 μm thick layer lining the luminal vessel surface, accordingly termed endothelial surface layer [132] or, by some authors, glycocalyx [35,36,137] (Fig.5).

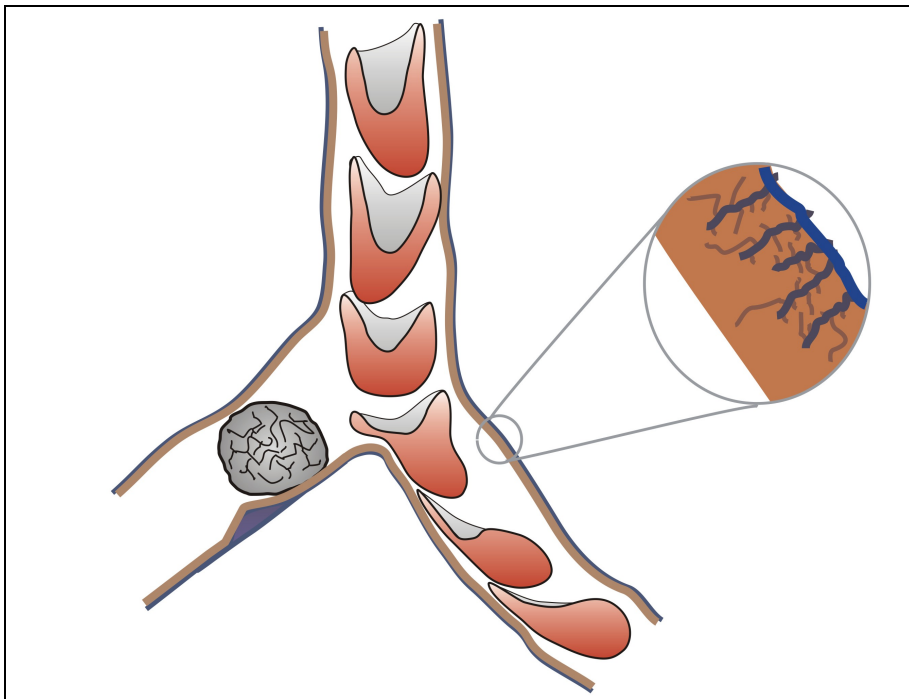


Figure 5. Model image of capillary blood flow *in vivo* in the presence of a thick, gel-like layer. (adopted from Pries et al. [131])

Various experimental approaches presented so far have contributed to the development of the concept of an endothelial surface layer, ESL, and to the estimation of its thickness and composition [130,137]:

- Based on results of hematocrit (H_T) measurements in cheek pouch and cremaster muscle capillaries of male hamsters, Desjardins and Klitzman [42,43,88] hypothesized that a matrix consisting of charged macromolecules might retard the plasma motion along the luminal endothelial cell surface, and thus may lead to the surprisingly low H_T observed.

- Pries and colleagues compared the distribution of blood flow observed in microvascular networks with the predictions made by means of computer simulations based on existing *in vitro* ‘laws’ [124,128]. They concluded that a quasi-stationary plasma layer lining the endothelial surface might be responsible for the unexpectedly high flow resistance found for vascular networks *in vivo*. It is worthy of note that this network approach allows reliable estimation of the average layer thickness of the complete microvascular network rather than determination of ESL thickness of individual vessels.
- Vink and Duling [186,188] established a method which uses fluorescently-labeled dextran molecules (FITC[#]) to indirectly visualize the ESL of capillary-sized vessels within an intravital microscopy set-up. This approach thus provides the opportunity to determine the layer thickness as corresponding to the width of the dye-exclusion zone. It is worthy of note that this method is confined to vessel diameters of at most 15 μm .
- Damiano and coworkers [39] introduced a method to trace the motion of fluorescent micro-particles in microvessels, called micro-particle image velocimetry, or μ -PIV. Based on the cross-sectional velocity profiles obtained, they could analyze hemodynamic parameters, including the effective ESL thickness [96,164].

The width of the ESL estimated with these methods ranges between 0.4 and 1.2 μm which is about one magnitude of size larger than the thickness of the ‘irregular, flocculent layer’ [144] observed with transmission electron microscopy (TEM) [5]. The obvious discrepancy between *in vivo* and *in vitro* estimates is probably caused by the staining procedures preceding TEM-observations leading to a collapse of the delicate ESL-components due to their extremely great vulnerability to dehydration [5].

In recent years, relatively new microscopic approaches utilizing confocal and photon laser microscopy have been used to assess the *ex vivo* dimensions of the ESL in isolated arteries [104,183] and on cultured endothelial cells from the human umbilical vein [7]. The measured ESL thickness ranges even between 2 and 4.5 μm . However, the spatial resolution of these techniques is relatively low, currently amounting to $\sim 0.6 - 0.9 \mu\text{m}$. Thus, further improvement is needed to provide reasonable precision in measurements.

According to a hypothesis of Pries *et al.* [130], the ESL is composed of two domains:

[#] FITC, fluorescein isothiocyanat

- the glycocalyx which in a strict sense is a thin layer of macromolecules directly anchored in the plasma membrane, including diverse glycoproteins and proteoglycans
- a thicker layer of loosely or transiently bound plasma components including proteins and glycans such as fibrinogen and hyaluronan (Fig. 6) [41,113,144].

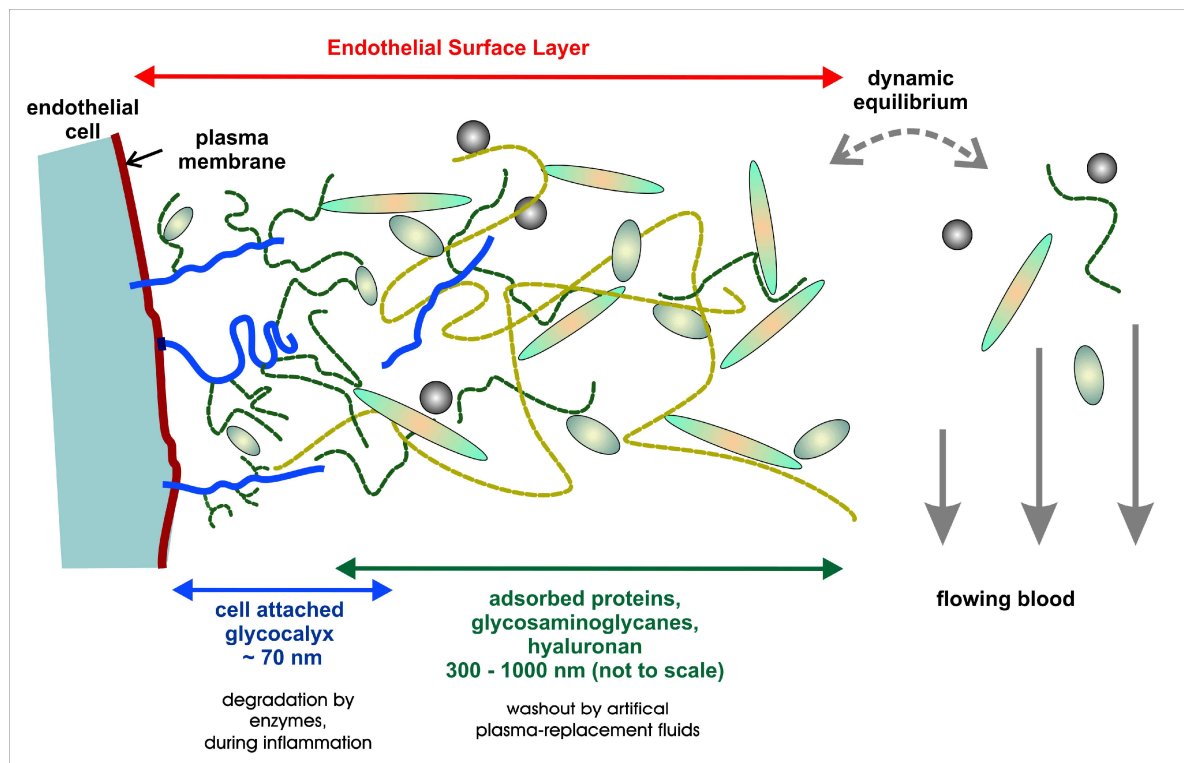


Figure 6. Schematic image of the composition of the ESL including a thin layer of membrane-bound molecules (glycocalyx) and a thick layer of transiently attached soluble plasma components. (Based on Pries *et al.* [130])

The results of these and subsequent studies [71,96,135,150,151,164,189] may explain why the ESL is likely to be the major factor for both the deviation of the *Fåhræus-Lindqvist* effect *in vivo* from that *in vitro* (Fig. 7) [129,132] and the strikingly low microvascular tube hematocrit *in vivo* [43,88,149] (Fig. 8).

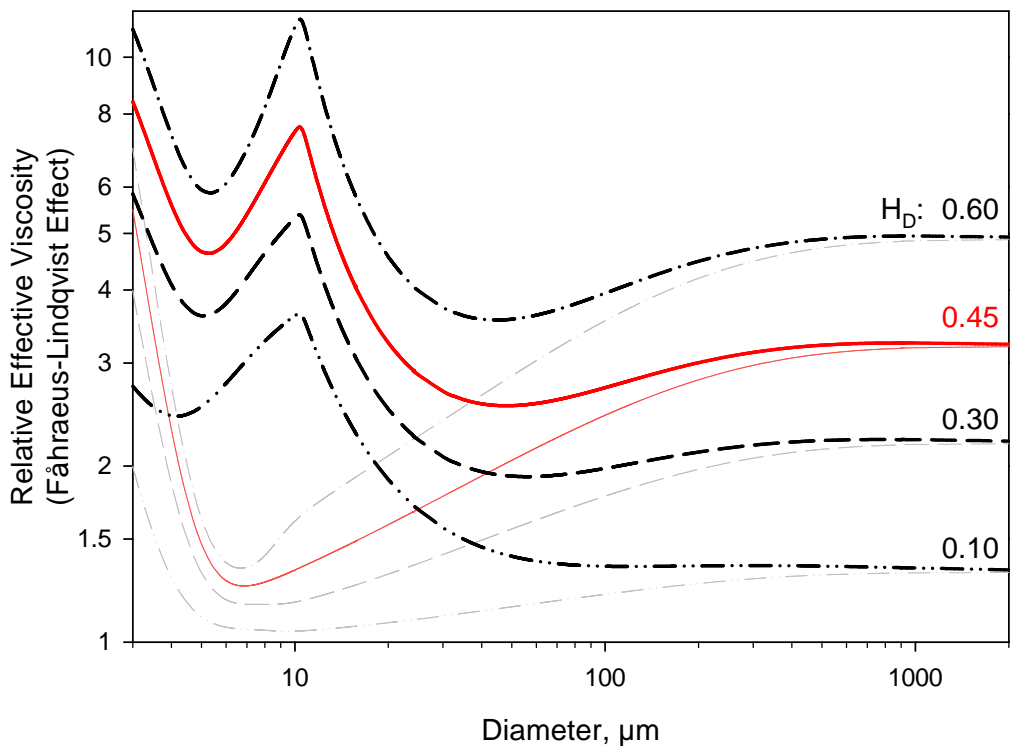


Figure 7. Predictions of relative effective viscosity as a function of diameter *in vivo* (heavy lines) for distinct levels of discharge hematocrit, H_D , involving the effect of a possibly diameter-dependent ESL thickness [132]; by comparison, respective *in vitro* viscosity data [123,124] is delineated (thin lines).

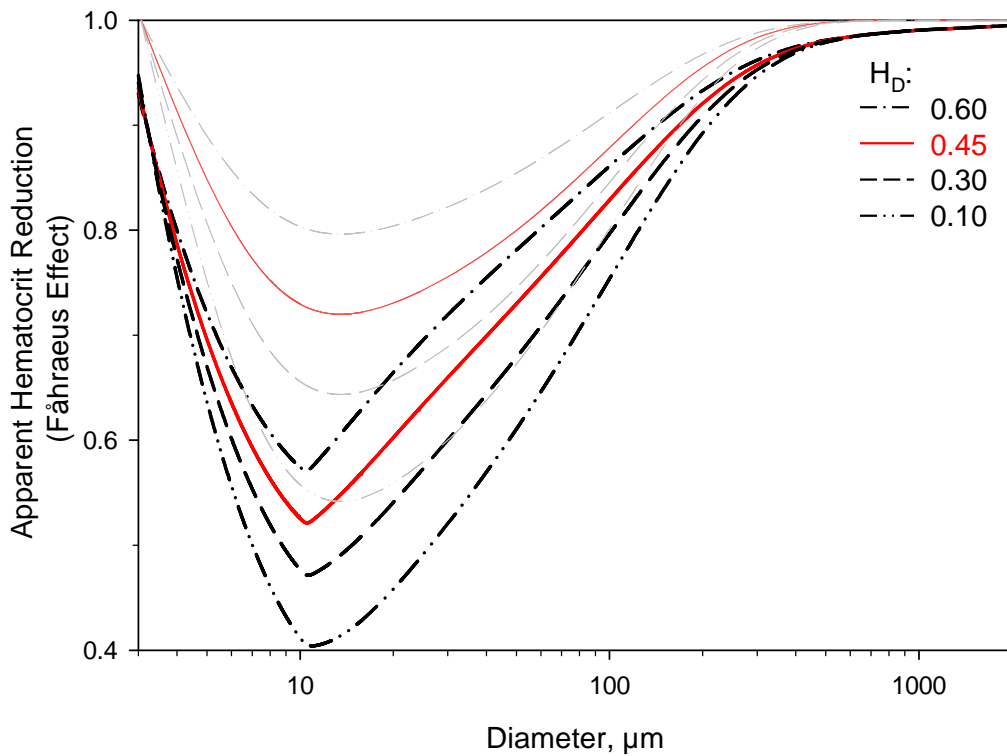


Figure 8. Fåhræus effect *in vivo* (heavy lines) [132] and *in vitro* (thin lines) [121] for distinct levels of discharge hematocrit, H_D .

So far, many hypotheses and models have been presented dealing with the biophysical aspects of the layer [26,36,37,75,171,172,202]. Such theories provide arguments why the ESL is, at least transiently, able to withstand the compressive forces exerted by the normal shear stress and moving red cells, but not by rolling leukocytes [50,150,186,195,199].

The layer affects the transendothelial transport of macromolecules [59,172,188], the transmission of shear stress towards the endothelial cytoskeleton [150,195] as well as early inflammatory processes [72,187,202] and the coagulation [132]. Damage of the blood-vessel interface may have a direct bearing on the development of diabetes [110], and atherosclerotic and ischemic [116] disease events such as stroke and myocardial infarction. Numerous studies [35,72,186,187] have demonstrated that the ESL can, at least partially, be degraded if subjected to inflammatory triggers such as tumor necrosis factor α (TNF- α) and oxidized low density lipoproteins (ox-LDL) as well as to reactive oxygen species (ROS) and hyaluronidase. Also, exposure to continuous epi-fluorescence leads to a shedding of the surface layer [39,96,104,164].

Even under physiological conditions, the features of the ESL such as its thickness, composition and permeability are supposed to vary temporally and spatially in a given species [104]. In addition, ESL properties may depend on vessel diameter [104,132], plasma composition [129,132], blood flow velocity, and on the hematocrit [132].

1.4. Mouse model with systemic hematocrit of up to 0.90

Recently, a mouse line (tg6) transgenic for the human erythropoietin (EPO) gene was generated which may serve as a model of strongly increased hematocrit. The glycoprotein EPO is mandatory for maintenance of erythropoiesis as it prevents erythroid progenitor cells, predominantly CFU-E[#], from apoptosis [8,25,79,159,160]. Naturally, expression of EPO mRNA is transiently induced by a reduction in partial oxygen pressure via binding of the nuclear factor HIF-1[¶] to hypoxia response elements (HRE) which are located in the 3'-flanking region of the EPO gene [46,73,74,153]. In contrast, tg6 mice constitutively overexpress EPO in an oxygen-independent manner leading both to excessive

[#] CFU-E, erythroid colony forming unit

[¶] HIF-1, hypoxia-inducible factor 1

erythrocytosis and polycythemia with levels of systemic hematocrit of ~0.80 to 0.90, and to a ~2.5-fold increase in total blood volume [190].

Surprisingly, tg6 mice can cope well with the elevated hematocrit although their cardiovascular system faces a significantly increased strain [191]. Numerous studies have been carried out in order to reveal the adaptive and compensative mechanisms allowing tg6 mice to survive for a relatively long term. Among those mechanisms are:

- increased flexibility of RBC due to doubled fraction of reticulocytes [190]
- enhanced erythro-phagocytosis [18]
- up-regulation of mitochondrial energy metabolism [103],
- natriuresis and diuresis [163] and
- ubiquitous vasodilation induced by augmented synthesis of NO and thrombin.

Especially vasodilation may appreciably reduce flow resistance due its strong inverse dependence on tube or vessel radius, as given by the Hagen-Poiseuille equation [68,141].

On the other hand, a number of specific traits of tg6 mice have been described, reflecting possible negative side effects of the chronically elevated hematocrit. Among those are reduced exercise performance [70,191], cellular and tissue damage in multiple organs [68,70,112,191], pulmonary hypertension [68], impaired hemostasis [155], 2 to 5-fold increased ET-1[#] levels [133,163], and activation of oxidative metabolism pathways [103,197]. Even though no signs of patent ischemic vascular disease are observed in these animals, mean life span (~7.4 months [191]) is significantly reduced relative to their wild-type littermates (~26.7 months [86]).

In essence, two pathophysiological mechanisms may be related to the premature death of tg6 mice: First, increased peripheral blood flow resistance demanding chronically increased cardiac performance ending up in congestive heart failure and acute ventricular dysfunction [141,191]. Second, chronic multiple organ damage at the level of the microvasculature (liver, kidney, PNS[¶] [70] and CNS^{*} [112]), becoming manifest predominantly in adult tg6 mice.

[#] ET-1, endothelin-1: is a strong vasoconstrictor, and as such the 'counterpart' of NO.

[¶] PNS, peripheral nervous system

^{*} CNS, central nervous system

Microhemodynamic changes and adaptations to increased hematocrit may therefore be involved in the pathophysiological processes associated with multiple organ degeneration. So far, there is only little knowledge of the microvascular rheology in these transgenic animals.

1.5. Objectives of the study

The objective of this study was to assess the consequences of strong elevations in systemic hematocrit for the hemodynamic and hemorheological properties in the microcirculatory system. In this context, the emphasis was on possible implications of the recently described gel-like layer lining the endothelial cell surface. For this purpose, a transgenic mouse model (tg6) was used to generate animals that exhibit very high hematocrit values of ~0.85.

In this context, two specific aims were addressed:

- Examination of the impact of an extremely elevated systemic hematocrit on viscosity, shear stress and additional parameters characterizing microvascular hemorheology, and on the thickness of the endothelial surface layer (ESL) *in vivo*.
- Discrimination between long-term adaptation of the microcirculatory system to elevated hematocrit and immediate hemodynamic effects of acute changes in hematocrit.

For this purpose, an intravital microscopy approach was used: Postcapillary microvessels in the cremaster muscle of tg6 mice and C57 wild-type control mice were investigated using micro-particle image velocimetry (μ -PIV). The respective data was analyzed according to the microviscometric approach of Damiano *et al.* [39].

In order to discriminate between long-term adaptation and sudden hemodynamic changes to elevated hematocrit, systemic hemodilution was performed representing an indirect experimental approach. Transgenic mice were hemodiluted to a hematocrit level similar to that of control mice, while the latter underwent a relative reduction of hematocrit corresponding to that in tg6 mice.

Findings in this model with severe changes of hematocrit are expected to improve the understanding of hemorheological mechanisms related to increased hematocrit. Such results may also be transferred to milder changes of hematocrit as they can occur in humans in the context of certain diseases [13,56,78,81,118].

2. Material and Methods

2.1. Summary of methods

Venular blood flow in the cremaster muscle of both epo transgenic (tg6) and wild-type control mice (C57Bl/6) was observed by means of intravital microscopy (IVM). Following the micro-particle image velocimetry (μ -PIV) approach described in detail by Damiano [39], the cross-sectional velocity distribution, $v(r)$, or velocity profile of each examined vessel (20-75 μm in diameter) was derived from the movement of fluorescent micro-particles, acting as passive flow tracers. These microspheres[#] were injected into the jugular vein immediately before recordings of blood flow were started. The cross-sectional distribution of shear rate, $\gamma(r)$, and shear stress, $\tau(r)$, could be analytically derived from the velocity profiles. The microviscometric method [39] which assumes blood to behave as a continuous fluid[¶] in vessels larger than 20 μm in diameter was employed to calculate the radial distribution of the viscosity, $\eta(r)$, from the shear rate and shear stress profiles. Based on the resulting viscosity profile, various microvascular flow parameters could be predicted, including axial pressure gradient, volume flow rate, relative apparent viscosity, and the ratio H_T/H_D . In addition, the effective hydro-dynamically relevant thickness of the ESL was determined, which hereafter is simply referred to as the ‘ESL thickness’. In the following, the successive experimental steps, as compiled in Fig. 9, are described in more detail.

[#] The term ‘microspheres’ is used synonymously with ‘micro-particles’ in the present study.

[¶] Continuous fluid: Blood actually being a heterogeneous red-cell suspension is regarded as a homogeneous linearly viscous incompressible fluid. According to Damiano [39] and Cokelet [34], blood viscosity of a linearly viscous fluid depends only on temperature and local hematocrit but is independent of shear rate, γ , provided that γ exceeds 50s^{-1} .

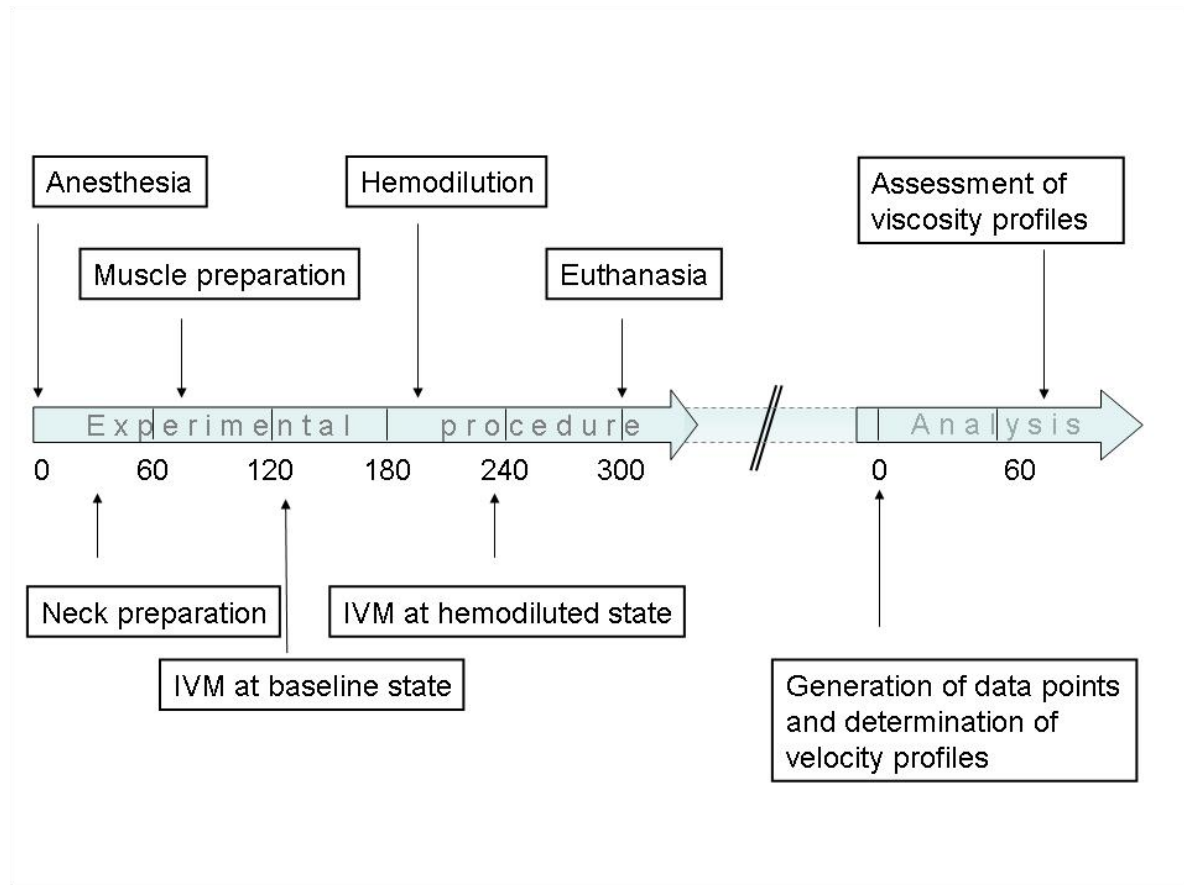


Figure 9. Experimental protocol and analytical procedure; values on the time-scale are given in minutes. IVM, intravital microscopy.

2.2. Preliminary remarks

All procedures were performed after approval by university and governmental committees on animal care (Tierversuchsantrag G239/02, accepted on February 25, 2003). Experiments and care of animals were in accordance with the declaration of Helsinki of the WMA on ethical considerations related to biomedical research from 1964 (last revised in 2000).

The transgenic (tg6) mice were obtained from the Institute of Veterinary Physiology in Zurich, Switzerland (Director Professor Max Gassmann). C57Bl/6 wild type mice were obtained from the ‘Forschungseinrichtung Experimentelle Medizin’ (FEM) of the Charité Berlin. Animals of each strain were housed under standardized conditions with free access to mouse chow and tap water.

2.3. Experimental groups

Male tg6 mice (N = 8; mean bw[#], 26.4 ± 1.7 g) and male C57Bl/6 wild-type mice (N = 8, mean bw 31.8 ± 3.3 g), hereafter referred to as epo mice and wt mice, respectively, underwent experimental investigation with the latter serving as control. The two groups are termed epo_{0.85} and wt_{0.46}, respectively, according to the strain and the mean systemic hematocrit. A total number of n = 32 vessels in the eight animals of the epo_{0.85} group (mean diameter 41.4 ± 12.3 μm) and n = 37 vessels in the eight animals of the wt_{0.46} group (mean diameter 35.0 ± 8.5 μm) were examined. As differences between animals within a given group are considered negligibly small, all vessels of each group were pooled (Fig. 10, top row).

For the next step of the experimental investigation, animals of the epo_{0.85} group underwent isovolemic hemodilution with either hydroxyethyl starch solution (HES 6%, 130/0.4, Voluven, Fresenius Kabi, Germany) or cell-free rat plasma (plasma). The groups emerging from this hematocrit reduction are termed epo_{H0.46} and epo_{p0.53}, according to the hemodilution agent (**H**ES or **p**lasma) utilized and the mean systemic hematocrit attained. If the mean arterial pressure fell below 50 mmHg during the steady state after hemodilution, the respective animal was excluded from the group and only the baseline data was analyzed. The resulting number of vessels in the epo_{H0.46} group (N =4) and epo_{p0.53} group (N = 3) amounted to n = 10 and n = 16, respectively (Fig. 10, middle row, left).

A 41% reduction in hematocrit was also applied to the control group. The resulting groups are named wt_{H0.30} and wt_{p0.24}, with a total of 15 (wt_{H0.30}) and 19 (wt_{p0.24}) vessels, respectively, being examined (Fig. 10, middle row, right).

In the consecutive statistical data analysis, both hemodilution groups of each strain were gathered into single groups (epo_{0.50}, wt_{0.27}) if no significant differences were found (Fig.10, bottom row).

[#] bw, body weight

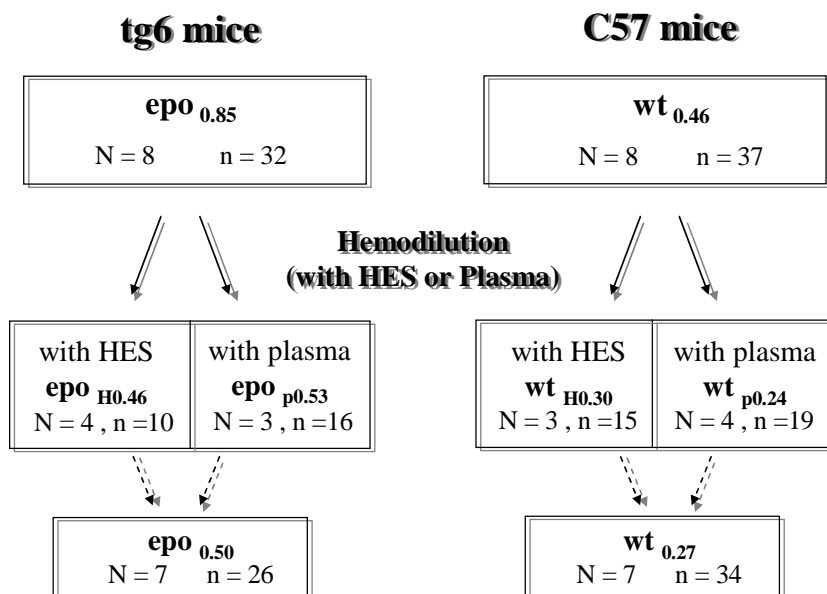


Figure 10. Schematic illustration of the division of experimental groups, with the subscript indicating mean systemic hematocrit; N, number of animals; n, number of vessels; HES, hydroxyethyl starch; plasma, rat plasma.

2.4. Anesthesia and animal preparation

Animals, ranging in age from 10 to 20 weeks, were allowed to breathe oxygen-enriched air to prevent acute hypoxia upon initiation of anesthesia [139]. All animals were anesthetized with an intraperitoneal bolus injection of a combination of xylazine (10 µg/g bw, Rompun 2%, Bayer, Leverkusen, Germany), ketamine (100 µg/g bw, Ketavet 100 mg/ml, Pharmacia, Karlsruhe, Germany) and atropine (0.1 µg/g bw, Atropinsulfat 0.5 mg/ml, Droben, Germany). The desired anesthetic level was achieved when the inter-toe reflex was missing or markedly delayed and spontaneous ventilation was still unimpaired. The mouse was fixated in supine position on a temperature-regulated heating pad to keep body temperature at ~37 °C. If required, additional amounts of the ketamine/xylazine-solution were administered (subcutaneous injection) during the experimental course to sustain anesthesia.

Subsequently, neck structures were dissected as follows:

- tracheotomy and intubation of the trachea using a PE[#]-tubing (1.22 mm outer diameter, Portex, Hythe, Kent, UK) to allow spontaneous respiration;

[#] PE, polyethylene

- preparation and cannulation of the right common carotid artery (PE-tube, 0.61 mm outer diameter);
- connection of the carotid catheter to a pressure transducer i) to continuously monitor mean arterial blood pressure (MAP) and heart rate (HR) and ii) to collect blood specimens;
- preparation and cannulation of the left external jugular vein analogously to that of the artery;
- connection of the venous catheter to a perfusor (Perfusor F, B. Braun, Melsungen, Germany) i) for continuous infusion of saline solution adjusted to a rate of 0.2 ml/h to maintain fluid balance and ii) for administration of drugs and liquids.

Micro-surgical steps of preparation of the right cremaster muscle followed those described by Baez [4] with some modifications. Preliminary measures and precautions included:

- gentle shaving of the ventral aspect of the lower abdomen,
- draining of the bladder to avoid unintended miction during the ensuing procedures,
- mounting the animal in slightly upright position onto a customized viewing stage designed for the intravital microscopic observation of small tissues, and
- intravenous injection of anti-P-selectin antibodies (RB40.34, 0.57 $\mu\text{g}/\mu\text{l}$) to suppress tethering and rolling of leukocytes along the venular vessel wall.

The initial incision was made in the skin and fascia above the right scrotum and was then extended along the top of the inguinal fold. As soon as the tissue was exposed, it was continuously irrigated with Ringer's solution (0.66 mol/l NaCl, 23.5 mmol/l KCl, 10mmol/l CaCl₂, 6 mmol/l MgCl₂, 90 mmol/l NaHCO₃) adjusted to pH 7.4 and equilibrated with 5% CO₂ and 95% N₂ to prevent spontaneous changes in vessel tone. The buffer's temperature was maintained at 34 °C with heating coils [53]. After careful separation of the entire connective tissue fascia from the muscle surface and subsequent midline incision of the muscle sack by means of thermal cautery, the open cremaster muscle pouch lay flat on the central glass cover slip of the stage. The muscle was gently extended [53] with thin threads (Prolene 6-0) placed along the edges of the muscle. Both epididymis and testicle were dissected from the muscle tissue and gently drawn aside rather than being delivered into the abdominal cavity as originally proposed by Baez [4]. Eventually, both the muscle tissue and the dissected entrails were covered with a transparent airtight PE-foil to preserve the tissue's osmotic balance and to prevent dehydration, and the superfusion was stopped.

2.5. Optical and electronic set-up for intravital microscopy

The experimental set-up is illustrated in figure 11. Blood flow was examined using an intravital microscope (Ernst Leitz, Wetzlar, Germany). The tissue was trans-illuminated with a standard microscope light source. Critical illumination was attained by adjusting the condenser height and aperture [90]. The microscopic field of view was depicted with a $\times 40$ water immersion objective (NA 1.15, Olympus, Tokyo, Japan) and captured with a CCD video camera (CF 8/5 NR, Kappa opto-electronics, Gleichen, Germany). In addition, both the coordinates (x , y , z) of the current spatial position of the microscope stage and a time course signal were superimposed on the video signal. During the recording, the tissue was epi-illuminated with intermittent stroboscopic flash light (model 11360 Strobex, Chadwick Helmuth, Mountain View, CA), while the intensity of trans-illumination was reduced to a level at which the vessel outline was just visible. By synchronizing (Fiber Optic Video Syn Module 9630, Chadwick Helmuth) the stroboscope and the CCD video camera, flash release was triggered such that each video frame was epi-illuminated twice. Thus, any fluorescent particle traversing the vessel section at the moment of flash release was represented twice on a single image.

Hence, the microscopic field of view was visualized both by continuous, low-powered trans-illumination and intermittent epi-illumination with two flashes per frame separated by a preset time delay. The final image as displayed on a video monitor was saved to a video recorder (DSR 20-P, Sony, Tokyo, Japan) on digital video tape (DV CAM 64, Sony) (Fig. 11). The resolving power of the optical set-up employed was $\sim 0.35 \mu\text{m}$, assuming a mean wavelength of 500 nm.

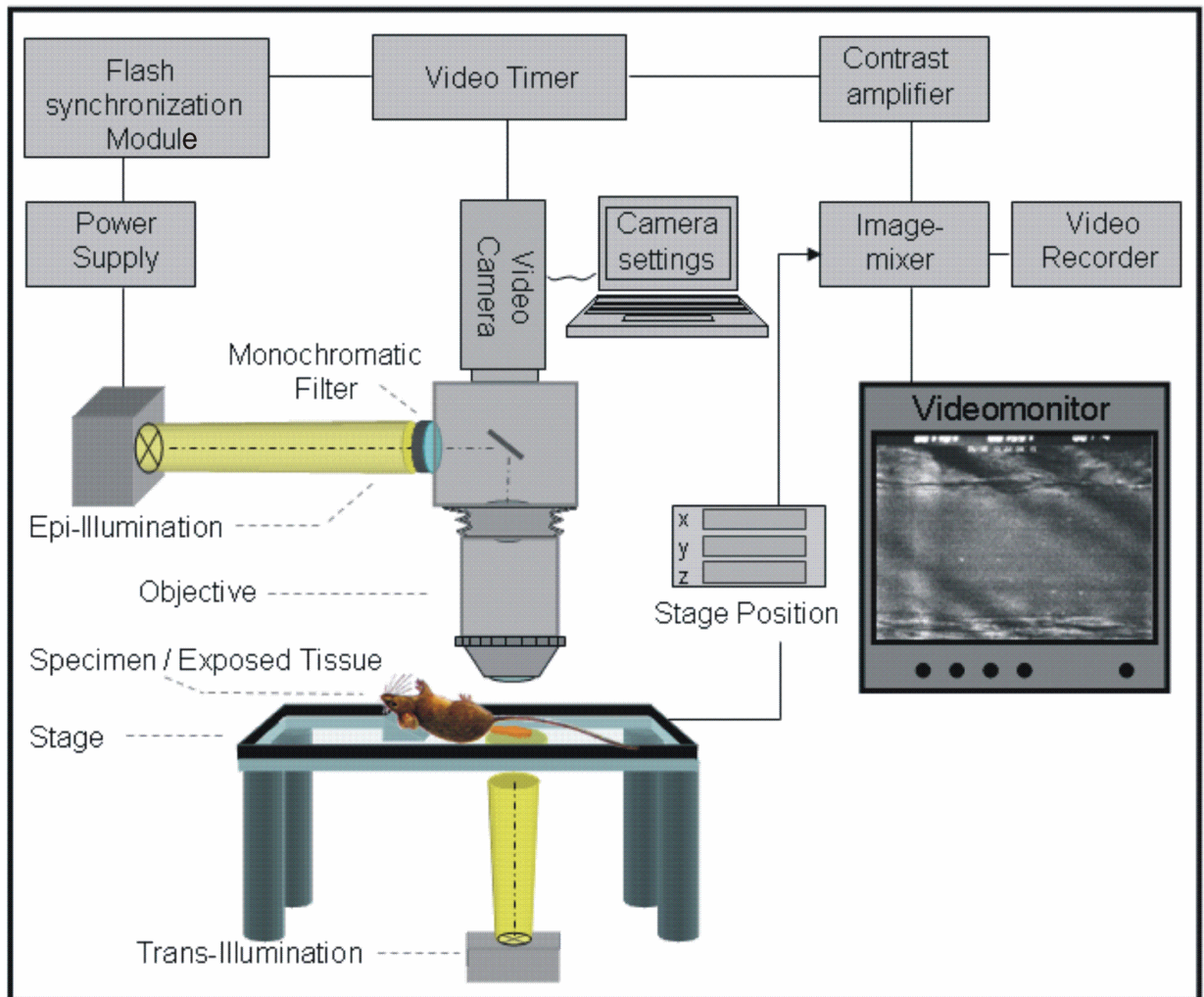


Figure 11. Experimental set-up for intravital microscopic observation; dash-dotted lines indicate the course of epi-illumination and trans-illumination, respectively; some details related to the animal and the microscopic stage (e.g. cannulation, heating pad, substage condenser) are not shown for reasons of clarity.

2.6. Intravital microscopy

Prior to intravital microscopic observation, papaverine ($2 \cdot 10^{-3}$ mol/l) was administered topically onto the cremaster muscle for ~10 minutes to prevent development of spontaneous arterial vasoconstriction and consecutive temporal variation of blood flow during the experimental observation. Following criteria had to be satisfied to include a vessel in further investigation:

- sufficient optical quality including a clearly visible vessel wall
- at most 3 adherent or rolling leukocytes in the microscopic field of view
- only minimal wall irregularity and variation in diameter

In addition, the examined vessel section had to be located at least 5 vessel diameters apart from the closest convergent bifurcation to ensure laminar and axisymmetric flow conditions.

It is immanent in the optical set-up used that the approximately cylindrical outlines of the vessel wall boundaries are projected as a two-dimensional or sectional image (Fig. 12A, B). Hence, there can be only one point along the optical axis, θ , at which the microscopic vessel image coincides with the equatorial plane of the vessel. Therefore, correct focusing ($\theta \rightarrow 0$) is crucial for valid and consistent determination of vessel diameter. The equatorial plane of the selected vessel was focused as proposed by Gretz *et al.* [65]: As the focus is traversing the equatorial plane of the vessel, the inner boundary of the vessel's wall goes from light (overfocused) to dark (underfocused). The vessel is considered focused at the point at which the contrast of the edge of the vessel intraluminal wall reverses, corresponding to the point of least contrast. This focusing was accomplished with high intensity trans-illumination. By rotating the CCD video camera, the microscopic image was adjusted such that the length axis of the vessel was approximately parallel to the upper and lower edge of the video monitor.

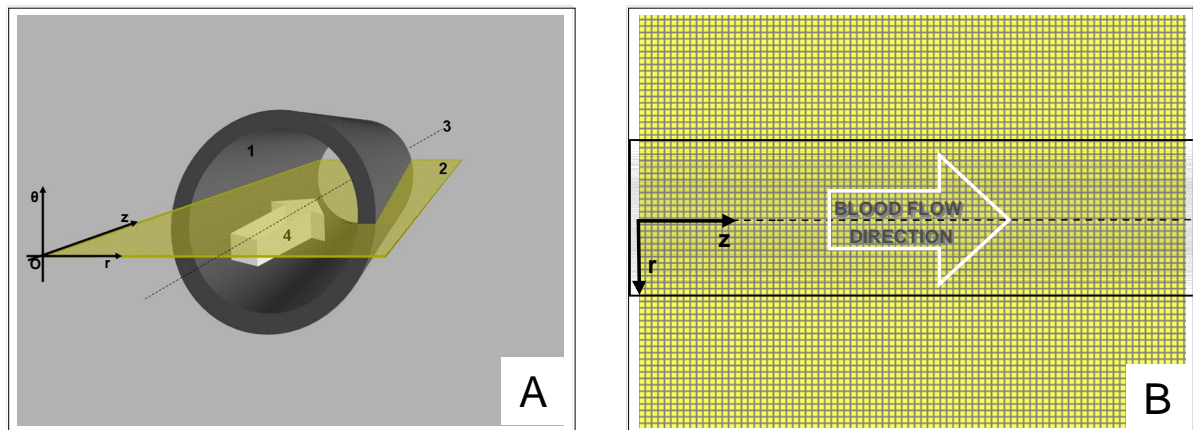


Figure 12. A, Schematic three-dimensional model of a vessel, including the vessel wall (1), the plane of focus (2), the vessel centerline (3), and the prevailing direction of flow (4). For reasons of clarity, the origin (O) of the coordinate system ($r;\theta;z$) is laterally displaced from the vessel centerline. B, Schematic two-dimensional image ($r;z$) of the microscopic field of view in the plane of focus ($\theta = 0$, yellow-colored scaffold).

Epi-illumination was turned on and a small volume ($\sim 10 \mu\text{l}$) of microspheres ($0.5 \pm 0.016 \mu\text{m}$ in diameter, FluoSpheres, Molecular Probes, Leiden, The Netherlands) suspended 1:19 in isotonic saline was slowly injected via the venous catheter. The chosen concentration of microspheres ($\sim 1.45 \cdot 10^7 \mu\text{l}^{-1}$) resulted in an optimal density of microspheres in the selected vessel section for the following off-line analysis, i.e. in the steady state each frame

showed ~4 doublets of micro-particles. Due to its dual-flash epi-illumination, each frame showed a double representation (doublet) of any traversing microsphere displaced by distance Δz . Flash time interval Δt (range, 0.5-10 ms) was adjusted such that the dual images of a microsphere in the vessel center were ~15-30 μm away from each other.

The topographical position of each vessel section, corresponding to the x/y/z-coordinates of the microscope stage (Fig. 11), was registered in order to retrieve the same vessel site after hemodilution, and to enable pairwise statistical comparison of data. Recording time was ~30-60 s per vessel.

2.7. Hemodilution

Initially, systemic baseline hematocrit was determined by collecting a small volume of blood (60 μl) from the carotid artery into a heparinized microtube and subsequent spinning of the blood sample for 5 minutes utilizing a table-centrifuge (Haematocrit, Hettich, Tuttlingen, Germany). As mentioned above, mean baseline hematocrit amounted to 0.85 ± 0.01 and 0.46 ± 0.02 for the epo group and wild-type group, respectively.

Adult Sprague Dawley rats (both male and female) underwent exsanguination via an arterial cannula to generate (cell-free) plasma, required for hemodilution experiments. The withdrawn blood sample was centrifuged at 2550 $G^{\#}$ (Megafuge 1.0, Heraeus, Hanau, Deutschland), followed by careful aspiration of supernatant of the spun blood, strictly avoiding undesired mixture with the buffy coat[¶] beneath. The plasma was filled into small plastic containers (1 ml) and stored at minus 30 °C.

The fluids used for isovolemic hemodilution (HES or thawed rat plasma) were administered via the venous catheter at a volume rate equal to that by which blood was simultaneously withdrawn from the carotid artery (~50 $\mu\text{l}/\text{min}$). On average, a total volume of 1.2 ml and 0.75 ml was exchanged in order to attain the desired target hematocrit in epo mice (0.50 ± 0.05) and wild-type mice (0.27 ± 0.04), respectively. This hematocrit reduction corresponds to a relative decrease of ~40%. In order to achieve steady state (i.e. homogenous

[#] G, gravitational force: Refers to an (artificially generated) acceleration experienced by an object, and is usually expressed as a multiple of standard gravity, g_n (~9.8 m/s^2).

[¶] Buffy coat: Thin boundary layer in between the plasma layer and the red cell layer generated by centrifugation of blood. It contains leukocytes and platelets.

distribution of the given fluid in the circulatory system), and to allow restoration of cardiovascular parameters, systemic hematocrit was reassessed not before 10 minutes after completion of hemodilution. If necessary, additional fluid could be exchanged.

Then, blood flow of the same vessel sections as before hemodilution was recorded again, using the μ -PIV approach as described before. Eventually, the animal was sacrificed with a lethal dose of pentobarbital (0.2 ml, 160 mg/ml, Narcoren, Merial, Hallbergmoos, Germany).

2.8. Off-line generation of data

The video recordings were digitized into 'avi'-format using in-house software. If needed, contrast and brightness of the images were optimized by means of a customized contrast amplifier. For following distance measurements, image software 'VMorph' was used.

For metrical calibration, an objective micrometer slide with 10 μm divisions (Carl Zeiss, Jena, Germany) was used. For the present optical set-up, the resulting pixel size amounted to 0.1282 $\mu\text{m} \times 0.1282 \mu\text{m}$.

2.9. Image analysis

The inner diameter (D) of the vessel was taken to be the shortest distance between the two opposing luminal edges of the endothelium as defined in the following way: At optimal focus adjusted as described before [65], the vessel wall appeared to be composed of 3 consecutive layers, each ~ 5 pixels in width. The 'inner' and the 'outer' band were dark, whereas the 'intermediate' band was bright (Fig. 13). This optical appearance is probably due to slightly different refractive indices[#] of plasma and tissue. Microspheres in close proximity to the vessel wall sometimes seemed to run alongside the interface between the inner dark and the intermediate bright layer. As microspheres are supposed to be essentially excluded from the endothelium, the middle pixel within the bright layer was considered the luminal edge of the endothelium. This assumption was consistently applied to all vessels.

[#] Refractive index: A material property that refers to the relative difference in the speed of light in a vacuum versus that in a given medium. A difference in the refractive indices of two adjacent (fluid) media gives rise to a bending of light rays as they pass from one medium to the other.

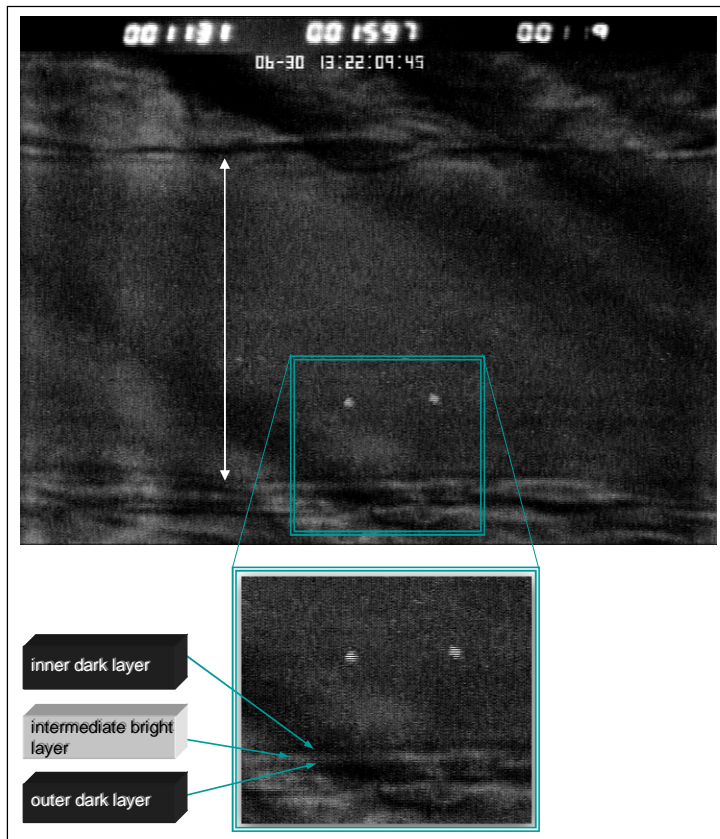


Figure 13. Typical bright field image of a 45.5- μm -diameter venule with a dual image of a microsphere (white dots). The white double arrow indicates the inner vessel wall. Detailed near-wall view (lower panel) reflects the common optical appearance of the luminal aspect of the vessel wall.

2.10. Collection of μ -PIV data and raw data plot

Both the center-to-center distance between dual images of a microsphere ($\Delta z = z_2 - z_1$) and its pseudo radial position, r^* , i.e. the distance between the microsphere and the inner vessel wall, were measured for each micro-particle in focus traversing the vessel section. The smallest possible r^* corresponds to half a sphere's diameter, i.e. 0.25 μm . The pseudo radial position, r^* , was transferred to the radial position, r , which corresponds to the distance between the microparticle and the vessel centerline, that is $r = R - r^*$, with R being half the vessel's diameter. Radial displacement of a microsphere between two corresponding flashes was negligibly small in most cases. If radial displacement was obvious, the radial positions of the upstream and the downstream image of the microsphere were averaged. A complete data set consisted of at least 50 of such measurements (Δz , r). The velocity, v , of any microsphere is given by $v = \Delta z / \Delta t$, where Δt is the preset flash time interval.

By plotting all velocity data, v , versus their corresponding radial position, r , a parabola-like distribution of data points was obtained (Fig. 14, top). Data points were folded over to one side of the vessel centerline assuming axisymmetric flow conditions to prevail (Fig. 14, bottom).

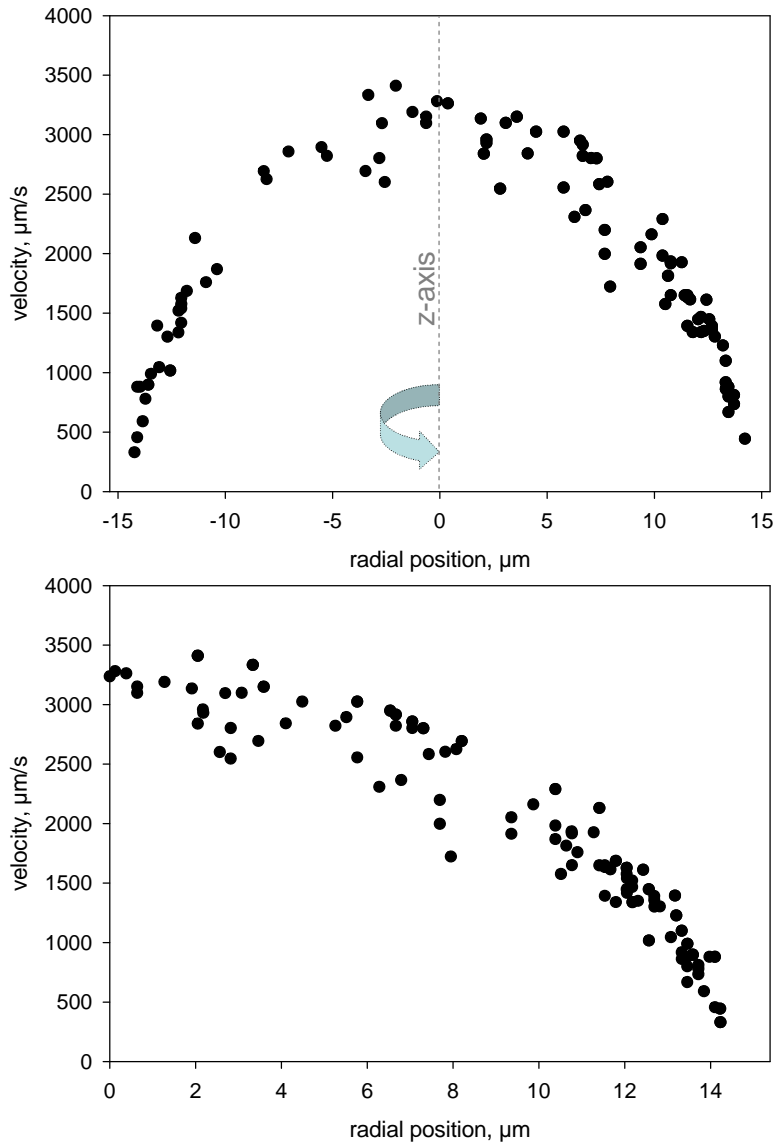


Figure 14. Complete raw μ -PIV data set with velocity data plotted against their corresponding radial position. The dashed line (z-axis) corresponds to the vessel centerline (top). For the next step of analysis, data points from the left-hand side are reflected to the right-hand side (bottom).

2.11. Selection and analysis of μ -PIV data

The plotted raw data points show a certain degree of scattering, as per exemplary plot in Fig. 14 (bottom panel). It is hypothesized that this scatter is mainly caused by the limited precision in localizing microspheres in a three-dimensional space or, more precisely, in the direction of the optical axis, y (Fig. 12A). Accordingly, not all microspheres which appear to be focused [65] necessarily flow exactly in the vessel's mid-sagittal plane which naturally accommodates fastest flow. Some microspheres with a measured radial position, r_{meas} , may actually lie on a slower concentric streamline since their true radial position, r_{true} ,

is closer to the vessel wall, i.e. $r_{\text{true}} > r_{\text{meas}}$. To a smaller degree, data scattering may also be produced by the mild pulsatility of venular flow, giving rise to a corresponding pulsatility curve with alternation of peaks and valleys. Microspheres recorded at off-peak times exhibit reduced velocity, while those scanned at or close to peak times exhibit the highest velocity for a given radial position.

The approach of data selection, thus, intends to eliminate data points generated by these errors from a given raw data set by selecting only the fastest data point for a given radial position. The filtering procedure is explained in detail by Damiano *et al.* [39]. Briefly, a data point, i , with given r_i and v_i is assumed to be relevant if there is no other point, j , with $r_j \geq r_i$ and $v_j \geq v_i$. As a result, the selected data points display a monotonic increase in velocity from the vessel wall ($r=R$) to the vessel center ($r=0$) (Fig. 15, left panel).

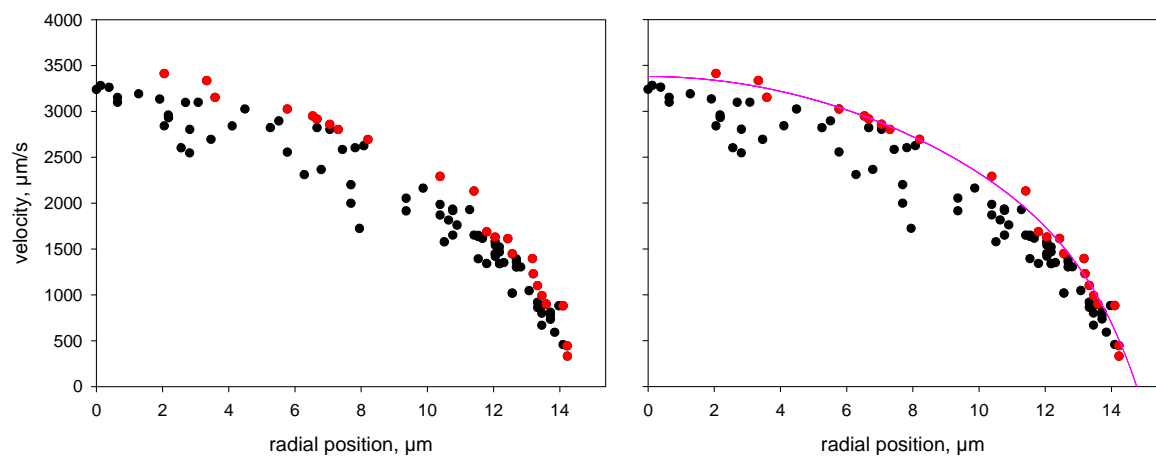


Figure 15. Monotonic filtering procedure selects relevant data points (red) from the raw data set (left plot), followed by the fitting of a curve (pink) to the filtered data points (right plot)

Subsequently, a curve is fitted to the selected data points, using standard non-linear regression of y on x , thus minimizing the sum of the squared vertical distances of the filtered data points from the fitted line (Fig. 15, right panel). The fitted line is described by the analytical model of Damiano *et al.* [39]. As for the *in vivo* case, the velocity fit has to satisfy the following constraints:

- The velocity curve must be continuous from the vessel centerline to the luminal surface of the ESL.
- The fit exhibits an exponential rather than a linear velocity distribution in the plasma-rich region near to the vessel wall.

The aim of the microviscometric analysis is to derive the cross-sectional viscosity distribution from the experimentally obtained velocity profile. The cross-sectional viscosity distribution is obtained by combining the radial profiles of local shear rate, γ_r , and local shear stress, τ_r . Briefly, the radial distribution of shear rate (Fig. 16, upper left panel), can be directly calculated by differentiating the velocity profile ($\gamma_r = dv/dr$). Since local shear stress is, by definition, a linear function of radial position, $\tau_r \sim r$ (Fig. 16, upper right panel), two data points exactly describe the shear stress profile:

- Due to the axisymmetry of flow, shear rate is supposed to vanish in the vessel center, ($\gamma_0 = 0$). Given the constitutive relationship between shear stress, shear rate and viscosity ($\tau = \gamma \cdot \eta$), the corresponding shear stress (τ_0) must be zero, too.
- Due to the continuum approximation, which the microviscometric approach is based on, plasma viscosity (η_{plasma}) is assumed to prevail in the near-wall fluid layers ($r \rightarrow R - t_{\text{ESL}}$). This gives rise to the corresponding local shear stress, τ_{wall} , given by the product of γ_{wall} times η_{plasma} .

The resulting viscosity profile (Fig. 16, lower left panel) then allows calculation of various flow parameters, including axial pressure gradient (dp/dz), volumetric flow rate (dQ/dt), relative apparent viscosity ($\eta_{\text{app rel}}$), and the H_T/H_D -ratio (Fig. 16, lower right panel).

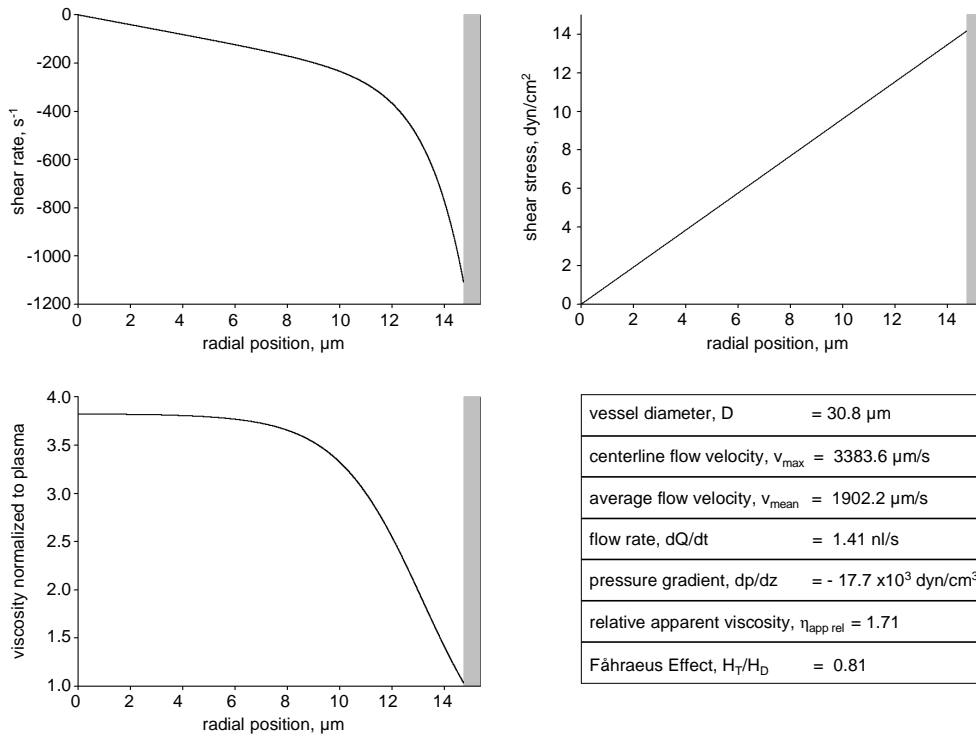


Figure 16. Exemplary illustration of the data output arising from the microviscometric analysis of the monotonically filtered μ -PIV data shown in Fig. 15. The shaded area on the right-hand ordinate of each plot corresponds to the vessel-specific estimate in ESL thickness, t_{ESL} (see Fig. 17).

The microviscometric concept is based on the following assumptions:

- Blood, albeit of particulate nature, is modeled as a continuous fluid with a spatially non-uniform viscosity when flowing through tubes or vessels [34].
- Blood is treated as a Newtonian fluid in so far as local viscosity only depends on the local hematocrit but not on variations in shear rate, provided the latter exceeds 50 s^{-1} . In other words, local viscosity is assumed to be a smooth monotonic function of local hematocrit, while variations in blood viscosity with shear rate at fixed hematocrit are assumed to be negligibly small [28].
- Conservation principles of mass and momentum have to be satisfied.
- Flow has to be steady, laminar and axisymmetric.

Hence, a fluid of radially constant viscosity (Newtonian fluid) generates a parabolic velocity profile, while any deviation from the parabolic velocity profile across the vessel lumen reflects a change in viscosity. This change is interpreted as a radial change in hematocrit.

Evidence of the accuracy of the microviscometric analysis and thus, support of the validity of the continuum approximation have been provided by *in vitro* experiments employing glass tubes (50–80 μm in diameter) perfused by human red cell suspensions (0.00–0.55, range of H_D) [96]. In these experiments, both the empirically estimated relative apparent viscosity, $\eta_{\text{app rel}}$, and the directly measured axial pressure drop, dp/dz , were compared with corresponding values predicted by applying the analytical model. Respective data exhibit remarkable agreement between predicted and measured values, as indicated by the correlation coefficients, r , of 0.80 and 0.84 for $\eta_{\text{app rel}}$ and dp/dz , respectively. Also, Cokelet has found support for the continuum approximation for tube/vessel diameters exceeding 20 μm [34].

2.12. Estimation of ESL thickness

As for the estimation of the hydrodynamically effective thickness of the ESL, t_{ESL} , some additional assumptions are introduced into the model:

- Red cells and fluorescent flow tracers cannot invade or penetrate the layer;
- The ESL is treated as a uniform porous layer in which fluid flow is modeled as flow in a Brinkman medium;
- The layer may allow only limited or no axial flow, depending on the assumed hydraulic permeability, which is the reciprocal of the hydraulic resistivity, K ;
- Shear stress is assumed to be continuously distributed across the ESL.

The estimate in ESL thickness is generally obtained by minimizing the least-squares error in the fit to the filtered μ -PIV data for all possible choices of α , with $\alpha = r_{\text{ESL}} / R$ (Fig. 17). The value r_{ESL} corresponds to the chosen radial position of the ESL interface, i.e. $r_{\text{ESL}} = R - t_{\text{ESL}}$.

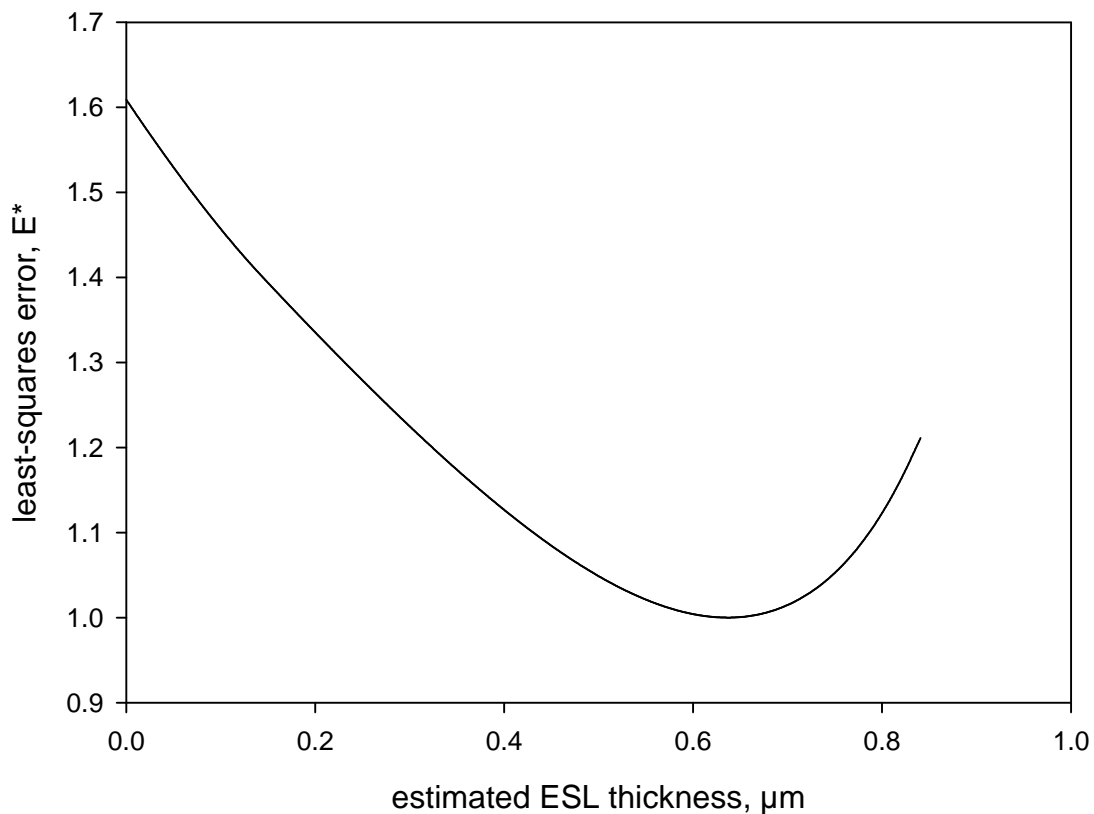


Figure 17. Curve obtained by an iterative procedure, which minimizes the least-squares error, E^* , in the fit to the μ -PIV data set shown in Fig. 15. The local minimum of the curve is regarded as the best estimation of the actual thickness of the ESL.

As a preliminary step of the estimation of ESL thickness, the near-wall course of the velocity profile is slightly modified to take the possible influence of flowing microspheres on near-wall fluid flow into consideration [164]. For this purpose, an analytical approach of Damiano *et al.* [38] is used to convert the translational speed of a near-wall microsphere (black dot) into the speed a fluid particle (plus symbol) would be likely to have at the same radial position in the absence of the microsphere (Fig. 18, upper left panel).

The velocity profile is then refitted to the corrected velocity data (solid line) and extrapolated (dotted line) to $r^* = 0$, corresponding to $r = R$. If the resulting velocity fit intersects the ordinate at zero velocity (Fig. 18, upper left panel), the vessel in question is assumed to lack any ESL. Under physiological conditions, however, the fitted line typically exhibits a negative intercept with the ordinate and a positive intercept with the abscissa (Fig. 18, upper right panel). The latter ($r = 0.58 \mu\text{m}$) is regarded as the best approximation to the actual ESL thickness, if - as is the case in the present study - the following assumptions are applied to the near-wall fluid flow:

- no-slip conditions, viz. vanishing blood flow at the ESL – vessel lumen interface
- no axial fluid flow through the layer, viz. infinite hydraulic resistivity ($K \rightarrow \infty$).

In contrast, assumption of pseudo-slip conditions (Fig. 18, lower left panel), which allows fluid flow right next to the luminal ESL surface, would result in a slightly higher estimate of t_{ESL} ($0.64 \mu\text{m}$). In addition, variation in the assumed hydraulic resistivity, K , within the ESL also affects the estimated t_{ESL} . In the case of finite hydraulic resistivity, e.g. $K = 10^9 \text{ dyns/cm}^4$, the resulting velocity profile within the ESL would adopt an exponential rather than a linear shape (Fig. 18, lower right panel), thereby leading to a higher estimate of t_{ESL} ($0.70 \mu\text{m}$) relative to that found for infinite K .

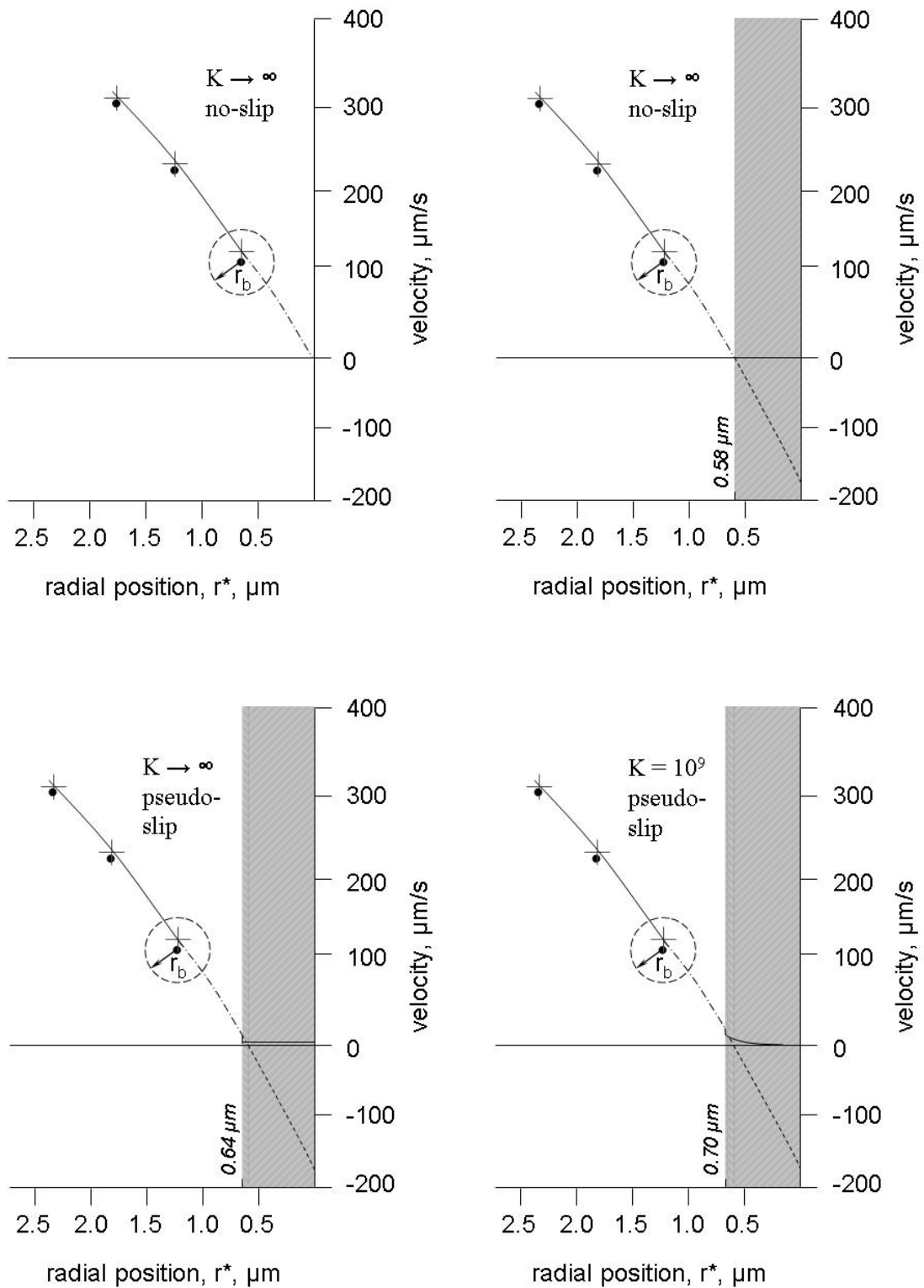


Figure 18. Schematic illustration of near-wall μ -PIV data and of the corresponding best velocity fit for different flow conditions, i.e. no-slip or pseudo-slip conditions, and finite or infinite hydraulic resistivity, K (dyns/cm^4). The shaded grey bands along the velocity axis denote the resulting estimates of ESL thickness. r_b , radius of a microsphere; + symbol, corresponding fluid particle.

2.13. Hemodynamic flow model

A hemodynamic flow simulation for an experimental vascular network in the rat mesentery with 546 vessel segments was used to calculate overall flow resistance and changes in the resistance with changing hematocrit and ESL thickness [121]. For the vessel lumen available for free fluid flow ($D - 2 \cdot t_{\text{ESL}}$), a parametric description of apparent viscosity, η_{app} , as a function of diameter and hematocrit ('*in vitro* viscosity law') was used [123]:

$$\eta_{\text{vitro}} = 1 + (\eta_{0.45} - 1) \cdot \frac{(1 - H_D)^C - 1}{(1 - 0.45)^C - 1}$$

where $\eta_{0.45}$ is the apparent viscosity for a discharge hematocrit of 0.45, and is given by:

$$\eta_{0.45} = 220 \cdot e^{-1.3D} + 3.2 - 2.44 \cdot e^{-0.06D^{0.645}}$$

The 'C' superscript is a parameter describing the dependence of apparent viscosity on discharge hematocrit in terms of the curvature of the resulting $\eta_{\text{rel}} - H_D$ - plot (Fig. 1), and is given by:

$$C = (0.8 + e^{-0.075D}) \cdot \left(-1 + \frac{1}{1 + 10^{-11} \cdot D^{12}} \right) + \frac{1}{1 + 10^{-11} \cdot D^{12}}$$

The ESL is modeled as an impermeable layer that restricts both blood and plasma flow, corresponding to infinite hydraulic resistivity. This corresponds to the concept advanced by Pries *et al.* [132], with the difference that a fixed ESL thickness was used for all vessels of the network. The assumed thickness of the ESL corresponds to that obtained from analysis of the velocity profiles (see 2.12.), and represents the group-specific average value. All resistance data was normalized with respect to the flow resistance obtained with a feed hematocrit of 0.46 (i.e. the hematocrit of the boundary vessels of the network), an ESL thickness of 0.5 μm , a mean corpuscular volume of 45 fl, and normal cell flexibility, corresponding to spontaneous conditions in wt mice.

2.14. Statistical analysis

For descriptive statistical analysis, SigmaPlot 8.0 software (Jandel, San Rafael, CA) was used. Box-whisker plots separate the data into quartiles, with the top of the box defining the 3rd quartile, the line within the box giving the median, and the bottom of the box showing the 1st quartile. The upper whisker defines the 95th percentile and the lower whisker the 5th percentile. Bar charts and tabular results represent mean values \pm SEM, except where otherwise noted.

SigmaStat 2.0 software (Jandel, San Rafael, CA) was utilized for deductive statistical analysis. A difference between two groups with respect to the tested parameter was considered significant at a level of $p < 0.05$, usually determined via Student's t-test. Non-parametric Mann-Whitney U-test was employed only if data was not normally distributed.

The level of significance is indicated in the figures by the number of asterisks as follows:

n.s.	$p \geq 0.05$
*	$p < 0.05$
**	$p \leq 0.01$
***	$p \leq 0.001$

2.15. Error sources

The estimates for micro-rheological parameters obtained by the μ -PIV approach in microvessels depend on the validity of the underlying assumptions and the deviations hereupon in the *in-vivo* setting. The most relevant factor *in vivo*, which could influence the flow profiles and thus the obtained results, is the non-standard geometry of microvessels as compared to the straight and circular shape assumed for the analytical approach. In an attempt to limit the respective problems, only relatively straight sections of venules with minimal visible irregularities of the wall were selected for experimental investigation. The remaining irregularities in vascular geometry and resulting *in-vivo* flow profiles will contribute to the overall amount of measurement variance. In the absence of precise

knowledge on their magnitude and due to the lack of a corresponding analytical theory, it is, however, not possible to quantify this effect.

Another assumption of the microviscometric approach is that the blood flow is axisymmetric and laminar. In order to minimize any deviation from these conditions, a distance to the next branch point of at least 5 vessel diameters to the site of measurement was maintained. Deviations from the assumed flow regimen will contribute to the variance in the measurement and thus to the standard deviation in the results.

As for the viscosity – hematocrit relations, the microviscometric analysis employed in the present study is based on comprehensive bulk viscosity data obtained by Chien et al. [28]. For their measurements, Chien and colleagues used red cell suspensions of human blood. It is well-known that the biophysical and rheological properties of human RBCs deviate from those of mice. Even among different mouse strains (e.g. C57 and tg6), there seem to exist differences in these properties, possibly affecting the behavior of microvascular blood flow. As long as strain-specific viscosity values for the mouse are not available, predictions of discharge hematocrit, H_D , and tube hematocrit, H_T , obtained from the viscosity profile (Fig. 16, lower left panel) may incur respective errors [96]. For that reason, the present study only addresses the ratio, H_T/H_D , where most of the involved errors cancel out.

The hydraulic resistivity, K , of the endothelial surface layer [59] is a measure for the retardation of plasma flow through the ESL. The estimates for the luminal edge of the ESL from near-wall velocity profiles are affected by the assumed hydraulic resistivity, such that smaller values of K lead to higher estimates in the layer thickness, and vice versa. However, Damiano et al. [39] have shown no significant sensitivity in the estimates for layer thickness on K over the range of values considered ($\infty > K > 10^9$ dyn s/cm⁴).

As for the precision of the estimates of layer thickness, Damiano et al. [39] repeatedly analyzed different vessels and found a standard error of ± 0.026 μm for layer thickness of 0.5 μm and a standard error of ± 0.017 μm for layer thickness of 0.2 μm . This implies not only all randomized, methodological errors, but also the biological variation between different vessels. Thus, it can be assumed that the absolute methodological error is below the level of respective layer thickness.

3. Results

3.1. Systemic hemodynamic parameters

3.1.1. Hematocrit

group	systemic hematocrit
epo _{0.85}	0.85 ± 0.01
epo _{0.50}	0.50 ± 0.05
epo _{H0.46}	0.46 ± 0.05
epo _{p0.53}	0.53 ± 0.02
wt _{0.46}	0.46 ± 0.02
wt _{0.27}	0.27 ± 0.04
wt _{H0.30}	0.30 ± 0.03
wt _{p0.24}	0.24 ± 0.01

Table 1. Systemic hematocrit in epo mice and wild-type mice before and after isovolemic hemodilution; values denote means ± SD.

Systemic hematocrit (Hct), expressed hereafter as a decimal fraction, declined in epo mice upon isovolemic hemodilution (HD) with HES or plasma from 0.85 to 0.46 (epo_{H0.46}) and 0.53 (epo_{p0.53}), respectively, thereby approaching baseline Hct of C57 wild-type (wt) control mice (0.46). In wt mice, HD resulted in a reduction in Hct to 0.30 (wt_{H0.30}) and 0.24 (wt_{p0.24}), respectively, corresponding to a mean Hct of 0.27 and a relative decrease of 41% (Tab. 1). Statistically significant on a $p < 0.001$ level were the differences in systemic hematocrit between the epo_{0.85} group and the corresponding HD groups, as were the differences between the wt_{0.46} group and the corresponding HD groups, and between the HD groups themselves within a given mouse strain, i.e. epo_{H0.46} vs. epo_{p0.53}, and wt_{H0.30} vs. wt_{p0.24}.

3.1.2. Mean arterial pressure and heart rate

During the course of the experiment, both epo mice and wt mice showed an overall drop in mean arterial pressure (MAP), which was slightly more pronounced in epo mice ($p < 0.001$) than in wt mice ($p < 0.05$). In epo mice, the main portion of pressure drop occurred upon hemodilution ($p < 0.01$), while a rather continuous decline of MAP was observed in wt mice. In the latter, hemodilution did not lead to a significant drop of pressure (Fig. 19, upper panel).

In contrast, heart rate (HR) remained almost constant prior to HD in both mouse groups but displayed an increase after HD which was stronger in the epo group ($p < 0.001$) than in the wt group ($p < 0.05$) (Fig. 19, lower panel). It appears likely that the increase in HR compensates for the decreased MAP in order to sustain cardiac output.

The relative changes in MAP and HR in epo mice upon hemodilution are consistent with the findings made by Frietsch *et al.* [55] for a similar hematocrit reduction. However, absolute values in HR of epo mice and wt mice are relatively low as compared to pertinent literature data [141,145]. This might be due to the well-known depressant cardiovascular effect of the anesthetic agents employed [89].

At any period of the experiment (P1 - P4), MAP in epo mice was statistically not different from that in wt mice. This is consistent with the findings of previous studies [141,190,191]. Likewise, HR did not differ significantly between the two mouse strains with regard to P1 and P2. During intravital microscopy (P3 and P4), however, HR was significantly higher in epo mice than in wt mice (P3, $p < 0.01$ and P4, $p < 0.001$).

Results

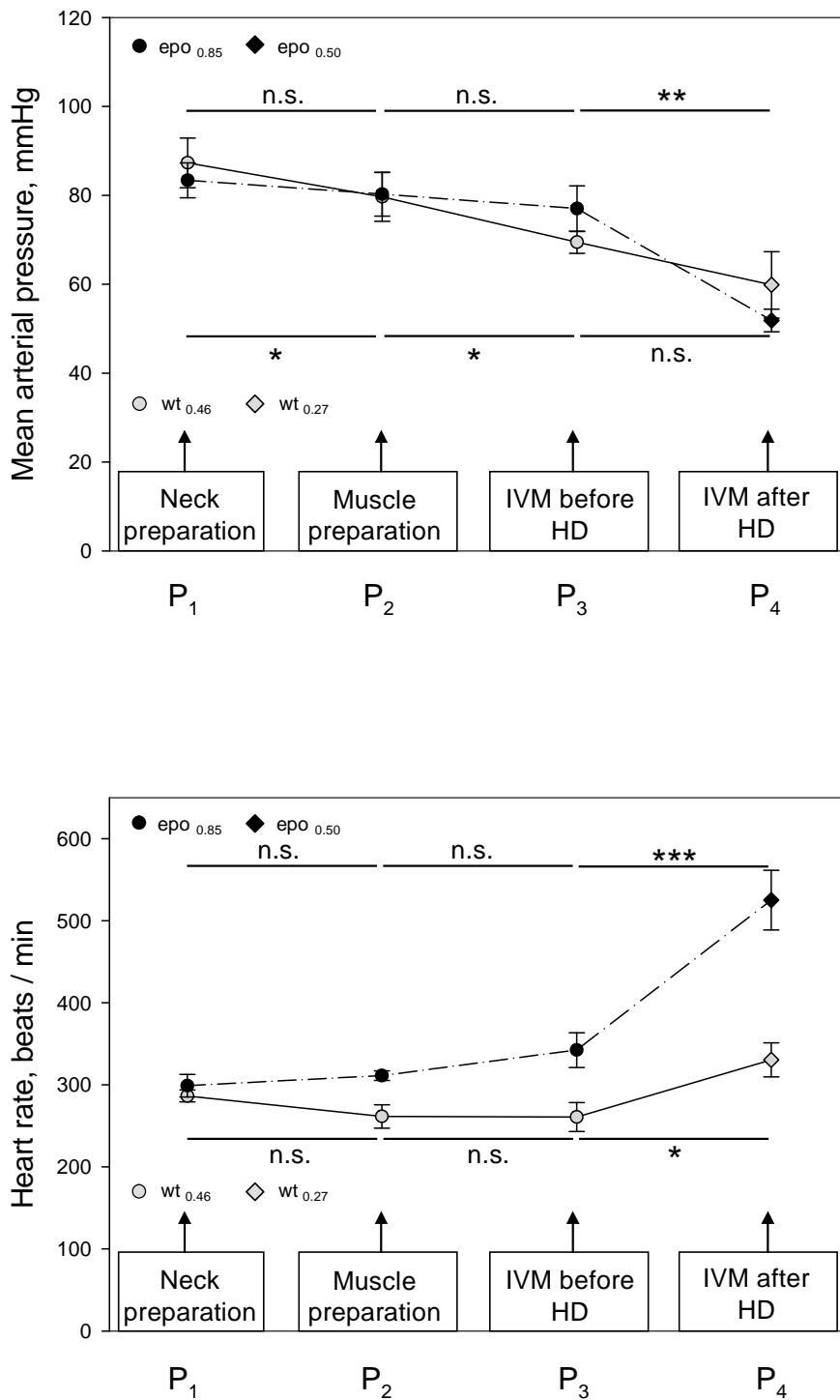


Figure 19. Upper panel: Course of mean arterial pressure in epo mice (dark) and wt mice (light grey) expressed as mean \pm SEM of the respective experimental period (P) with P₁ corresponding to the neck preparation, P₂ to the cremaster muscle preparation, P₃ to intravital microscopy (IVM) before hemodilution (HD), and P₄ corresponding to IVM after HD. Differences were tested for significance using paired t-test (P₁ vs P₂ and P₂ vs. P₃) or t-test (P₃ vs. P₄). Upper and lower bars correspond to dark and light grey symbols, respectively.

Lower panel: Course of heart rate in epo mice (dark) and wt mice (light grey). Differences were tested for significance using paired t-test (P₁ vs. P₂ and P₂ vs. P₃) and unpaired t-test (P₃ vs. P₄), respectively.

3.2. Microrheological parameters

3.2.1. Blood flow velocity

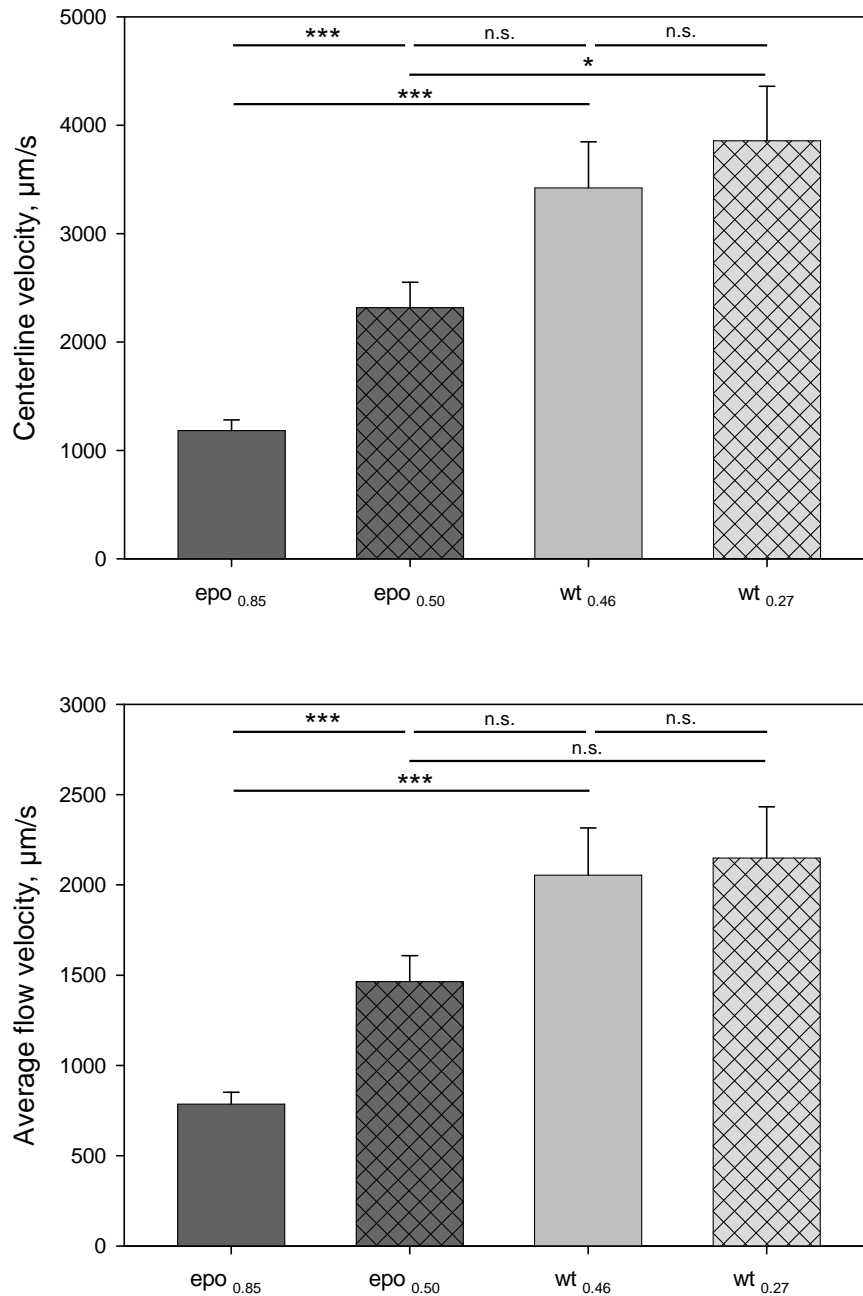


Figure 20. Centerline velocity (upper panel) and average flow velocity (lower panel) in both epo mice (dark grey) and wt mice (light grey) before and after isovolemic hemodilution. Differences were tested for significance using paired t-test or Mann-Whitney U-test for paired and unpaired data samples, respectively.

At baseline, centerline flow velocity (v_{\max}) was significantly lower in epo mice (epo_{0.85}) than in wt mice ($p < 0.001$, Mann-Whitney U-test). Upon HD of epo mice, v_{\max} increased by 96% ($p < 0.001$, paired t-test), thereby approaching baseline level of wt mice. In contrast, wt mice only showed a slight, insignificant increase in v_{\max} after HD (Fig. 20, upper panel).

Similar to v_{\max} , average flow velocity (v_{mean}) in epo mice was nearly 3-fold lower than in wt mice ($p < 0.001$), and almost doubled after hemodilution ($p < 0.001$). In contrast to epo mice, HD of wt mice only led to a marginal rise of v_{mean} ($p > 0.05$) (Fig. 20, lower panel). Significant correlation between v_{mean} and vessel diameter was only found in wt mice, with a coefficient of determination, r^2 , of 0.181 and 0.110 in the wt_{0.46} and wt_{0.27} group, respectively (data not shown).

3.2.2. Flow rate

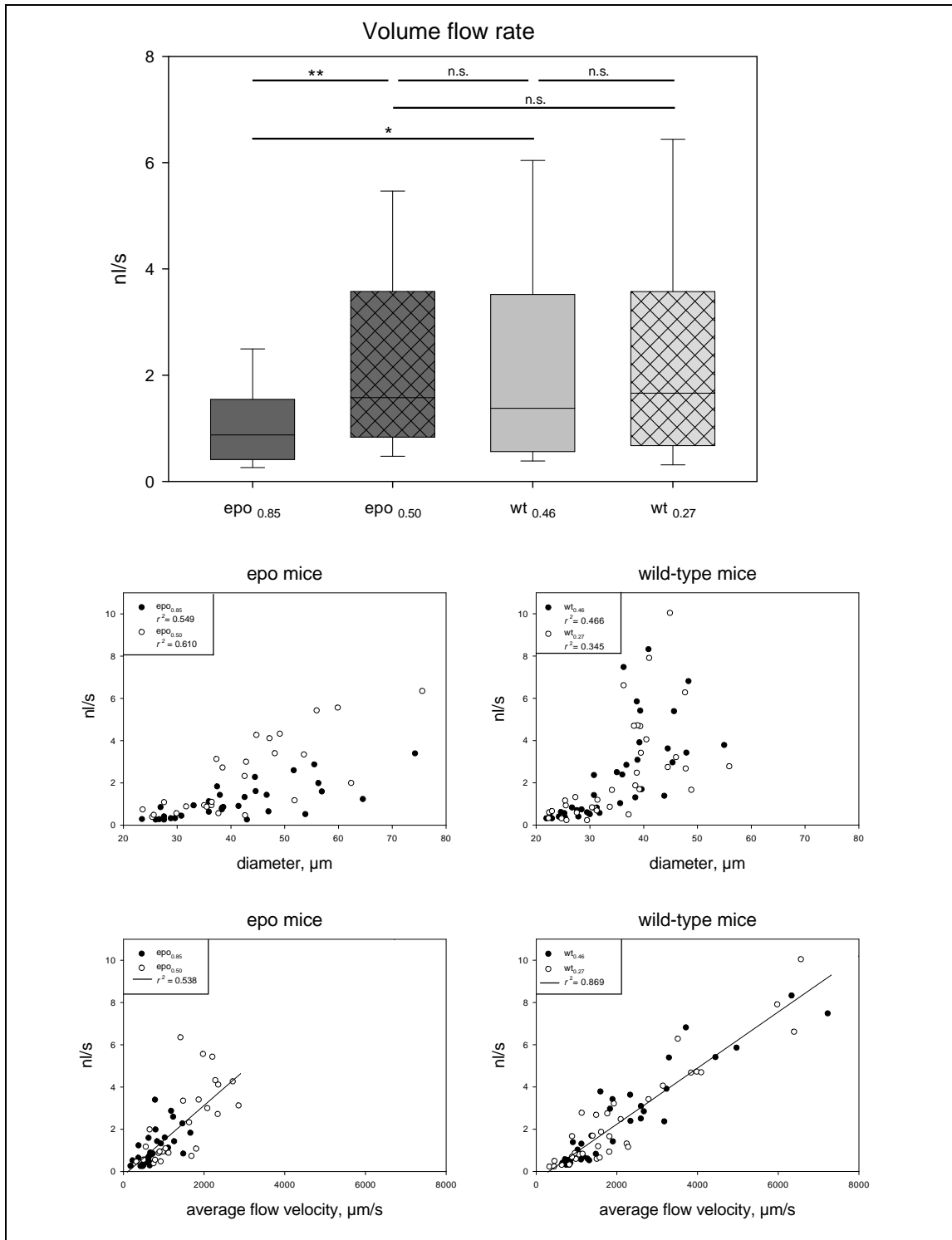


Figure 21. Upper panel: Volume flow rate in epo mice (dark grey) and wt mice (bright grey) before and after hemodilution. Differences were tested for significance using Wilcoxon Signed Rank test or Mann-Whitney U-test for paired and unpaired data samples, respectively.

Mid/Lower panels: Volume flow rate as a function of vessel diameter (mid panels) and average flow velocity (lower panels) in epo mice (left panels) and wt mice (right panels). r^2 , coefficient of determination

Volume flow rate (dQ/dt), which is a function of v_{mean} times vessel diameter, was significantly lower in epo mice than in wt mice with regard to baseline conditions ($p < 0.05$) (Fig. 21). Hemodilution led to a 90%-increase in dQ/dt in epo mice ($p < 0.01$). Post-hemodilution values in epo mice were thus very similar to baseline levels of their wt counterparts ($p > 0.05$). In contrast, no significant increase in dQ/dt was observed in wt mice after hemodilution (Fig. 22).

As expected, dQ/dt did show significant correlation with vessel diameter on the one hand, and with v_{mean} on the other hand (Fig. 21, middle and lower panels). Linear regression analysis of the v_{mean} - dQ/dt plot (Fig. 21, lower panels) revealed a slightly steeper regression line in the epo group than in the wt group which may be attributed to the, on average, slightly larger vessel diameter in the former group ($p < 0.05$) (Tab. 2).

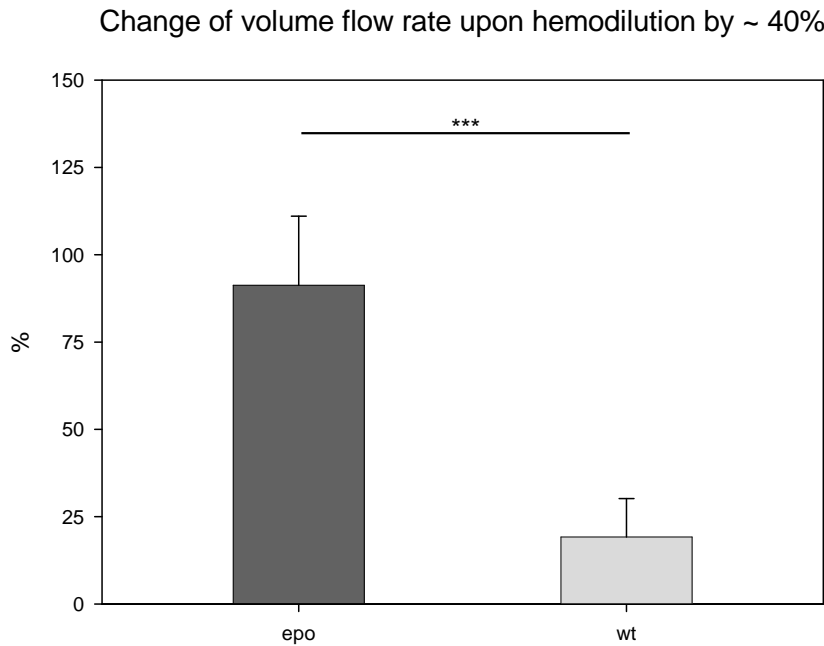


Figure 22. %-Change of volume flow rate in epo mice (dark grey) and wt mice (bright grey) upon hemodilution; columns denote mean \pm SEM; difference was tested for significance using Mann-Whitney U-test.

group	vessel diameter, μm
epo 0.85	40.7 ± 12.2
epo 0.50	42.2 ± 12.6
epo H0.46	47.6 ± 14.4
epo p0.53	38.8 ± 10.4
wt 0.46	34.5 ± 8.3
wt 0.27	35.5 ± 8.6
wt H0.30	36.2 ± 8.5
wt p0.24	35.0 ± 9.0

Table 2. Vessel diameter of the different experimental groups; values denote means \pm SD.

3.2.3. Velocity profiles

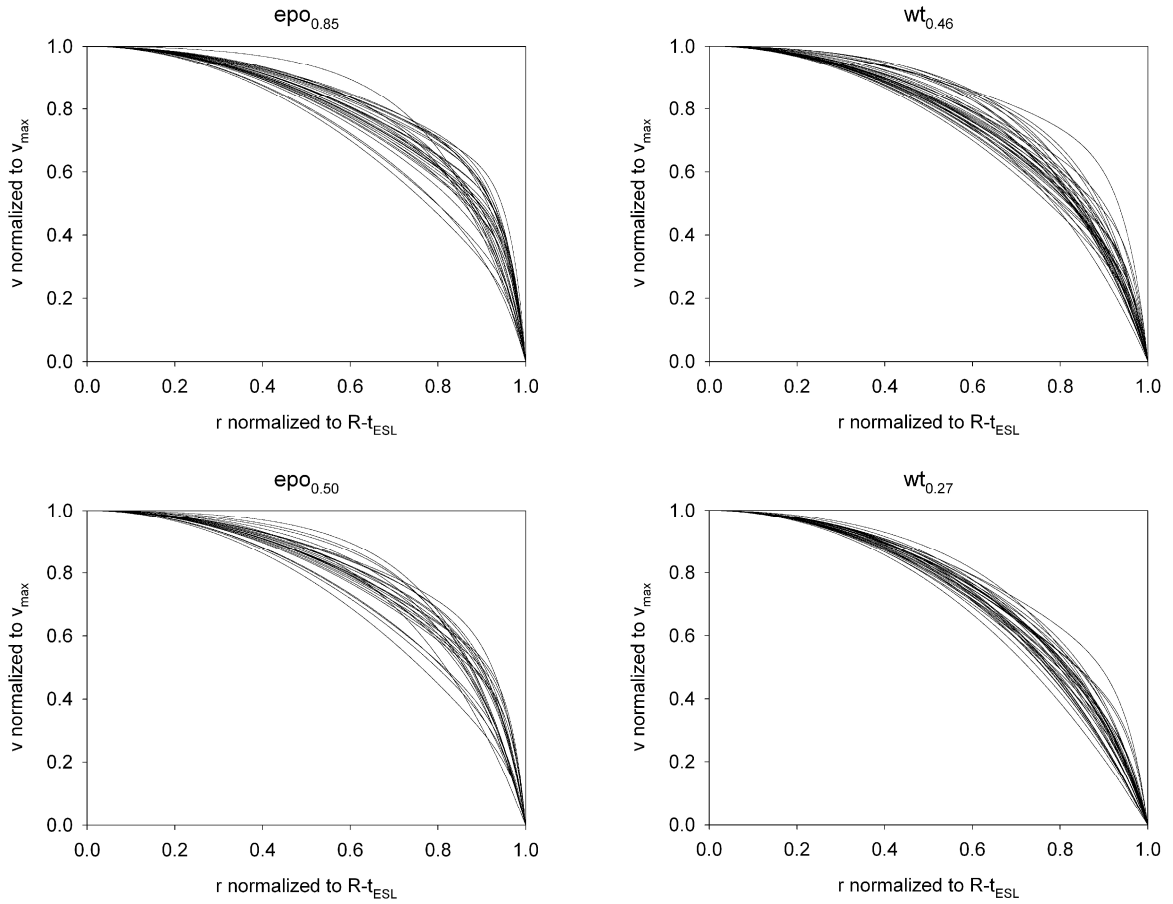


Figure 23. Assembly of all velocity profiles of each group. All data is normalized to the centerline velocity (v_{\max}) and $r = R - t_{\text{ESL}}$, respectively.

In order to assess and to compare the velocity profiles with respect to their shape, each profile was normalized to its centerline velocity (v_{\max}) and to the radial position, equal to the respective vessel radius minus ESL thickness ($r = R - t_{\text{ESL}}$). Each plot in figure 23 accommodates all those profiles belonging to one of the four groups, viz. $\text{epo}_{0.85}$, $\text{epo}_{0.50}$, $\text{wt}_{0.46}$, and $\text{wt}_{0.27}$. It reveals the apparent tendency towards increasingly parabolic-shaped profiles with decreasing level of systemic hematocrit.

Division of v_{\max} by v_{mean} yields an index that allows quantitative assessment of these profiles with respect to their shape or, more precisely, to their degree of bluntness. Figure 24 confirms the visual impression of figure 23: The $\text{epo}_{0.85}$ group is characterized by the lowest velocity ratio corresponding to highest degree of bluntness, while groups with gradually lower Hct exhibit progressively higher v_{\max}/v_{mean} ratios. Somewhat surprisingly, a significant difference in v_{\max}/v_{mean} ratio remains between $\text{epo}_{0.50}$ and $\text{wt}_{0.46}$, despite similar Hct. This discrepancy might be due to the significantly lower mean shear rate in the former

group (Fig. 26), an assumption which is supported by *in vitro* findings [136]. Interestingly, epo mice reached significantly higher ratios when hemodiluted with HES instead of plasma ($p < 0.05$, Tab. 3) which may be attributed to the higher target hematocrit in the latter and/or to differences in the hemodynamic effects of these fluids themselves.

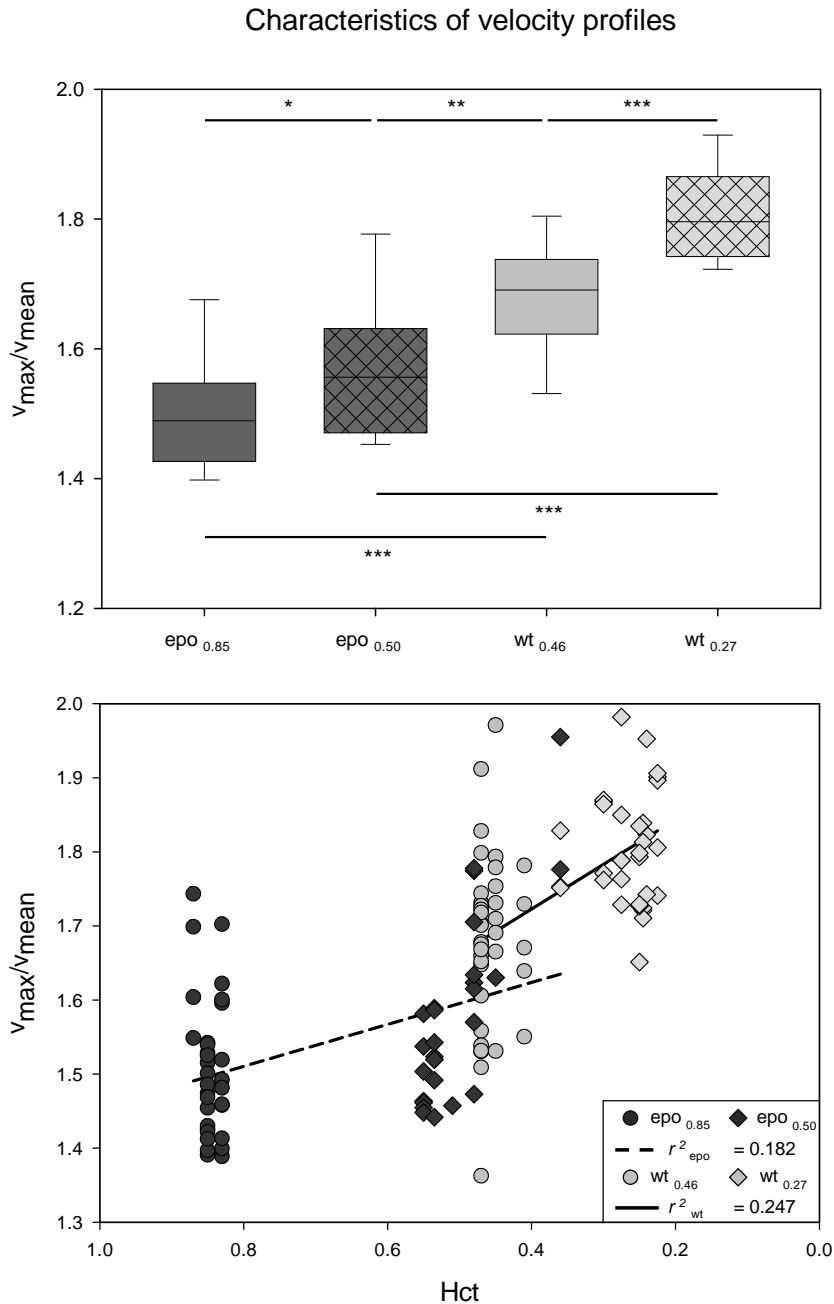


Figure 24. Upper panel: Box-plot showing the ratio of centerline and average flow velocity (v_{max}/v_{mean}), which is a measure of the degree of bluntness of the velocity profiles, illustrated on Fig. 17. Differences were tested for significance using t-test.

Lower panel: Dependence of v_{max}/v_{mean} ratio on systemic hematocrit, Hct, in epo mice (dark) and wt mice (light grey) both before (circles) and after hemodilution (rhombs). Note, the abscissa is scaled inversely. r^2 , coefficient of determination.

Results

group	v_{\max}/v_{mean}
epo _{0.85}	1.51 ± 0.09
epo _{0.50}	1.58 ± 0.13
epo _{H0.46}	1.65 ± 0.15
epo _{p0.53}	1.54 ± 0.09
wt _{0.46}	1.68 ± 0.12
wt _{0.27}	1.81 ± 0.09
wt _{H0.30}	1.83 ± 0.09
wt _{p0.24}	1.80 ± 0.08

Table 3. Ratio v_{\max}/v_{mean} in epo mice and wt mice before and after isovolemic hemodilution; values denote means \pm SD.

Vertical straggling of data points (Fig. 24, lower panel) and profiles (Fig. 23) can partly be explained by the different agents used for hemodilution in epo mice (Tab. 3), and by the estimated ESL thickness (Fig 25, lower panel). Multivariate regression analysis, applied to all groups as a whole, revealed that a combination of systemic hematocrit (given as a decimal fraction) and ESL thickness (given in μm) does predict v_{\max}/v_{mean} most accurately ($r^2 = 0.568$):

$$v_{\max}/v_{\text{mean}} = 1.788 + (0.153 \cdot \text{ESL}[\mu\text{m}]) - (0.392 \cdot \text{Hct})$$

The present v_{\max}/v_{mean} ratios or bluntness factors are on average higher than the values reported by Tangelder *et al.* [177] for a similar Hct: They obtained a median value of ~ 1.5 for blood flow in rabbit mesenteric arterioles (D, 18-32 μm) at a Hct level of 0.45. To a major part, this discrepancy may be due to the difference in the velocity fitting procedure. In Tangelder's approach, for instance, the curves were not forced to intersect the vessel wall ($r = 1$) at zero velocity, but rather displayed a positive intercept, corresponding to pseudo-slip conditions. In addition, Tangelder used dye-labeled platelets (mean diameter $\sim 1\mu\text{m}$) to trace the blood flow, which may provide a lower resolution of the near-wall velocity distribution.

Results

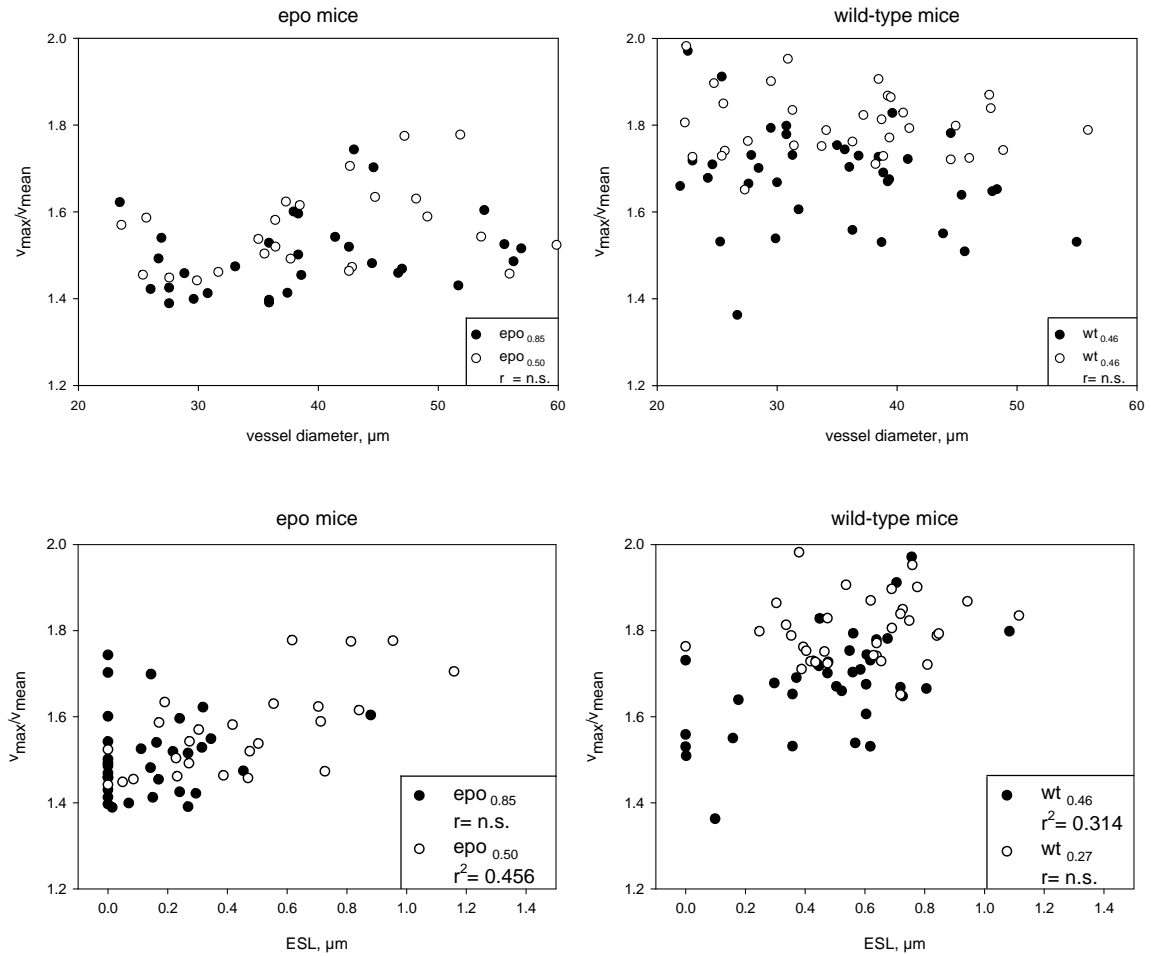


Figure 25. Upper panels: Dependence of the ratio v_{\max}/v_{mean} on the corresponding vessel diameter in epo mice (left panel) and wt mice (right panel) both before (closed circles) and after (open circles) hemodilution; coefficient of correlation was not significant in any group as far as only data points corresponding to $\leq 60\mu\text{m}$ -diameter vessels were considered.

Lower panels: Dependence of the ratio v_{\max}/v_{mean} on the width of the ESL; significant correlation was found for the $\text{epo}_{0.50}$ group and $\text{wt}_{0.46}$ group; r^2 , coefficient of determination.

3.2.4. Shear rate and shear stress

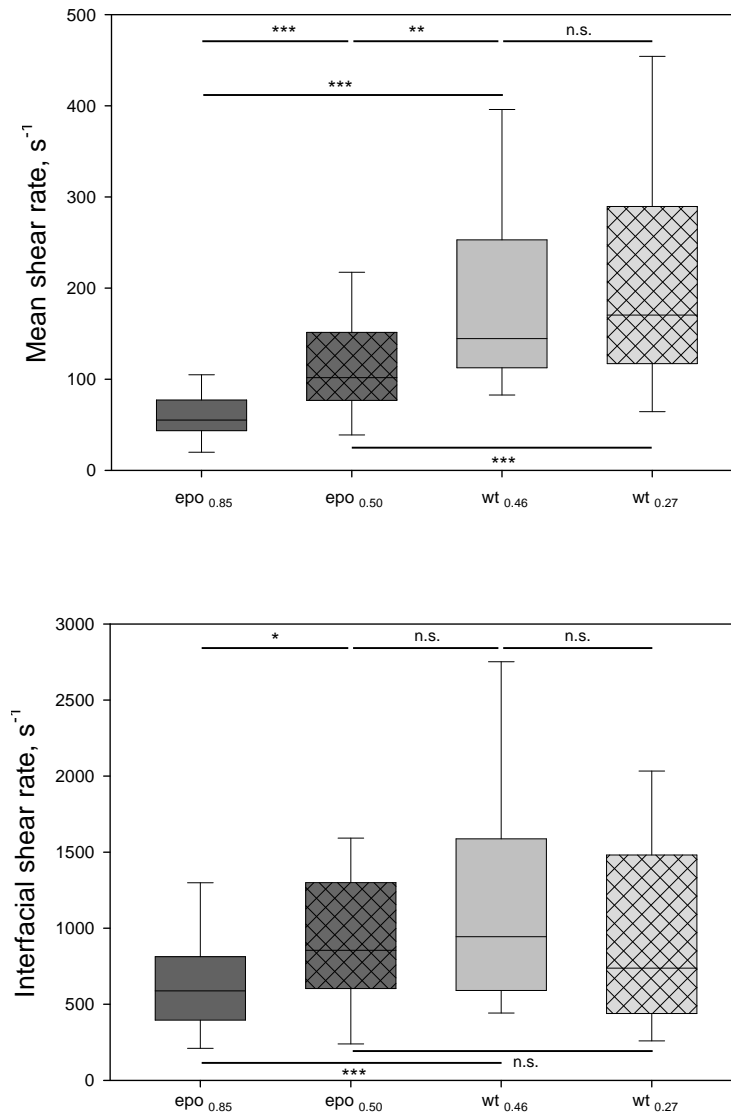


Figure 26. Upper panel: Mean shear rate (i.e. shear rate averaged over the vessel cross-section) in epo mice and wt mice before and after hemodilution.

Lower panel: Interfacial shear rate (, i.e. the shear rate at the luminal aspect of the ESL) in epo mice and wt mice before and after hemodilution obtained by extrapolating the radial shear rate profile to the luminal ESL surface($r=R-t_{ESL}$).

Consistent with the findings on average flow velocity (Fig. 20), the mean shear rate continuously increased with decreasing systemic hematocrit in terms of the group-specific mean (Fig. 26, lower panel).

In contrast, shear rates prevailing at the luminal surface of the vessel wall ($r = R-t_{ESL}$), hereafter referred to as interfacial shear rate, exhibited relatively small inter-group

differences, indicating the tendency to keep this hemodynamic parameter constant over a large range of hematocrit (Fig. 26, upper panel). Interfacial shear rates in wt mice (mean \pm SEM, $1226 \pm 130 \text{ s}^{-1}$) exhibited remarkable consistency with those found by Damiano *et al.* [39] ($1237 \pm 158 \text{ s}^{-1}$) for the same mouse strain. No significant differences in interfacial shear rate were detected between the HES group and the plasma group in either the epo or the wt mice.

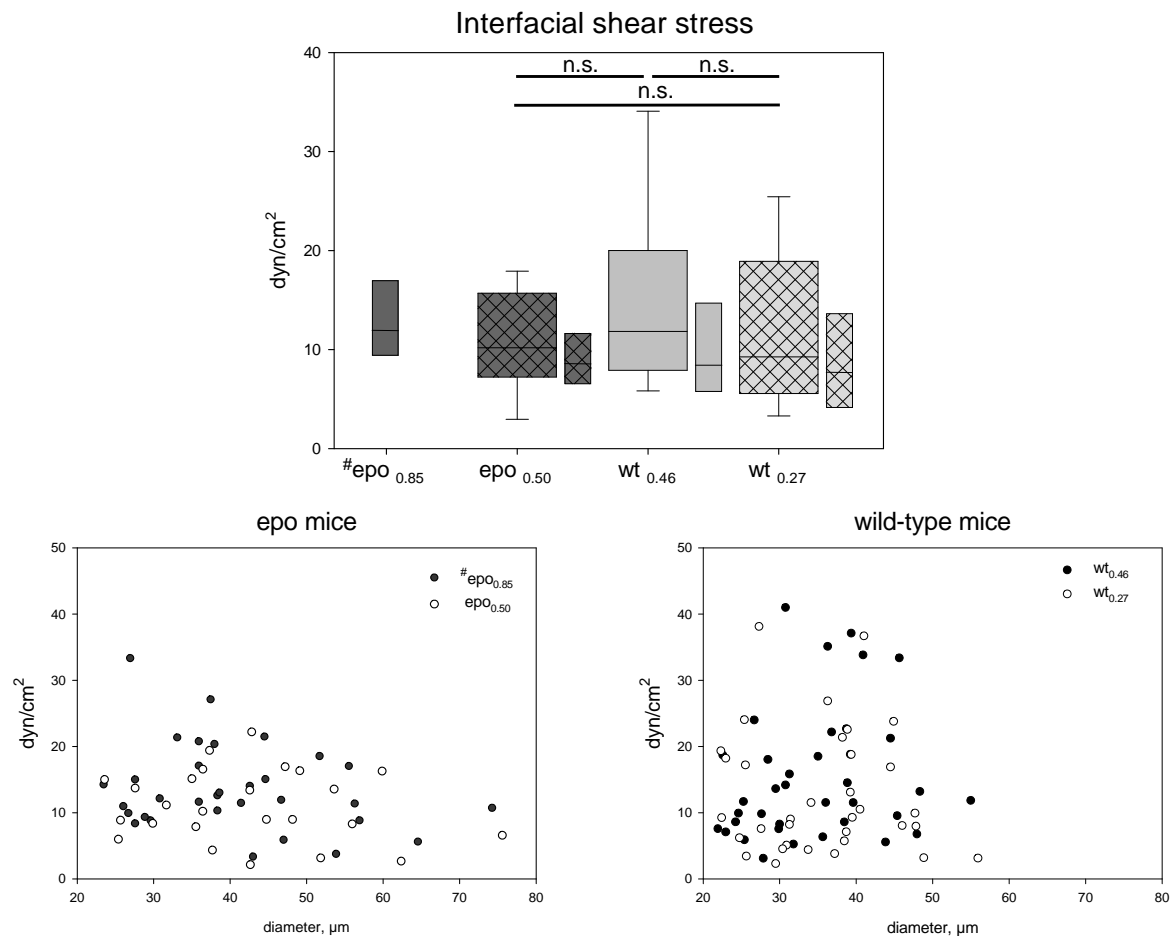


Figure 27. Upper panel: Interfacial shear stress, $\tau(R- t_{ESL})$, in epo mice (dark grey) and wt-mice (light grey), before and after hemodilution. Large boxes denote experimental values, while small ones represent theoretical reference values according to Sharan *et al.* [154]. Experimental data of the epo_{0.85} group is not shown; instead, the estimated shear stress ($\#epo_{0.85}$) is presented. Lower panels: $\tau(R- t_{ESL})$ plotted against vessel diameter for epo mice (left panel) and wt mice (right panel) both before (closed symbols) and after hemodilution (open symbols). Baseline data of epo mice ($\#epo_{0.85}$) is calculated according to Sharan [154].

Interfacial shear stress, i.e. the shear stress present at the inner vessel surface ($r=R- t_{ESL}$), was neither significantly different between epo_{0.50} group and any wt group, nor between the wt groups. Thus, the animals seem to preserve interfacial shear stress levels over a substantial range of hematocrit. When compared to the range of baseline data in wt mice (3

- 40 dyn/cm²), respective post-hemodilution values in epo mice are distributed over a smaller range with an apparent upper limit of ~22 dyn/cm² (Fig 27, lower panels). No significant differences in interfacial shear stress were detected between the HES and the plasma group in both epo mice and wt mice, respectively.

For comparison, theoretical reference values of wall shear stress, τ_R , are represented by the small boxes within Fig. 27. For calculation of these data, an equation presented by Sharan *et al.* [154] is used. The respective approach models red cell suspensions perfusing a microvessel as a two-phase fluid, and assumes parabolic velocity profiles.

$$\tau_R = \frac{4 \eta_{rel\ app} \cdot v_{mean} [\mu m / s]}{0.5 \cdot D [\mu m]}$$

For each vessel, experimental data ($\eta_{rel\ app}$, v_{mean} , D) of the present study is used as input for the above equation. Baseline values of $\eta_{rel\ app}$ in epo mice, which could not be determined with the present analytical approach, are obtained from the *in vitro* viscosity law (Fig. 28) [124].

As illustrated in figure 27 (upper panel), the resulting wall shear stress is essentially lower than the corresponding experimental data. However, relative inter-group differences in τ_R are similar to those between the experimentally obtained interfacial shear stress. With respect to the epo_{0.85} group, the above equation predicts only a mild increase in τ_R , which is attributable to the low average flow velocity and the, on average, slightly larger vessel diameter. These two parameters (v_{mean} , D) nearly offset the approximately 3.5-fold higher apparent viscosity as predicted by *in vitro* viscosity law (Fig. 28) [124]. In the epo_{0.85} group, interfacial shear stress could not be determined with the present microviscometric approach, since local viscosity of the near-wall fluid layers cannot be assumed to equal plasma viscosity at a systemic hematocrit of ~0.85, as usually done for moderate or low levels of systemic hematocrit.

3.2.5. Relative apparent viscosity

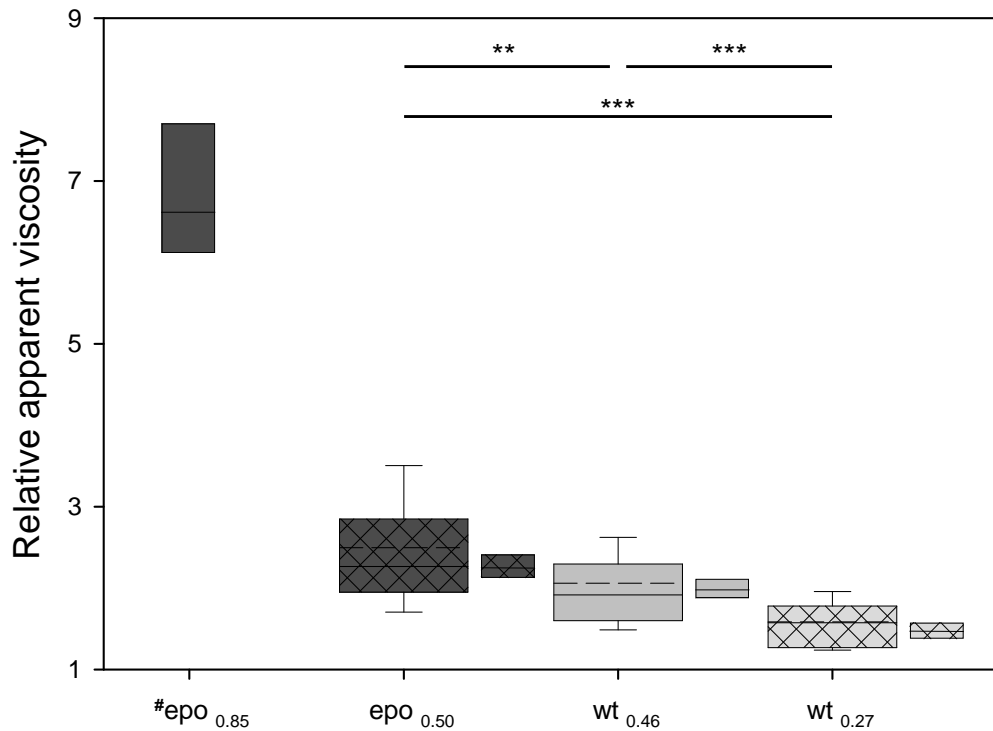


Figure 28. Relative apparent viscosity in epo mice (dark grey) and wt mice (bright grey), both before and after hemodilution. Differences were tested for significance using Wilcoxon Signed Rank Test and Mann-Whitney U-test for paired and unpaired data samples, respectively. Experimental data of the epo_{0.85} group is not shown due to methodical limitations (see discussion). *In vitro* viscosities, calculated with the *in vitro* viscosity law of Pries *et al.* [124], are denoted by the small boxes (median $\pm 1^{\text{st}}/3^{\text{rd}}$ quartile). Note that these predictions are made on a vessel-specific basis rather than on group-averages with regard to the input data for the viscosity law, i.e. vessel diameter, species-specific mean corpuscular volume.

group	$\eta_{\text{rel app}}$
epo _{0.85}	-
epo _{0.50}	2.50 ± 0.80
epo _{H0.46}	1.95 ± 0.33
epo _{p0.53}	2.84 ± 0.82
wt _{0.46}	2.06 ± 0.67
wt _{0.27}	1.58 ± 0.29
wt _{H0.30}	1.51 ± 0.29
wt _{p0.24}	1.65 ± 0.29

Table 4. Relative apparent viscosity in epo mice and wt mice, before and after isovolemic hemodilution with HES or plasma. Values denote means \pm SD.

As shown in figure 28, relative apparent viscosity, $\eta_{\text{rel app}}$, declined gradually and almost linearly with decreasing hematocrit according to the group-specific median. Experimental data (large boxes) also shows remarkably good agreement with theoretical *in vitro* data

(small boxes), with the latter being calculated for each single vessel with the *in vitro* viscosity law of Pries *et al.* [124]. Due to constraints of the microviscometric analysis, experimental baseline data for epo mice could not be determined. Therefore, only theoretical data derived from the aforementioned viscosity law [124] is presented for this group. Accordingly, relative apparent viscosity of epo mice is predicted to be about 3.5-fold higher than in wt mice.

Upon hemodilution, the relative decrease in $\eta_{\text{rel app}}$ in epo mice may exceed the corresponding decrease of hematocrit, while the reverse is found in wt mice (Fig. 29).

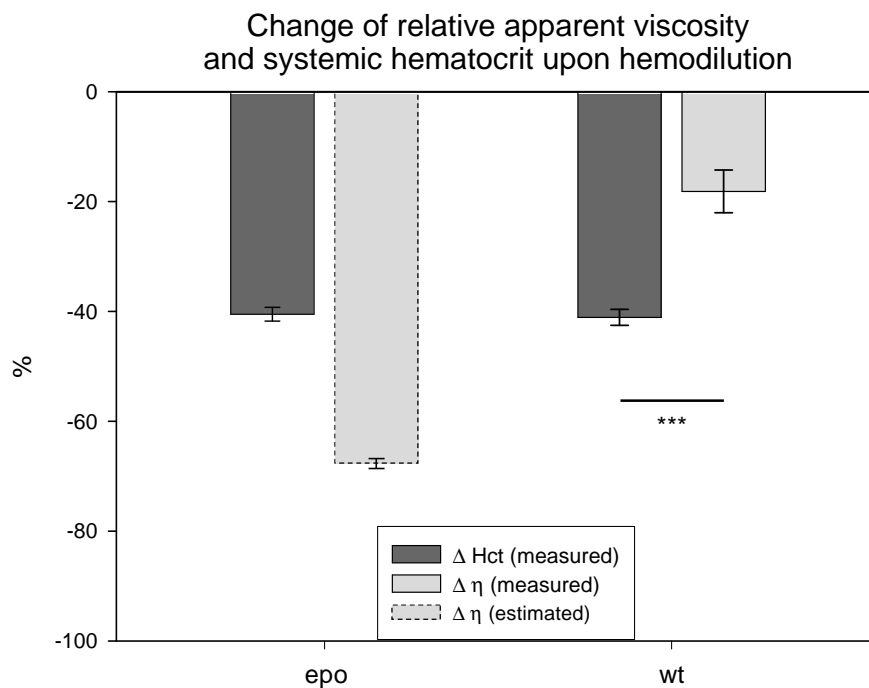


Figure 29. %-Change of relative apparent viscosity (light grey) compared to that of systemic hematocrit (dark grey) upon isovolemic hemodilution. The change in viscosity in epo mice is based on the analytically predicted *in vitro* data shown in Fig. 28. Bars denote mean \pm SEM.

In Fig. 30 (lower panel), relative apparent viscosity obtained by microviscometric analysis of the present μ -PIV data is plotted against mean systemic hematocrit of the respective group. Post-hemodilution values are denoted by triangles, with up and down triangles corresponding to the HES groups and plasma groups, respectively. Reference *in vitro* viscosity data, originally collected from flow in small glass tubes and subsequently described by the parametric *in vitro* viscosity law [124], is shown in the upper plot of Fig. 30. Adjustment of the *in vitro* viscosity law to both the mean corpuscular volume (MCV) of wild-type mouse erythrocytes (45 fl) and the current mean vessel diameter (38 μm) yields the dashed line in the lower panel of Fig. 30. Reference *in vivo* viscosity data based

either on network analysis [124] or on intravascular pressure drop measurements [92] is substantially higher than the present data at comparable vessel diameters and hematocrit (data not shown). No significant dependence of relative apparent viscosity on vessel diameter within the examined range was found in any of the experimental groups (plot not shown).

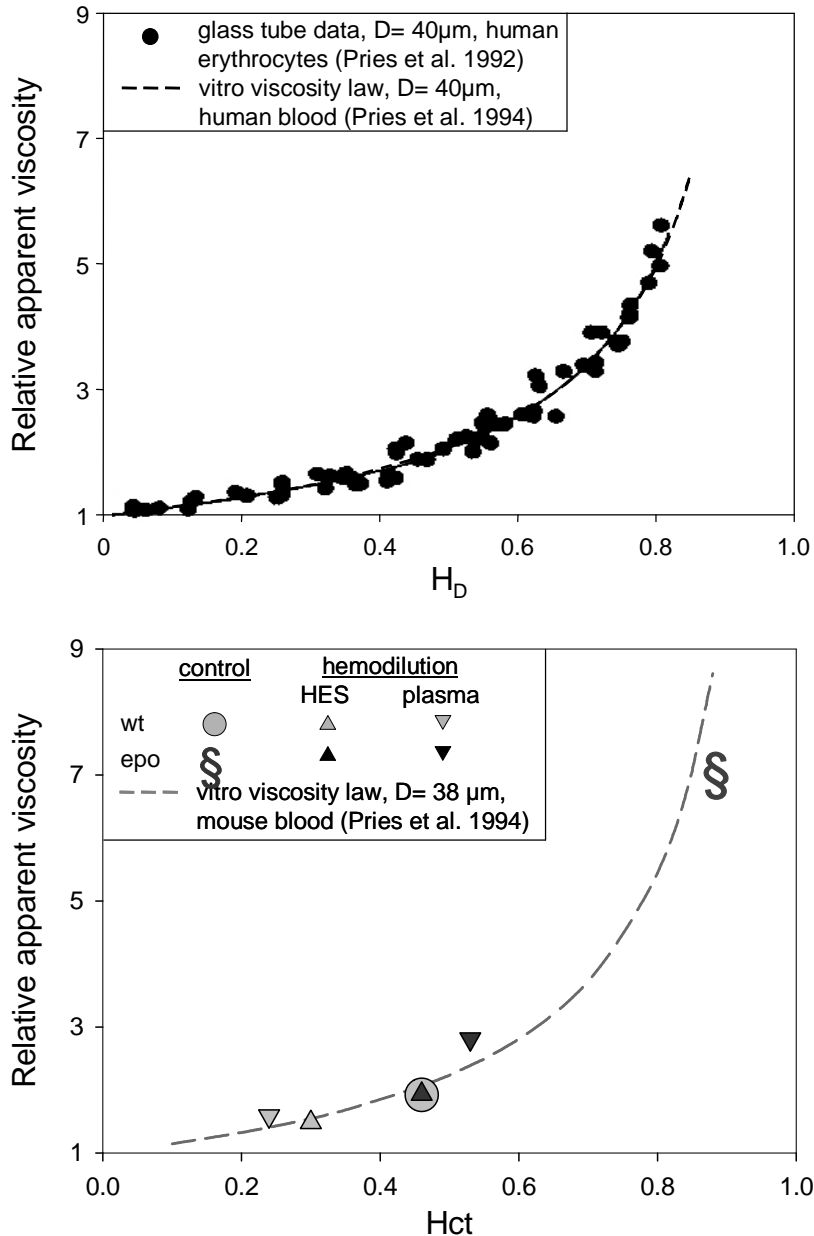


Figure 30. Upper panel: Dependence of relative apparent viscosity (circles) on discharge hematocrit (H_D) for fixed tube diameter ($40\ \mu\text{m}$) as obtained from glass tube experiments performed with human red cells (MCV 92 fl) [123]. Best non-linear fit to the experimental data is represented by the solid/dashed line, according to the *in vitro* viscosity law [124].

Lower panel: Dependence of relative apparent viscosity, $\eta_{\text{rel app}}$, on systemic hematocrit (Hct) as obtained from microviscometric analysis. Symbols represent median values of the respective group as a whole. These data exhibit remarkable consistency with those obtained from the *in vitro* viscosity law (dashed curve), with the latter being adjusted to both mouse blood (MCV 45 fl) and average vessel diameter of the present study ($D=38\ \mu\text{m}$). The arrow indicates the expected baseline value of $\eta_{\text{rel app}}$ in epo mice obtained by extrapolation of the non-linear fit to $Hct = 0.85$. Note, H_D is supposed to equal systemic hematocrit in the range of vessel diameter considered [42,125].

3.2.6. Microvascular hematocrit

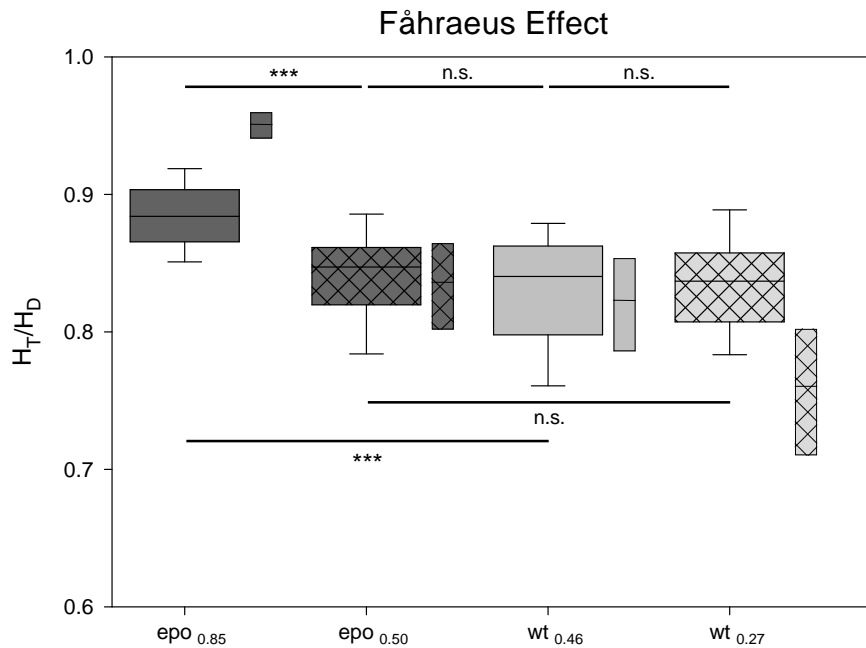


Figure 31. Ratio of H_T/H_D (Fåhraeus effect) of the four experimental groups (large boxes). Small boxes represent predicted *in vitro* reference data according to Pries *et al.* [124]. Differences between the experimental groups were tested for significance with t-test, except for $epo_{0.85}$ vs. $wt_{0.46}$ (Mann-Whitney U-test).

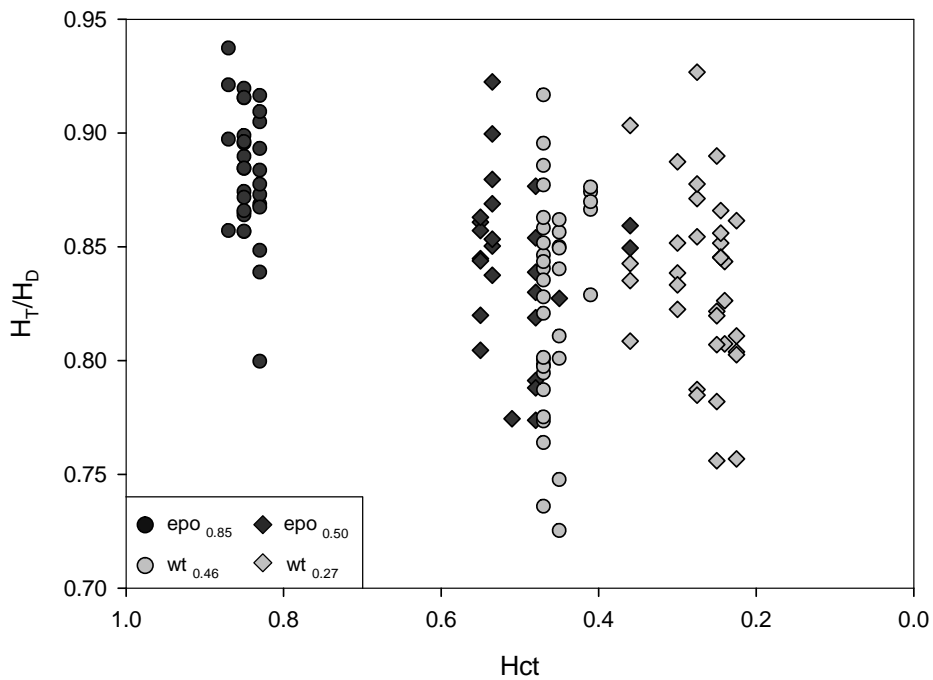


Figure 32. Relationship between H_T/H_D -ratio and systemic hematocrit. Each data point denotes a single vessel. Note, the abscissa is scaled inversely.

The ratio H_T/H_D , describing the *Fåhræus effect*, exhibited a significant decline in epo mice upon HD ($p < 0.001$). In contrast, no significant decrease in H_T/H_D was found in their wild-type littermates upon acute reduction of Hct (Fig. 31).

The relationship between H_T/H_D -ratio and hematocrit is displayed in figure 32. Significant correlation was only obtained in epo mice ($r^2 = 0.316$). Thus, hematocrit seems to be the main factor for the decline in H_T/H_D -ratio in epo mice, while additional factors may contribute to both the vertical data scatter and the lack of change in terms of the mean value in wt mice. Vertical data scatter, especially with respect to wt mice (light gray), may in part be attributed to two parameters pertaining to vessel geometry: First, the large range of vessel diameter (D) which is known to affect the *Fåhræus effect* at given hematocrit (see Fig. 8); second, the ESL thickness (t_{ESL}). Multivariate analysis was performed to assess their influence. The resulting parametric description indicates that a linear combination of D and t_{ESL} provides the most accurate prediction ($r^2 = 0.518$) of the level of the H_T/H_D -ratio (Fig. 33). Accordingly, H_T/H_D is positively correlated with D , but negatively with the t_{ESL} .

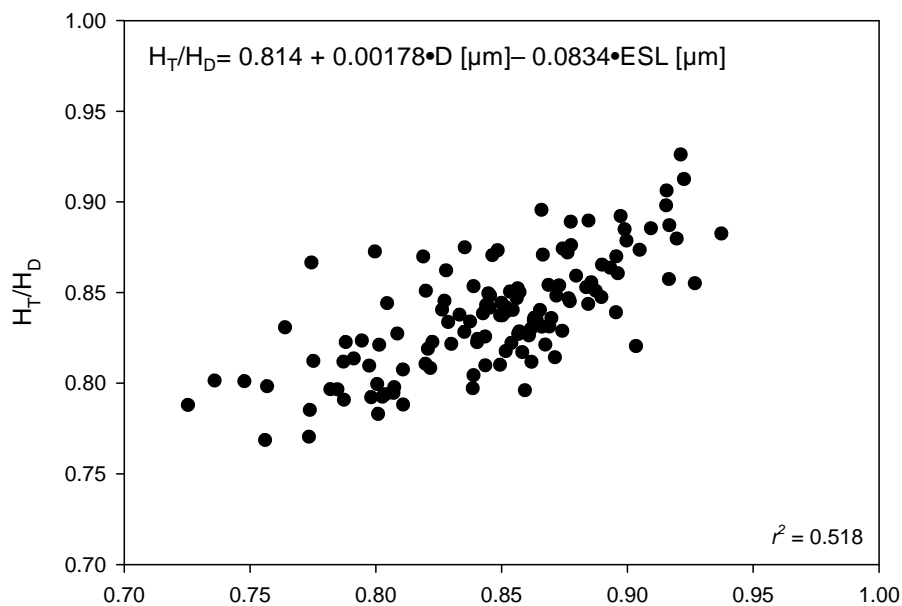


Figure 33. Scatter plot of H_T/H_D -ratios as determined by microviscometric analysis (x) vs. those predicted by means of a linear multivariate analysis (y). The plot accommodates data of all vessels, irrespective of the experimental group. r^2 , coefficient of determination.

3.2.7. ESL thickness

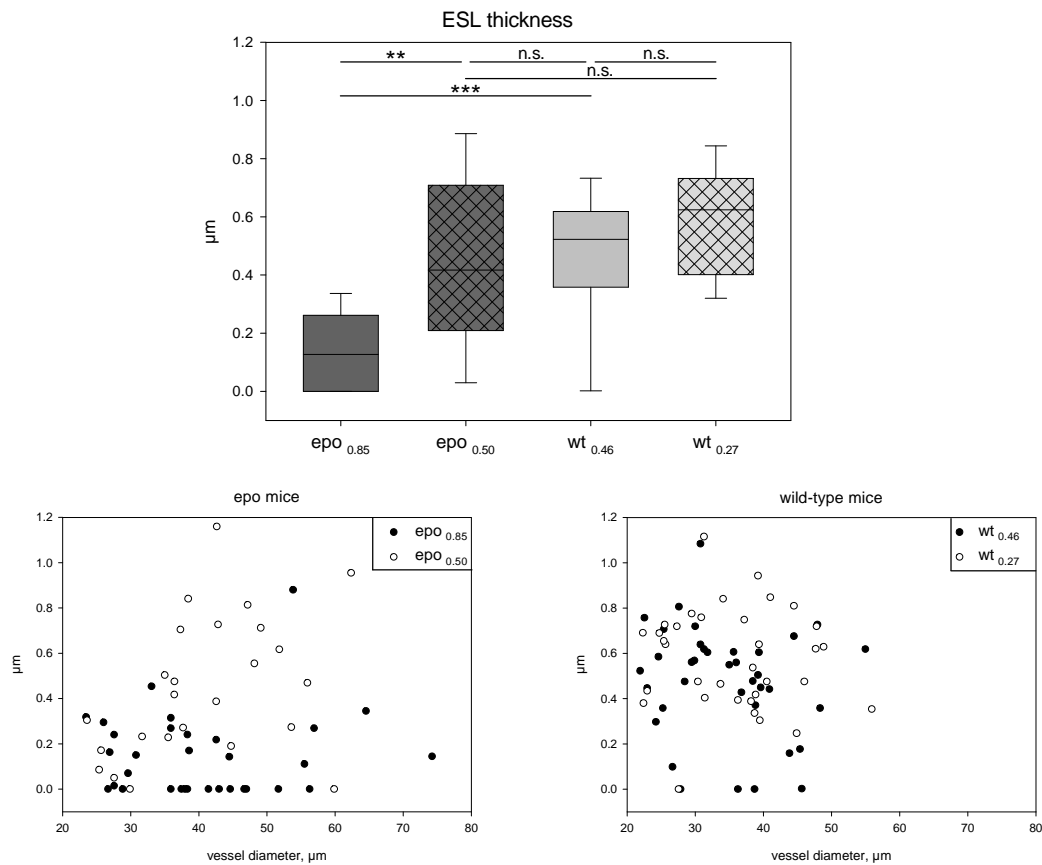


Figure 34. Upper panel: Estimated ESL thickness in epo mice and wt mice both before and after hemodilution. Differences were tested for significance using the paired t-test or Mann-Whitney U-test, respectively.

Lower panels: Scatter plot of ESL thickness as a function of vessel diameter, D , for epo mice (left panel) and wt mice (right panel) both before and after hemodilution; no significant correlation was detected.

Median ESL thickness in epo mice is $0.13 \mu\text{m}$ which is substantially lower than the corresponding baseline value in wt mice, i.e. $0.52 \mu\text{m}$ ($p < 0.001$). As obvious from the lower left panel in Fig. 34, a total lack of ESL is detected in the majority of vessels of the $\text{epo}_{0.85}$ group (filled circles). In the other experimental groups, only a relatively small number of vessels shows a complete lack of ESL. After hemodilution of epo mice, ESL thickness shows a significant increase, attaining a median value of $0.42 \mu\text{m}$ ($p < 0.01$) which is not significantly different from wt baseline. The slight increase in ESL thickness upon HD in wt mice does not reach significance ($p > 0.05$).

Table 5 discriminates the estimates of ESL thickness with respect to the fluid used for hemodilution, i.e. HES and plasma: epo mice hemodiluted with HES reach a greater ESL thickness as compared to the corresponding plasma group ($p < 0.05$). Accordingly, the rise in ESL thickness of epo mice diluted with HES is stronger ($p < 0.001$) than that found in the

plasma group ($p=0.01$). In wt mice, only hemodilution with plasma leads to a significant increase in ESL thickness ($p<0.01$), whereas no significant change is observed in the HES group ($p>0.05$).

The relationship between systemic hematocrit and ESL thickness (given as group-specific mean values) is shown in Fig. 35.

group	ESL thickness, μm
epo _{0.85}	0.15 ± 0.19
epo _{0.50}	0.45 ± 0.31
epo _{H0.46}	0.62 ± 0.26
epo _{p0.53}	0.35 ± 0.30
wt _{0.46}	0.47 ± 0.25
wt _{0.27}	0.58 ± 0.23
wt _{H0.30}	0.50 ± 0.23
wt _{p0.24}	0.64 ± 0.20

Table 5. Estimated ESL thickness in epo mice and wt mice before and after isovolemic hemodilution with HES or plasma; values denote means \pm SD.

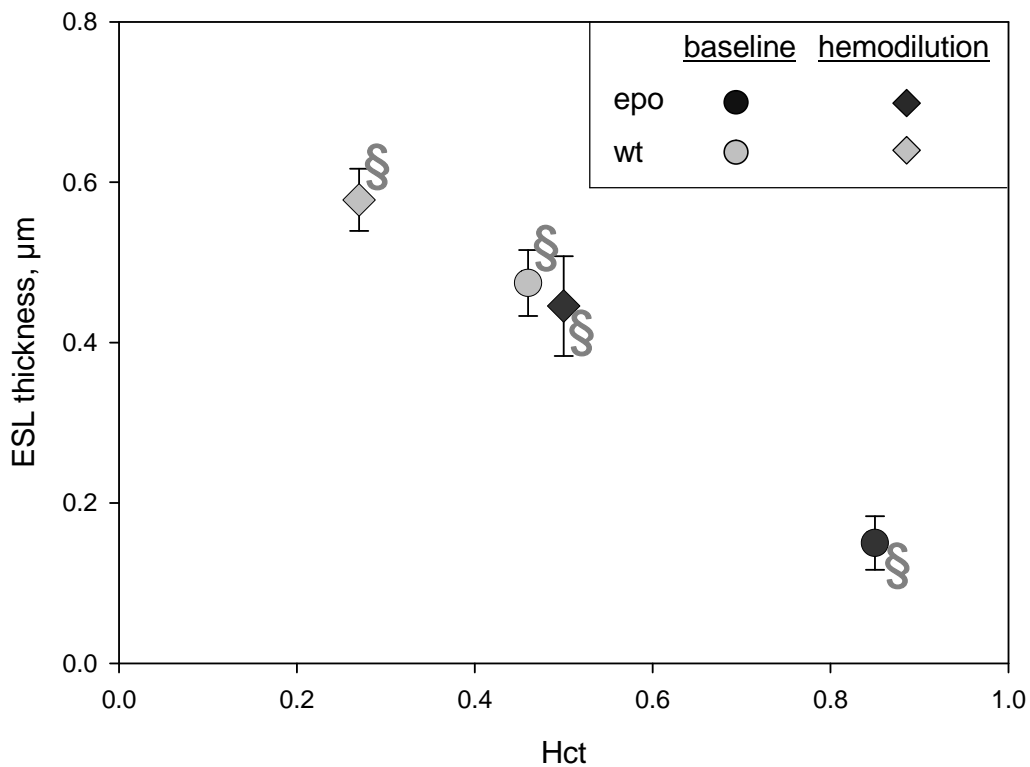


Figure 35. ESL thickness as a function of systemic hematocrit. Symbols represent mean values \pm SEM, while arrows indicate corresponding median values.

4. Discussion

4.1. Key findings

The main finding of the present analysis is that epo transgenic mice with systemic hematocrit levels of ~ 0.85 show a reduced ESL thickness ($\sim 0.1 \mu\text{m}$) in post-capillary microvessels relative to levels found in wild-type control mice ($\sim 0.5 \mu\text{m}$). Isovolemic hemodilution of epo mice to normal systemic hematocrit levels (~ 0.50) led to an immediate restoration in ESL thickness close to wild-type levels. This indicates that the observed ESL-reduction in epo mice under baseline conditions is reversible and mainly due to compression (rather than degradation) by a high hematocrit core of red cells within microvessels.

In addition, microvascular average flow velocity and volumetric flow rate in epo mice were 2.5-fold and 1.6-fold lower, respectively, than in wild-type control vessels with similar diameter. Upon hemodilution of epo mice, these flow quantities attained control levels of wild-type mice.

Hemodynamic flow simulations suggest that the combined effects of increased red-cell flexibility [190], larger red-cell volume, Fåhræus-Lindqvist effect, and reduced ESL thickness restore microvascular flow resistance in epo mice to normal levels found in wild-type mice, and thus compensate for the direct hemodynamic effects of the elevated systemic hematocrit.

4.2. Endothelial surface layer

The endothelial surface layer (ESL) is a gel-like structure [158] coating the luminal side of the vessel wall. It is considered to be composed of a highly hydrated, cell-bound macromolecular fiber matrix (~13% solid fraction [171,195]), usually termed glycocalyx [171], and an even more dilute and, thus, more fragile layer of plasma proteins (~0.1% solid fraction [149]), which are transiently attached to the scaffold forming the glycocalyx. According to this definition, the ESL is, hereafter, referred to as the sum of the glycocalyx and the plasma protein layer above. While the thickness of the glycocalyx is on the order of about 50 nm, as detected *in vitro* by means of transmission electron microscopy [162], the overall *in vivo* thickness of the ESL in microvessels under physiological conditions may range between 0.4 and 1 μm [39,42,186]. Its thickness as well as its composition and permeability are supposed to vary with time and space and to adapt to changing external factors [127,171,187].

In this context, the finding of the present study, i.e. that epo mice exhibit a substantially reduced ESL thickness relative to wt controls (Fig. 34, 35), suggests that also the hematocrit level may play a substantial role for the *in vivo* dimensions of the ESL. In the following, conceivable pathomechanisms related to ESL damage/thinning under conditions of increased hematocrit are discussed:

At hematocrit levels as high as 0.85, one has to consider the red cell column to exert substantial mechanical forces, directed perpendicularly and tangentially towards the inner vessel surface. A perpendicularly directed force would generate a sort of ‘squeezing’ effect. These compressive forces [183] which may be even enhanced by slow-flow conditions might overcome the hydraulic forces generated within the ESL [149] and lead to its apparent collapse. Justification for this hypothesis is provided by *in vivo* observations [186] and by models of capillary blood flow presented by Weinbaum *et al.* [195] and Secomb *et al.* [151], in which even a single red cell, if flowing slowly enough (<20-50 $\mu\text{m/s}$), is able to transiently penetrate and compress the ESL. On the other hand, if the hematocrit is very high, compression is not exerted by a single, slowly flowing red cell but by a continuous stream of red blood cells flowing at higher velocities, possibly leading to permanent compression of the ESL. Due to their flow dynamics, erythrocytes also generate tangentially directed forces, i.e. shearing forces, which may exert a kind of ‘scratching’

effect on the ESL. These cell-related effects have to be distinguished from the concept of a time-invariant wall shear stress in a strict sense. The latter refers to the shearing effect generated by the flow of a homogeneous fluid. In the present study, wall shear stress was found to be just slightly higher in epo mice than in their wt siblings, and on average well below 20 dyn/cm^2 (Fig. 27, upper panel). This value is also considered as an upper limit of force which the ESL is able to withstand [151]. As shown in a model by Secomb *et al.* [152], wall shear stress *in vivo* may exhibit significant variability due to irregularities in vessel shape. According to this model, a fully developed ESL is able to buffer the shear stress peaks to a considerable extent. This buffering function, however, is substantially diminished when ESL thickness is reduced to $0.05 \mu\text{m}$. Thus, the reduced ESL thickness in epo mice in concert with the very high hematocrit entailing occasional outward-bulging of red cells from the inner cell core [85] may actually lead to excessive local shear stress peaks way above 20 dyn/cm^2 . This could hamper macromolecular plasma constituents from binding to the molecules linked to the ESL. It appears unlikely that, for example, increased red cell flexibility is able to balance the perpendicular and tangential forces caused by the red cell bulk.

Second, the ESL might also be disrupted by deleterious chemical substances, especially by those which exhibit higher concentrations in epo mice relative to wt mice, viz. reactive oxygen species (ROS), cytokines [103] and nitric oxide (NO) [141]. The implications of elevated concentrations of ROS, e.g. oxidized lipoproteins, in terms of their ESL-damaging effect *in vivo* have been extensively investigated in previous studies [35,140,187]. Because NO was found both to induce generation of ROS, e.g. the tissue-toxic peroxynitrite, and to increase vascular permeability by itself [16], the integrative effect of both substances (ROS and NO) may lead to significant damage of the ESL. A complex system of anti-oxidative enzymes, comprising superoxide dismutase, katalase, peroxidase, glutathione, and others, normally protects the tissue (and the ESL) by scavenging substances like ROS. Large amounts of such oxidative agents may, however, challenge the anti-oxidative system, which is supported by findings on both the cerebral and erythrocyte-related metabolism in epo mice [18,103].

Eventually, a sort of viscous circle may be established where the question of cause and effect is difficult to address. Once the ESL is mechanically reduced, detrimental agents can get in closer proximity to the vessel wall. There, they may lead to additional chemical

degradation of the ESL due to rapid depletion of the anti-oxidative enzymes located in the vasculature, and vice versa.

The main finding of a strongly reduced ESL thickness, which might also correspond to an overall increased permeability [59], may have a number of functional consequences [130,195]. A thinned ESL enlarges the effective vessel lumen available to the bloodstream. This will reduce flow resistance, especially in smaller vessels due to its inverse relation to the fourth power of vessel radius. Interestingly, hemodilution of epo mice led to a marked increase in the layer thickness. This, in turn, may attenuate the decline in viscosity arising from hematocrit reduction. Also in wt mice, the ESL thickness slightly increased upon hemodilution, though not significantly. Thus, alteration in ESL thickness may represent a possible mechanism to modulate the flow resistance according to the currently prevailing hematocrit.

Among the physiological functions of the ESL is not only the 'regulation' of flow resistance [36,129,149,151] but also that of coagulation and transendothelial transport of plasma proteins [75], as well as the transmission of the interfacial shear stress into the endothelial cell via the cytoskeleton [130,150], and its role in modulating inflammatory processes [72,107]. With respect to the latter, deterioration of an 'intact' endothelial cell surface may also lead to increased susceptibility to tethering and adhesion of leukocytes. Indeed, previous studies show vascular degeneration and signs of latent chronic vascular inflammation in various organs of epo mice, e.g. in the liver, the kidney [70], and the brain [112]. Increased plasma concentrations of the *von Willebrand factor* [112] also indicate damage of the endothelial cell surface. This is unlikely to be a direct effect of increased erythropoietin levels. Instead, the present results suggest that damage of the ESL may account for the observed vascular degeneration leading, for example, to increased local shear stress as outlined above. Endothelial cell dysfunction is also assumed to be related to increased cardiovascular risk [168].

Also erythrocytes may suffer from increased and rapidly changing external stress and bending forces [50,151,152]. These forces are expected to increase when ESL thickness is reduced [152]. This may lead to cell trauma [82] and a strongly reduced life span of erythrocytes in the epo transgenic animal [18]. Consistent with this hypothesis, several studies on these mice have found elevated plasma concentrations of hemolytic products

such as free hemoglobin and LDH, increased osmotic fragility of red cells [155], enlargement of the spleen, and an increased number of reticulocytes in the blood, indicating augmented consumption of erythrocytes [190].

The finding of the present study that lowering the hematocrit to 'normal' levels by hemodilution seems to be adequate to re-establish the ESL supports the assumption of hematocrit-dependency of ESL thickness (Fig. 35). *In vitro* experiments performed in special flow chambers have shown that de-novo synthesis of macromolecules induced by changes in shear stress results in an increase in the thickness of the glycocalyx [3]. Since this process has been shown to take up to 1 week [117], it is unlikely to contribute to the observed ESL thickening, which must have taken place within 60 minutes after hemodilution, corresponding to the period of time necessary to collect the μ -PIV data in a given animal. This strongly indicates that the relatively quick ESL thickening accompanying hemodilution in epo mice is caused by a spontaneous relief from the compressive forces exerted by the aforementioned red cell core and by spontaneous adhesion of plasma components rather than their de-novo synthesis. On the other hand, the almost abolished ESL observed under control conditions in epo mice may be primarily the result of mechanical compression rather than chemical degradation

In wt mice, the effect of hemodilution on ESL thickness was milder than in epo mice (Fig. 34 and 35). Only in the plasma group, the increase in ESL thickness reached the level of significance ($p < 0.05$), whereas the respective increase in the HES group was not significant (Tab. 2). For the most part, the discrepancy between both groups pertaining to ESL thickness may be attributed to the difference in the group-specific hematocrit levels (Tab. 1), considering the approximately linear relationship between ESL thickness and systemic hematocrit (Fig. 35). Even though an influence of the fluid itself on the layer thickness cannot be ruled out [129], an explicit and consistent effect was not observed in the present investigation.

The estimated ESL thickness in wt mice (mean 0.47 μm) found in the present study under baseline conditions (Hct 0.46) is within the range of values reported by previous studies, irrespective of the experimental or analytical approach used [96,164,186].

4.3. Hemodynamics

Strong elevations in systemic hematocrit are generally supposed to impair hemodynamic and hemorheological properties due to a disproportional increase in flow resistance [66,138] (Fig. 3). This assumed relationship between flow resistance and hematocrit is based on measurements of viscosity performed in rotational viscometers, which per se provide information on the bulk rheological properties of blood. For instance, at extremely high hematocrit levels of about 0.85 pertinent *in vitro* literature data predicts at least a 4 to 5-fold higher bulk viscosity than at a physiological hematocrit level of 0.45 [28,29,123,124,190]. In addition, rotational viscometers will yield at high shear rates approximately the same viscosity as found in bulk vessels ($D \geq 1000 \mu\text{m}$) for a given hematocrit [93,108]. The corresponding exponential increase in viscosity with hematocrit may, however, be substantially attenuated in capillary-sized tubes and microvessels due to the Fåhræus effect (Fig. 3). Therefore, it may be inappropriate to extrapolate bulk viscosity data directly to microvessels. On the other hand, *in vivo* viscosity data for hyperphysiological hematocrit levels is generally very sparse and limited to hematocrits of about 0.65. For instance, Lipowsky *et al.* [94] determined the flow resistance in mesenteric microvessels of cats hemoconcentrated to hematocrits of up to 0.67 (mean 0.63). Respective results indicate that hemoconcentration from Hct 0.34 to Hct 0.63 leads to a doubling in flow resistance. However, the dual micro-pipette technique which was used in the study referred to in order to determine flow resistance (=measured axial pressure drop divided by estimated volumetric flow rate) is extremely cumbersome and very sensitive to measurement errors.

In light of these experimental limitations, a flow simulation model of an experimental microvascular network [121] was used to estimate the relative difference in flow resistance between epo mice and wt mice. (For more details on that approach, the reader is referred to the ‘Material and Methods’ section, 2.13.) The present analysis suggests that the epo transgenic mice, which grow up with excessive polycythemia, are able to lower their blood flow resistance to a considerable extent *in vivo*. As mentioned in the key findings, several compensating mechanisms seem to contribute to this reduction. The quantitative effects on flow resistance these factors are predicted to have in the considered microvascular network are summarized in figure 36.

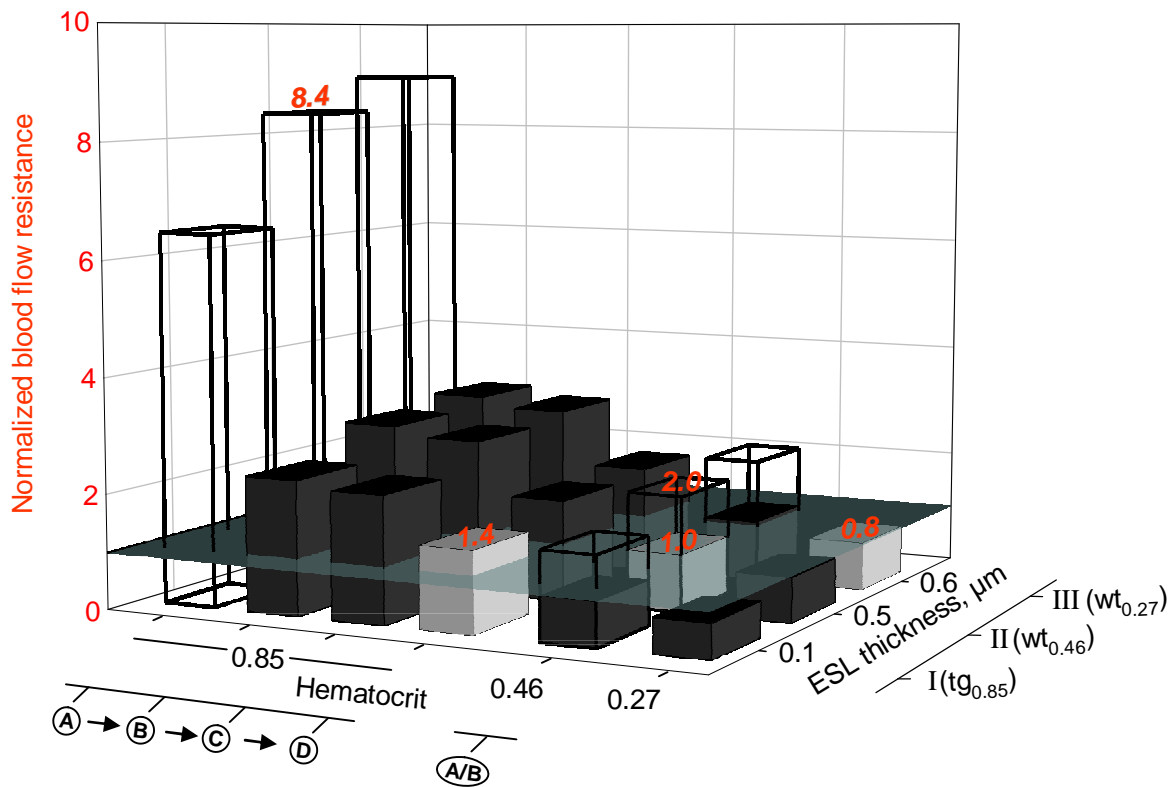


Figure 36. Dependence of flow resistance in an experimental microvascular network on ESL thickness (I-III) and hematocrit (0.27, 0.46, 0.85). In addition, four other factors are considered.

A: Bulk viscosity was assumed for all vessels independent of vessel diameter (transparent columns).

B: Reduction of apparent viscosity with declining vessel diameter according to *Fåhræus-Lindqvist effect* was taken into account.

C: Effect of increased red cell volume, MCV (wt 45 fl vs. epo 57 fl), was included.

D: Impact of increased cell flexibility on bulk viscosity according to [190] was integrated.

All values are calculated with a hemodynamic flow simulation using an experimental vascular network in the rat mesentery with 546 vessel segments [124]. For the vessel lumen available for free flow (D – 2•ESL), a parametric description of apparent viscosity *in vitro* as a function of diameter and hematocrit (*in vitro* viscosity law) is used [123]. No hydraulic conductivity in the ESL is assumed. This corresponds to the concept advanced by Pries et al. [132] with the exception that the indicated ESL thickness is used for all vessels. Values are normalized to the flow resistance obtained for wt mice under spontaneous conditions (ESL thickness II, Hct 0.46, MCV 45 fl, normal cell flexibility). Each column in light gray represents the predicted flow resistance of the experimental group considered (epo_{0.85}, wt_{0.46}, wt_{0.27}) if the assumed parameters are applied to it. Categories of ESL thickness (I-III) correspond to the group-specific median values rounded to one decimal place.

Figure 36 illustrates that, in addition to the well-known dependence on hematocrit, flow resistance is also affected by the *Fåhræus-Lindqvist* effect, by the cell flexibility, by the cell volume and by the ESL thickness. In the following, these factors and corresponding mechanisms are discussed in more detail.

- When assessing flow resistance, there is basically a great difference whether a single large vessel or a microvascular network is considered. Due to the *Fåhræus-Lindqvist* (FL) effect, transition from large vessels (D ~1000 μm) to microvessels will yield for

a given hematocrit a substantially lower apparent viscosity and flow resistance, respectively (Fig. 1). This is especially relevant for very high levels of hematocrit where the FL effect may be more salient than at physiological levels (Fig. 37). Accordingly, the FL effect accounts for the greatest reduction of flow resistance relative to that of the other factors considered (Fig. 36, A→B).

- Another possible factor known to affect flow resistance by influencing vessel geometry is the endothelial surface layer (ESL) [128]. Because of its presumably high hydraulic resistivity (K [dyn/cm⁴]), corresponding to strong attenuation of plasma flow, the ESL reduces the vessel cross-section available to the blood stream. Due to the inverse fourth power dependence of the flow resistance, R , on vessel radius, r , ($R \sim 1/r^4$) even a slight decrease in vessel diameter can significantly increase the resistance, and vice versa. A decrease in ESL thickness corresponds to an increase in effective vessel diameter, which is similar to the effect of NO as described before. When applied to the current finding of a $\sim 0.4 \mu\text{m}$ thinner ESL in epo mice as compared to wt mice, this would lead to a decline in resistance by just $\sim 5\%$ in a single vessel of $38 \mu\text{m}$ in diameter. This relatively small decrease is because the ESL occupies only a relatively small portion of the cross-section on this vessel scale. In contrast, in smaller-diameter microvessels the effect on the resistance is greater since the ESL takes a correspondingly larger portion of the vessel cross-section. Considering a complete microvascular network comprising microvessels with different diameters and an ESL thickness reduced consistently by $0.4 \mu\text{m}$, the calculated overall flow resistance decreases by $\sim 18\%$ (Fig. 36). This decrease is quantitatively similar to that caused by heparinase treatment [128].

As hypothesized by Pries *et al.* [132], in multi-file flow ‘cell-to-cell interactions and collisions lead to a radial displacement of cells toward the wall, bringing them into close contact with the ESL’. This may give rise to an additional retardation of the blood flow. Thus, the total effect of the ESL on flow resistance could actually exceed the purely geometrical effect, especially at very high hematocrits where radial displacement of cells is likely to occur more frequently. Therefore, the above-mentioned 18% decrease may even underestimate the actual decrease in flow resistance induced by an ESL reduction in the microvascular network considered at a hematocrit of 0.85.

- Epo mice exhibit an elevated fraction of reticulocytes which represent the youngest generation of mature erythrocytes [190]. These cells naturally possess a slightly larger mean corpuscular volume, MCV (epo 57 fl vs. wt 45 fl [190]). A change in cell volume may affect blood viscosity due to the FL effect. This effect describes for a given hematocrit the dependence of relative apparent viscosity not only on tube size, but more precisely, on relative tube size, i.e. the ratio of tube size over particle size: In tubes smaller than 1000 μm in diameter, apparent viscosity generally decreases as tube diameter is reduced. Only at diameters below about 5 μm viscosity starts to rise steeply again. As for the relative tube size, an increase in particle size has the same effect as a smaller-diameter tube. Accordingly, an increase in MCV will generate a slight decrease of viscosity in tubes larger than 5 μm in diameter leading to an apparent rightward shift of the viscosity curve as illustrated in figure 37. For the considered range of corpuscular volume (45 - 57 fl) this effect is, however, relatively small. It would be most pronounced at elevated hematocrits and if the tube or vessel diameter considered falls into a region where the viscosity curve exhibits a relatively high slope.

Effect of hematocrit and MCV on the Fåhræus-Lindqvist effect

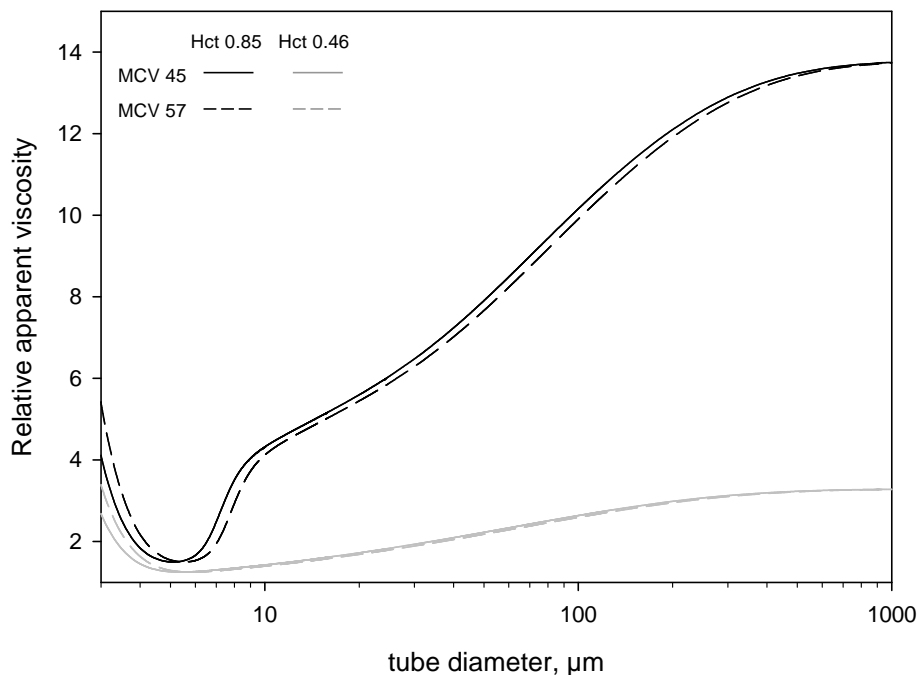


Figure 37. Influence of change in cell volume (45fl, dashed lines; 57fl, solid lines) on the dependence of relative apparent viscosity on tube diameter for high (black) and moderate (grey) levels of hematocrit *in vitro*.

- Young erythrocytes are also known to be more flexible than mature cells [156,157]. Numerous studies have addressed the effect of altered cell deformability on apparent viscosity *in vitro* [29,148,175,201]. Hardening of red cells has been shown to increase bulk viscosity as measured in a Couette viscometer[#]. However, this effect was seen to be significant only at hematocrits above ~0.40 [29,161]. For increased red cell flexibility, Vogel *et al.* [190] demonstrated a reduction in bulk viscosity by factor 2 to 3 as compared to a suspension containing normally flexible erythrocytes. In line with the findings on chemically hardened cells, this effect was only significant for high hematocrits (~0.89), but nearly absent for normal hematocrit levels (~0.44). Results of a recent study [55] have confirmed the almost missing difference in bulk viscosity between epo mice and wt mice when the hematocrit is reduced to the level of wt mice.

In vivo and *in situ* studies on the effect of altered red cell deformability on blood flow are scarce and limited to hematocrits ≤ 0.45 . Moreover, the results obtained with artificially hardened cells are not consistent, probably due to methodical differences [24,44,175]. The actual effect may depend on the hemodynamic conditions and adaptations [95], and on the severity and kind of rigidification [30]. In addition, in most experimental *in vivo* settings, the hardened red cells injected into the vascular system are rapidly removed (>70% within 25 minutes after injection) from the circulation by sequestration occurring preferentially in the spleen [30,161]. Hence, assessment of the influence of reduced cell flexibility on flow resistance *in vivo* and, especially, its dependence on hematocrit is difficult.

As for increased cell flexibility, extrapolation of corresponding viscometric *in vitro* data to the *in vivo* situation may inherit significant error as well. Unfortunately, its potential relevance for effective viscosity at high hematocrits *in vivo* cannot be proven by current experimental data as the μ -PIV approach fails for such hematocrit levels. More detail on methodical limitations is given below. Notably, strongly increased plasma NO-levels (3-fold increase in epo mice [141]) may even reduce red cell flexibility [9] and thus attenuate the potentially beneficial effect on flow resistance. Thus, quantification of the effect of enhanced cell flexibility on resistance

[#] Couette viscometer, a special type of rotational viscometer based on cone-plate viscometer

in vivo based on *in vitro* findings [190] may not be very precise and should be handled with caution (Fig. 36, C→D).

At least, the assumption that increased cell flexibility does **not** substantially affect blood viscosity at physiological hematocrit levels *in vivo* is supported by the finding of the present study: Epo mice hemodiluted to about the hematocrit level of wt control mice did not reach lower but even slightly higher viscosities as compared to their wt siblings (Fig. 28/30). It is unlikely that erythrocytes of epo mice have lost the higher flexibility by the hemodilution procedure. A possible explanation for the hematocrit dependency of the effect of cell deformability on viscosity lies in the difference between cell-cell and cell-plasma interaction. At increased hematocrit (i.e. increased volume fraction of cells and decreased volume fraction of the suspending fluid trapped between the cells), the relative contribution of cell-cell collisions to the overall amount of energy dissipation during blood flow and thus to the apparent viscosity exceeds that of cell-plasma interactions. The latter, in turn, may gain in importance with decreasing hematocrit [29]. Hence, at moderate or low levels of hematocrit, increased cell deformability will probably not reduce flow resistance to a significant extent.

The elevated plasma levels of nitric oxide (NO) [141] resulting from increased activity of the endothelial NO-synthase (eNOS) as detected in the lung tissue [68] and in the endothelium of the thoracic aorta [141] of epo mice may lead to generally increased vessel diameters. According to the Hagen-Poiseuille law, in which flow resistance is inversely related to the 4th power of vessel radius, increased vessel size will decrease flow resistance. A recent study, however, has found no significant difference in mean anatomical diameter of both arterial and small venous vessels between epo mice and wt mice [54]. In addition, NO may also influence flow resistance by rheological mechanisms, i.e. by reducing erythrocyte aggregation tendency. Some studies indicate that NO regulates red cell deformability in a concentration-dependent biphasic manner [9,19,173], with both very high and very low NO-concentrations reducing cell deformability. In contrast, He et al. [69] found no significant effect of NO on cell deformability *in vitro*. Therefore, the resistance effect of altered NO concentration was not included in the present analysis.

A further mechanism that could effectively diminish flow resistance is the reduction of true microvessel hematocrit below the systemic level, i.e. large vessel hematocrit. From a rheological point of view, both the vessel *Fåhræus effect* (FE) and the so-called *network Fåhræus effect* (NF) may contribute to a dynamic reduction of microvascular hematocrit below systemic hematocrit [126]. At very high levels of hematocrit, inward migration of red cells virtually does not occur, and the FE becomes negligibly small [6,121]. The NF supposes that red cells tend to follow the high flow pathways within a vascular network leading to an uneven distribution of hematocrit both at single vessel bifurcations and across this network. This results in a relatively small number of high-hematocrit pathways, being balanced by a relatively large number of low-hematocrit pathways. When averaged over the entire microvascular network, this phenomenon would give rise to a microvascular discharge hematocrit being lower than the discharge hematocrit of vessels feeding or draining the network. This phenomenon is, however, typically observed for hematocrits of up to ~0.30 [88,122]. On the other hand, high levels of systemic hematocrit are accompanied by a homogenization of microvascular hematocrit distribution. Hence, under basically slow-flow and high hematocrit conditions, all effects that could contribute to a dynamic reduction of microvascular hematocrit are unlikely to be significant enough in order to explain a lowered network flow resistance in the $epo_{0.85}$ group [51]. Consistent with this is the failure to find anatomical shunts between arterioles and venules in the cremaster muscle of hamsters, as demonstrated in a previous study [88]. In contrast, *in vivo* measurements of both intravascular and tissue pO_2 (partial oxygen pressure) in the subcutaneous tissue of conscious *epo* mice [54] suggest the existence of arterio-venous shunts which could effectively reduce hematocrit in the distal regions of the respective network. Hence, studies need to be conducted where microvessel hematocrit, blood flow and the vessel topography of complete microvascular networks in *epo* mice are assessed simultaneously in order to provide evidence for the existence of such an adaptive mechanism.

In contrast, an increased number of vessels arranged in a parallel manner is likely to reduce the overall flow resistance of the respective network according to Kirchhoff's circuit laws. Indirect evidence for an increased vessel number in *epo* mice is provided by their 2.5-fold higher total blood volume [190] and by the finding that average blood flow velocity in similar sized vessels is decreased 2.5-fold (Fig. 20), while cardiac output is not different

from wt mice [141,191]. In addition, immunohistochemical examination of the EDL[#]-muscle of epo mice revealed an about 65% higher capillary density relative to their wt littermates (Fig. 38). The discrepancy in vessel number between direct observations (1.65-fold) and estimates deduced from global hemodynamic parameters (2-fold) could be due to the existence of arterio-venous shunts in epo mice as hypothesized recently [54].

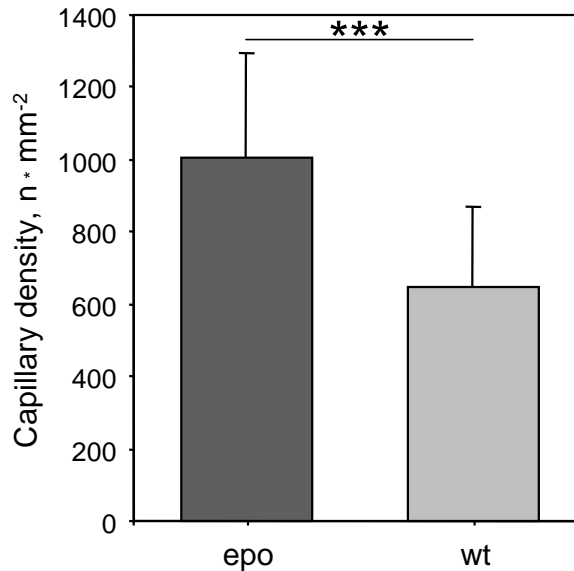


Figure 38. Functional capillary density (number of perfused capillaries, n, per unit area) in the extensor digitorum longus (EDL) muscle of epo mice and wt mice (unpublished data by O. Baum), values given as mean \pm SD; $p < 0.001$ (t-test).

Taken together, the factors considered could even overcompensate for the resistance effect of increased hematocrit. This is, however, unlikely to be the case. Instead, the ability of epo mice to reduce their flow resistance might in part be counteracted by the relatively low shear rates (Fig. 39).

At low and normal levels of hematocrit and high shear rates, bulk viscosity of whole blood as measured in rotational viscometers exhibits only a mild, inverse dependence on shear rate [28,93]. Only if shear rate falls below a certain threshold does viscosity start to rise significantly. For instance, at a hematocrit of 0.45, bulk viscosity increases markedly as shear rates become smaller than $\sim 10 \text{ s}^{-1}$ [28,55,190]. With increasing hematocrit, this threshold is shifting towards progressively higher shear rates. One might speculate that such a relation exists *in vivo* as well, even though direct extrapolation of this relation to the situation *in vivo* is not adequate [124,136] due to additional factors, e.g., radial shear rate

[#] EDL, (musculus) extensor digitorum longus

distribution, gravitational forces. Possibly, the combined effect of relatively low pseudo-shear rates prevailing in epo mice (Fig. 39) and excessive hematocrits of about 0.85 might increase viscosity and, thus, flow resistance *in vivo*.

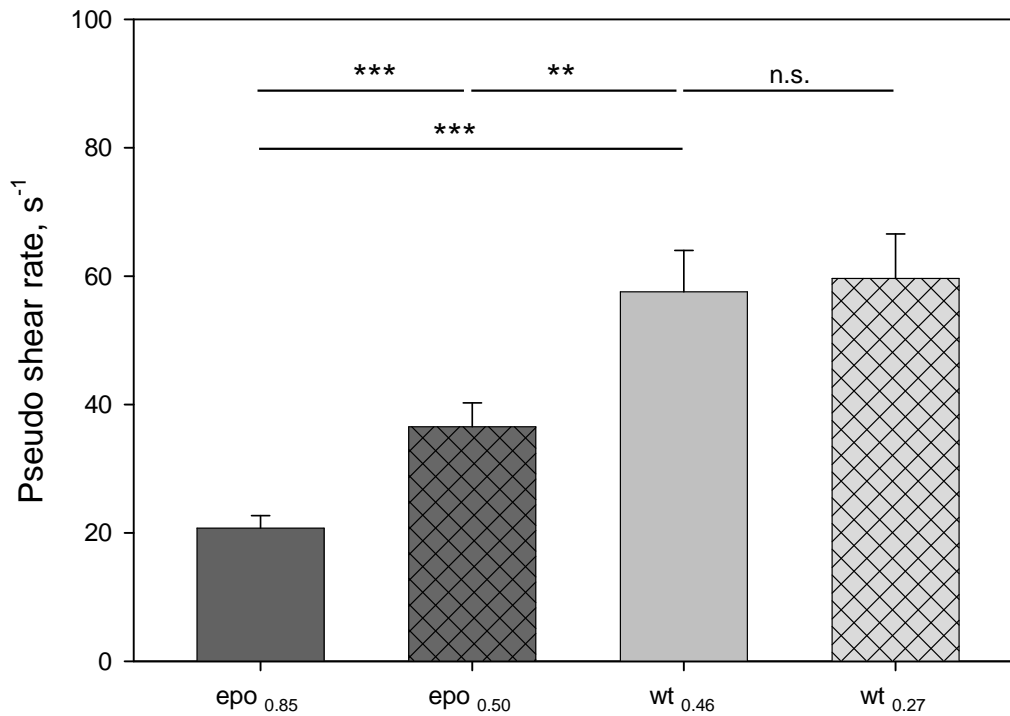


Figure 39. Pseudo-shear rate (equal to average flow velocity divided by vessel diameter) in epo mice and wt mice; columns represent mean \pm SEM

In essence, the integrative effect of all factors assessed above and summarized in Fig. 36 gives rise to an unexpectedly low overall network flow resistance in epo mice, which is similar to the level of wt mice. Strong support for this hypothesis is provided by the finding that mean arterial pressure, heart rate and cardiac output in epo mice are not significantly different from wt mice [141,190,191]. Accordingly, total peripheral resistance, which corresponds to the ratio of mean arterial pressure (minus central venous pressure) to cardiac output, is expected to be within the range of wt mice.

4.4. Blood viscosity *in vivo*

In the interpretation of the present data, some methodical constraints need to be considered. For normal and low levels of hematocrit, the microviscometric approach provides reliable hemodynamic and hemorheological results. It can be applied to blood flow in both venules and arterioles. The respective vessel diameter should be at least 20 μm . At such vessel dimensions blood flow can be well approximated with a continuum model, which the current analytical approach is based on [34]. The accuracy of the method in determining apparent viscosity under such conditions has been verified by previous glass tube experiments for hematocrits ranging from 0.17 to 0.55 [96].

At very high levels of systemic hematocrit, however, the analytical technique used is not able to determine shear stress and apparent viscosity properly (Fig. 26 and 27). In order to determine these two quantities accurately, the microviscometric method requires a known viscosity at a given radial location of the vessel cross-section in addition to the measured velocity profile or shear rate profile. This condition is usually met at the virtually cell-free fluid layers adjacent to the vessel wall, where generally plasma viscosity is assumed to prevail. Given a known local viscosity, the radial viscosity distribution and the apparent viscosity can be calculated. The assumption of the existence and width of such a cell-free zone, however, refers to an idealized two-phase flow model with a red cell core and a continuous cell-free layer. Of note, the term ‘cell-free layer’ (CFL) must not be confused with the ESL. In contrast to the latter, the CFL represents a portion of the vessel lumen available to the free blood stream. Numerous investigations have shown the width of the CFL both to be inversely related to the level of hematocrit [85,99,154,167,179,180] and to exhibit considerable temporal variation [85] due to transient protrusion of peripheral cells. For glass tubes 40 to 83 μm in diameter, Bugliarello *et al.* [22] observed a decrease in mean CFL thickness from 12 μm to 2 μm as hematocrit was increased from 0.10 to 0.40. Maeda *et al.* [99] examined the CFL in microvessels (25 – 35 μm in diameter) of the isolated rabbit mesentery. Increasing feed hematocrit from 0.08 to 0.45 led to a decrease in CFL width from ~ 5 μm to ~ 1 μm . Hence, for very high hematocrit levels, an effectively cell-free layer of sufficient width does not seem to be present. Under these conditions, true viscosity of the near-wall fluid layers might substantially exceed plasma viscosity, giving rise to a rather cell-poor layer (of unknown hematocrit and unknown viscosity). Without a

reasonable knowledge of viscosity at a certain radial position, neither the radial shear stress distribution nor the apparent viscosity can be properly assessed.

It has to be stated that the present viscosity values[#] are considerably lower than respective *in vivo* estimates in the pertinent literature [92,124]. They rather seem to reflect the *in vitro* viscosity (Fig. 30) as measured in glass tubes. Two reasons may account for this finding.

- As for the determination of the viscosity, the microviscometric analysis considers only the fluid within the ‘effective’ vessel lumen, i.e. the lumen available for the blood stream (anatomical or bright-field diameter – 2 • ESL thickness). Thus, the ‘effective’ vessel lumen does not imply the ESL. As stated by Pries et al. [132], the flow conditions within the ‘effective’ vessel lumen may resemble those in glass tubes of same inner diameter. Thus, also, the viscosity of the blood perfusing the ‘effective’ vessel lumen may be similar to the apparent viscosity as measured in glass tubes, which naturally lack any ESL. The effective blood viscosity may increase to levels actually expected according to the predicted overall flow resistance in microvascular networks [124] only after involving the ESL and potentially related hemorheological effects in terms of mechanical interactions with adjacent red cells.
- It is generally accepted that white cells can play a critical role in determining intravascular resistance to flow [134]. This appears to be relevant in venules in particular where interactions between leukocytes and the vessel wall frequently occur. According to Lipowsky, increased incidence of rolling and adhering leukocytes, triggered for instance by the surgical trauma related to the cremaster muscle preparation, could increase viscosity by up to 74% [20,93]. As for the total peripheral flow resistance, the role of white cells may be less important because rolling and adherence does not occur in arterial vessels under normal flow conditions. In the present study, the rolling of leukocytes was prevented by P-selectin antibodies (RB 40.34) administered systemically to all animals. This may, in part, account for the unexpectedly low relative apparent viscosity in the venules examined.

Surprisingly, the effective viscosity in hemodiluted epo mice did not fall below the level of wt mice (Fig. 28/30), despite the higher cell flexibility that was probably maintained. Two

[#] This refers to all groups but the epo_{0.85}. In the latter, determination of apparent viscosity was not possible as explained above.

factors might contribute to this finding: First, the ESL seems to be rapidly reconstituted upon hemodilution. Secondly, and as explained above, *in vitro* data on the effect of increased cell flexibility on bulk viscosity suggests that at physiological levels of hematocrit the positive rheological impact of this cell property becomes much less distinct [55,190]. With regard to flow in small tubes ($<30\ \mu\text{m}$), the relative contribution of cell deformability to overall flow resistance might be further diminished at lowered hematocrit, as the extent of cell deformation in the microcirculation is generally smaller than in bulk flow. This is due to the special flow phenomena in small tubes, i.e. the dynamic reduction of microvessel hematocrit (*Fåhræus effect*) and the prevailing flow patterns. These features of tube flow give rise to reduced incidence of cell-to-cell and cell-to-wall collisions and, consequently, reduced amount and frequency of cell deformation.

4.5. Implications and conclusions

In numerous population studies, elevated systemic hematocrit is accompanied by an increase in total peripheral resistance due to a decrease in cardiac output, or a compensatory increase in mean arterial pressure (MAP) [17,61,63,66,94,111,138,146,176]. Recent animal studies indicate that acute mechanisms such as NO-induced vasodilation may prevent the increase in resistance upon mild elevations of hematocrit, at least in the short term [100,101]. However, the compensatory capacity of such mechanisms was limited to relative increases of baseline hematocrit by ~20%, beyond which the peripheral resistance did start to rise.

In light of these findings, it is surprising that under the chronic conditions in epo transgenic mice the nearly 100% higher hematocrit relative to wild-type baseline is not accompanied by a decrease in cardiac output nor an increase in MAP [141,190,191]. Hence, total peripheral resistance does not differ significantly between epo mice and their wild-type littermates either. A couple of possible mechanisms which may reduce total peripheral resistance below the actually anticipated level for such high hematocrits have been established in recent years, i.e. NO-induced increase in vessel diameter [141] and increased erythrocyte flexibility [18,190]. However, despite increased NO-levels [141], intravital microscopic studies have revealed that only larger-diameter post-capillary venules (>45 μm) show increased diameters compared to their wild-type counterparts [54]. The corresponding effect on total peripheral flow resistance is relatively small since the bulk of resistance is generated on the arterial rather than on the venous side of the circulatory system. As for the effect of the 1.5 - 3-fold increased cell deformability on flow resistance, only *in vitro* data is available [190]. In addition, the observed *in vitro* effect can only partly explain the remarkably low peripheral flow resistance seen *in vivo* (Fig. 36).

A growing body of evidence indicates the existence of a thick endothelial surface layer (ESL), which is only present *in vivo* [117] and not available for free blood flow [88,128,129,132]. This layer and changes in its thickness may influence flow resistance. In the present study, a decrease in ESL thickness by about 0.4 μm is found in venules of epo mice. Provided that this finding also applies to capillaries and small arterioles, it could give rise to an additional reduction in flow resistance by about 20% (Fig. 36). The hemodynamic effect of an ESL reduction is, thus, relatively weak, as compared to that of

increased cell flexibility. Hence, maintenance of total peripheral resistance is achieved rather by the integration of several compensatory effects, i.e. the *Fåhræus-Lindqvist effect*, increased total blood volume, reduced ESL, increased effective vessel diameter, increased cell flexibility, and increased cell volume (Fig. 36).

The functional consequences of ESL thinning and potential damage may, however, underlie pathophysiological events such as endothelial and organ degeneration [70]. In general, vascular pathologies [137] related to ESL injury include atherosclerosis [181,182], microangiopathy in diabetes [110], and tissue damage induced by ischemia-reperfusion [107,116]. When associated with high hematocrit, degenerative processes may be further aggravated. In fact, on the microvascular level, epo mice reveal signs of endothelial degeneration, rendering the organism more vulnerable to vascular disease events, especially in older specimens [70]. This could possibly account for the reduced life span of epo mice [191] relative to wt mice [86].

In contrast to epo mice, polycythemic humans such as patients suffering from polycythemia vera (PV) generally exhibit insufficient adaptation to increased hematocrit, leading to hypertension as a result of increased pulmonary and peripheral flow resistance, and to elevated cardiovascular risk, e.g. thromboembolism [17,31,52,170]. In addition, it has been shown that the increased risk of thrombosis in PV patients is associated with vascular damage and endothelial cell dysfunction [109]. It might be speculated that compression and/or damage of the ESL, evoked by the high hematocrit, brings platelets and leukocytes into close proximity to the vessel wall. This, in essence, undermines the role of the ESL and makes the vascular interface a more proinflammatory and prothrombogenic surface relative to normocythemic humans. Thus, apart from hemodynamic factors, also a compromised function/integrity of the ESL could contribute to the increased cardiovascular risk in polycythemic patients. To test this hypothesis, more insight into micromechanics of the ESL in polycythemia is needed, e.g. to differentiate between effects of reversible compression versus structural damage of the ESL.

5. Summary

Elevated systemic hematocrit (Hct) is known to increase cardiovascular risk, such as deep vein thrombosis, myocardial infarction, and stroke. Besides an impairment of the hemodynamic conditions due to the increased blood viscosity and resistance to blood flow, another possible mechanism could be a disturbance of the blood-endothelial cell (EC) interface. It has been shown that the flowing blood interacts with the EC surface via an approximately 0.5 μm thick layer, termed glycocalyx, or endothelial surface layer (ESL), which is relevant for various physiological and pathophysiological processes, including inflammation, transendothelial molecular transport, and atherosclerosis. The consequences of increased Hct levels for the functional properties of this interface in microvessels are incompletely understood.

To examine the effects of elevated Hct on ESL thickness, microvascular hemodynamics and hemorheology, an erythropoietin-transgenic mouse line (tg6) exhibiting Hct levels as high as 0.85 without alteration of total peripheral resistance was used. Intravital microscopy of cremaster muscle venules ($n_{\text{vessel}} = 32$), both before and after systemic hemodilution, was combined with micro-particle image velocimetry (μ -PIV) to determine specific flow quantities (flow velocity, shear rate, shear stress, viscosity, flow rate) and ESL thickness. C57 wild-type mice (wt, Hct 0.46) served as control ($n_{\text{vessel}} = 37$). A flow simulation model was used to assess the effects of changes in Hct and ESL on overall flow resistance in a microvascular network.

Tg6 mice showed reduced flow velocity (2.5-fold) and flow rate (2-fold) relative to their wt counterparts. ESL thickness in tg6 mice was substantially smaller (median, 0.13 μm) than in control mice (median, 0.52 μm). Flow simulations show that the increase in luminal vessel diameter in tg6 mice due to the reduced ESL accounts for less than 20% of the maintenance of network flow resistance. The simulations further indicate that only the integrative effect of several compensatory mechanisms (increased cell flexibility, larger cell volume, Fåhræus-Lindqvist effect, increased vascular volume, and diminished ESL) could keep flow resistance similar to wt levels, despite the much higher Hct. Upon hemodilution of tg6 mice to an Hct of 0.50, ESL thickness increased almost to wt levels (median, 0.42 μm), as did flow velocity and flow rate. This relatively rapid reconstitution of physiological ESL thickness suggests that compression, i.e. mechanical interaction between the blood and the endothelium, rather than chemical degradation is the primary mechanism of its initial reduction.

In conclusion, excessive Hct levels in tg6 mice are associated with a reversible loss of ESL thickness. This contributes, in part, to compensation of increased flow resistance. However, it may also evoke pathophysiological effects linked to an impaired function of the blood-EC interface, suggesting that the pathological phenomena previously observed in tg6 mice (chronic multiple organ damage, EC degeneration) might relate predominantly to the biological implications of the nearly abolished ESL rather than to compromised hemodynamic conditions.

6. Zusammenfassung

Es ist bekannt, daß ein erhöhter systemischer Hämatokrit (Hkt) das Risiko für Herz-Kreislaufkrankungen, wie beispielsweise venöse Thrombosen, Herzinfarkt und Schlaganfall, erhöht. Neben einer Verschlechterung der Hämodynamik durch die erhöhte Blutviskosität und den erhöhten Strömungswiderstand stellt die Störung des Blut-Endothel Interfaces einen anderen möglichen Pathomechanismus dar. Es ist gezeigt worden, daß das strömende Blut über eine etwa 0,5 μm dicke Schicht, genannt Glykokalyx oder auch endotheliale Oberflächenschicht (ESL), mit der Gefäßwand interagiert. Diese Schicht ist in zahlreiche physiologische und pathophysiologische Prozesse involviert, wie beispielsweise Entzündung, transendothelialer Molekültransport und Atherosklerose. Die Auswirkungen von erhöhtem Hämatokrit auf die funktionellen Eigenschaften dieses Interfaces in Mikrogefäßen sind nur unvollständig verstanden.

Um die Auswirkungen eines erhöhten Hämatokrits auf die ESL-Dicke, die mikrovaskuläre Hämodynamik- und Rheologie zu untersuchen, wurde ein transgener Mausstamm (tg6) verwendet. Durch Überexpression von Erythropoetin erreichen diese Mäuse Hämatokritwerte von etwa 0,85, zeigen aber dennoch einen normalen peripheren Strömungswiderstand. Intravitalmikroskopie von post-kapillären Venolen des M. cremaster ($n_{\text{Gefäß}} = 32$) vor und nach Hämodilution wurde mit einer mikropartikulären Geschwindigkeitsmessung (μ -PIV) kombiniert, um bestimmte Strömungsparameter (Strömungsgeschwindigkeit, Scherrate, Schubspannung, Fließrate) und die ESL-Dicke zu bestimmen. C57 Wildtyp Mäuse (wt, Hkt 0,46) dienten als Kontrollgruppe ($n_{\text{Gefäß}} = 37$). Ein Strömungssimulationsmodell wurde verwendet, um die Auswirkungen von Veränderungen des Hämatokrits und der ESL-Dicke auf den Strömungswiderstand eines Gefäßnetzwerkes quantitativ zu beurteilen.

Tg6 Mäuse zeigten eine Verminderung der Strömungsgeschwindigkeit (2,5-fach) und der Fließrate (2-fach) relativ zu den Kontrolltieren. Die Dicke der ESL in tg6 Mäusen (Median 0,13 μm) war deutlich geringer als in den wt Mäusen (Median 0,52 μm). Die Strömungssimulationen zeigen, daß die Vergrößerung des Gefäßlumens, bedingt durch den fast kompletten Verlust der ESL, weniger als 20% zur Aufrechterhaltung des Strömungswiderstands der tg6 Mäuse beiträgt. Erst durch die Kombination verschiedener Kompensationsmechanismen (Erhöhung von Erythrozytenflexibilität, vergrößertes Zellvolumen, Fåhræus-Lindqvist Effekt, vergrößertes Gefäßvolumen und reduzierte ESL)

kann der Netzwerkwiderstand - trotz stark erhöhtem Hämatokrit - auf dem Niveau der wt Mäuse gehalten werden. Nach Hämodilution der transgenen Tiere auf einen Hämatokrit von 0,50 stieg die ESL-Dicke (Median 0,42 μm) ebenso wie Strömungsgeschwindigkeit und Fließrate nahezu auf die entsprechenden Werte der Kontrolltiere an. Diese relativ schnelle Wiederherstellung einer physiologischen ESL-Dicke legt nahe, daß ihre ursprüngliche Verringerung weniger auf chemischen Abbau als auf Kompression, d.h. mechanische Interaktion zwischen Blut und Endothel, zurückzuführen ist.

Es lässt sich konkludieren, daß extrem hohe Hämatokritwerte mit einem reversiblen Verlust der ESL assoziiert sind. Das trägt dazu bei, die hämatokritbedingte Zunahme des Strömungswiderstands auszugleichen. Es kann aber andererseits auch pathophysiologische Effekte hervorrufen, welche mit gestörter Funktion des Blut-Endothel Interfaces verknüpft sind. In Analogie dazu könnten die für diese Tiere bereits bekannten pathophysiologischen Effekte des hohen Hämokrits (Multiorganschäden, endotheliale Degeneration) eher mit den biologischen Implikationen einer stark reduzierten ESL assoziiert sein als mit einer Verschlechterung der Hämodynamik.

7. References

7.1. Literature

1. Albrecht KH, Gaehtgens P, Pries A, et al. The Fahraeus effect in narrow capillaries (i.d. 3.3 to 11.0 micron). *Microvasc Res* 1979; 18(1): 33-47.
2. Allport LE, Parsons MW, Butcher KS, et al. Elevated hematocrit is associated with reduced reperfusion and tissue survival in acute stroke. *Neurology* 2005; 65(9): 1382-7.
3. Arisaka T, Mitsumata M, Kawasumi M, et al. Effects of shear stress on glycosaminoglycan synthesis in vascular endothelial cells. *Ann N Y Acad Sci* 1995; 748: 543-54.
4. Baez S. An open cremaster muscle preparation for the study of blood vessels by in vivo microscopy. *Microvasc Res* 1973; 5(3): 384-94.
5. Baldwin AL and Winlove CP. Effects of perfusate composition on binding of ruthenium red and gold colloid to glycocalyx of rabbit aortic endothelium. *J Histochem Cytochem* 1984; 32(3): 259-66.
6. Barbee JH and Cokelet GR. The Fahraeus effect. *Microvasc Res* 1971; 3(1): 6-16.
7. Barker A, Konopatskaya O, Near C, et al. Observation and characterisation of the glycocalyx of viable human endothelial cells using confocal laser scanning microscopy. *Phys. Chem. Chem. Phys.* 2004; 6: 1006-1011.
8. Barrio Rendo ME. Erythropoietin requirement for the maintenance of normal levels of erythropoiesis in the normal adult mouse. *Acta Physiol Pharmacol Ther Latinoam* 1997; 47(4): 225-8.
9. Bateman RM, Jagger JE, Sharpe MD, et al. Erythrocyte deformability is a nitric oxide-mediated factor in decreased capillary density during sepsis. *Am J Physiol Heart Circ Physiol* 2001; 280(6): H2848-56.
10. Beall CM and Goldstein MC. Hemoglobin concentration of pastoral nomads permanently resident at 4,850-5,450 meters in Tibet. *Am J Phys Anthropol* 1987; 73(4): 433-8.
11. Beall CM, Brittenham GM, Strohl KP, et al. Hemoglobin concentration of high-altitude Tibetans and Bolivian Aymara. *Am J Phys Anthropol* 1998; 106(3): 385-400.
12. Beall CM. Oxygen saturation increases during childhood and decreases during adulthood among high altitude native Tibetans residing at 3,800-4,200m. *High Alt Med Biol* 2000; 1(1): 25-32.
13. Beall CM, Laskowski D, Strohl KP, et al. Pulmonary nitric oxide in mountain dwellers. *Nature* 2001; 414(6862): 411-2.
14. Beall CM. High-altitude adaptations. *Lancet* 2003; 362 Suppl: s14-5.
15. Beall CM, Song K, Elston RC, et al. Higher offspring survival among Tibetan women with high oxygen saturation genotypes residing at 4,000 m. *Proc Natl Acad Sci U S A* 2004; 101(39): 14300-4.
16. Beckman JS, Beckman TW, Chen J, et al. Apparent hydroxyl radical production by peroxynitrite: implications for endothelial injury from nitric oxide and superoxide. *Proc Natl Acad Sci U S A* 1990; 87(4): 1620-4.
17. Bertinieri G, Parati G, Ulian L, et al. Hemodilution reduces clinic and ambulatory blood pressure in polycythemic patients. *Hypertension* 1998; 31(3): 848-53.
18. Bogdanova A, Mihov D, Lutz H, et al. Enhanced erythro-phagocytosis in polycythemic mice overexpressing erythropoietin. *Blood* 2007; 110(2): 762-9.
19. Bor-Kucukatay M, Wenby RB, Meiselman HJ, et al. Effects of nitric oxide on red blood cell deformability. *Am J Physiol Heart Circ Physiol* 2003; 284(5): H1577-84.

20. Braide M, Amundson B, Chien S, et al. Quantitative studies on the influence of leukocytes on the vascular resistance in a skeletal muscle preparation. *Microvasc Res* 1984; 27(3): 331-52.
21. Brown DW, Giles WH and Croft JB. Hematocrit and the risk of coronary heart disease mortality. *Am Heart J* 2001; 142(4): 657-63.
22. Bugliarello G and Hayden JW. Detailed characteristics of the flow of blood in vitro. *Trans Soc Rheol* 1963; 7: 209-230.
23. Burch G. Erythrocytosis and ischemic myocardial disease. *Am Heart J* 1961; 62: 139-40.
24. Cabrales P. Effects of erythrocyte flexibility on microvascular perfusion and oxygenation during acute anemia. *Am J Physiol Heart Circ Physiol* 2007; 293(2): H1206-15.
25. Casadevall N and Vainchenker W. [Erythropoiesis and its regulation]. *Rev Prat* 1993; 43(11): 1335-40.
26. Chen X, Jaron D, Barbee KA, et al. The influence of radial RBC distribution, blood velocity profiles, and glycocalyx on coupled NO/O₂ transport. *J Appl Physiol* 2006; 100(2): 482-92.
27. Cheng TO. High hematocrit value is a risk factor for myocardial infarction. *J Thorac Cardiovasc Surg* 1999; 117(1): 199-200.
28. Chien S, Usami S, Taylor HM, et al. Effects of hematocrit and plasma proteins on human blood rheology at low shear rates. *J Appl Physiol* 1966; 21(1): 81-7.
29. Chien S, Usami S, Dellenback RJ, et al. Blood Viscosity: Influence of Erythrocyte Deformation. *Science* 1967; 157(3790): 827-829.
30. Chien S. Red cell deformability and its relevance to blood flow. *Annu Rev Physiol* 1987; 49: 177-92.
31. Chievitz E and Thiede T. Complications and causes of death in polycythaemia vera. *Acta Med Scand* 1962; 172: 513-23.
32. Cinar Y, Demir G, Pac M, et al. Effect of hematocrit on blood pressure via hyperviscosity. *Am J Hypertens* 1999; 12(7): 739-43.
33. Cokelet GR and Goldsmith HL. Decreased hydrodynamic resistance in the two-phase flow of blood through small vertical tubes at low flow rates. *Circ Res* 1991; 68(1): 1-17.
34. Cokelet GR. Poiseuille Award Lecture. Viscometric, in vitro and in vivo blood viscosity relationships: how are they related? *Biorheology* 1999; 36(5-6): 343-58.
35. Constantinescu AA, Vink H and Spaan JA. Elevated capillary tube hematocrit reflects degradation of endothelial cell glycocalyx by oxidized LDL. *Am J Physiol Heart Circ Physiol* 2001; 280(3): H1051-7.
36. Damiano ER. The effect of the endothelial-cell glycocalyx on the motion of red blood cells through capillaries. *Microvasc Res* 1998; 55(1): 77-91.
37. Damiano ER and Stace TM. A mechano-electrochemical model of radial deformation of the capillary glycocalyx. *Biophys J* 2002; 82(3): 1153-75.
38. Damiano ER, Long DR, El-Khatib FH, et al. On the motion of a sphere in a Stokes flow parallel to a Brinkman half-space. *J Fluid Mech* 2004; 500: 75-101.
39. Damiano ER, Long DR and Smith ML. Estimation of viscosity profiles using velocimetry data from parallel flow of linearly viscous fluids: application to microvascular haemodynamics. *J Fluid Mech* 2004; 512: 1-19.
40. Danesh J, Collins R, Peto R, et al. Haematocrit, viscosity, erythrocyte sedimentation rate: meta-analyses of prospective studies of coronary heart disease. *Eur Heart J* 2000; 21(7): 515-20.
41. Delvos U, Preissner KT and Muller-Berghaus G. Binding of fibrinogen to cultured bovine endothelial cells. *Thromb Haemost* 1985; 53(1): 26-31.

42. Desjardins C and Duling BR. Microvessel hematocrit: measurement and implications for capillary oxygen transport. *Am J Physiol* 1987; 252(3 Pt 2): H494-503.
43. Desjardins C and Duling BR. Heparinase treatment suggests a role for the endothelial cell glycocalyx in regulation of capillary hematocrit. *Am J Physiol* 1990; 258(3 Pt 2): H647-54.
44. Driessen GK, Fischer TM, Haest CW, et al. Flow behaviour of rigid red blood cells in the microcirculation. *Int J Microcirc Clin Exp* 1984; 3(2): 197-210.
45. Droma Y, Hanaoka M, Basnyat B, et al. Genetic contribution of the endothelial nitric oxide synthase gene to high altitude adaptation in sherpas. *High Alt Med Biol* 2006; 7(3): 209-20.
46. Eckardt KU, Boutellier U, Kurtz A, et al. Rate of erythropoietin formation in humans in response to acute hypobaric hypoxia. *J Appl Physiol* 1989; 66(4): 1785-8.
47. Erikssen G, Thaulow E, Sandvik L, et al. Haematocrit: a predictor of cardiovascular mortality? *J Intern Med* 1993; 234(5): 493-9.
48. Fahraeus R. The suspension stability of the blood. *Physiol Rev* 1929; 9: 33-47.
49. Fahraeus R, and Lindqvist, T. The viscosity of the blood in narrow capillary tubes. *Am J Physiol* 1931; 96: 562-568.
50. Feng J and Weinbaum S. Lubrication theory in highly compressible porous media: the mechanics of skiing, from red cells to humans. *J. Fluid Mech.* 2000; 422: 281-317.
51. Fenton BM, Carr RT and Cokelet GR. Nonuniform red cell distribution in 20 to 100 micrometers bifurcations. *Microvasc Res* 1985; 29(1): 103-26.
52. Fernandez-Luna JL, Silva M, Richard C, et al. Pathogenesis of polycythemia vera. *Haematologica* 1998; 83(2): 150-8.
53. Frasher WG, Jr. Preparation of living tissues for microscopy. *Microvasc Res* 1973; 5(3): 430-5.
54. Frietsch T, Gassmann M, Groth G, et al. Excessive erythrocytosis does not elevate capillary oxygen delivery in subcutaneous mouse tissue. *Microcirculation* 2007; 14(2): 111-23.
55. Frietsch T, Maurer MH, Vogel J, et al. Reduced cerebral blood flow but elevated cerebral glucose metabolic rate in erythropoietin overexpressing transgenic mice with excessive erythrocytosis. *J Cereb Blood Flow Metab* 2007; 27(3): 469-76.
56. Fujimaki T, Matsutani M, Asai A, et al. Cerebral venous thrombosis due to high-altitude polycythemia. Case report. *J Neurosurg* 1986; 64(1): 148-50.
57. Fujimoto N, Matsubayashi K, Miyahara T, et al. The risk factors for ischemic heart disease in Tibetan highlanders. *Jpn Heart J* 1989; 30(1): 27-34.
58. Gagnon DR, Zhang TJ, Brand FN, et al. Hematocrit and the risk of cardiovascular disease--the Framingham study: a 34-year follow-up. *Am Heart J* 1994; 127(3): 674-82.
59. Gao L and Lipowsky HH. Measurement of solute transport in the endothelial glycocalyx using indicator dilution techniques. *Ann Biomed Eng* 2009; 37(9): 1781-95.
60. Gelfi C, De Palma S, Ripamonti M, et al. New aspects of altitude adaptation in Tibetans: a proteomic approach. *Faseb J* 2004; 18(3): 612-4.
61. Gobel BO, Schulte-Gobel A, Weisser B, et al. Arterial blood pressure. Correlation with erythrocyte count, hematocrit, and hemoglobin concentration. *Am J Hypertens* 1991; 4(1 Pt 1): 14-9.
62. Gonzales GF. Peruvian contributions to the study on human reproduction at high altitude: from the chronicles of the Spanish conquest to the present. *Respir Physiol Neurobiol* 2007; 158(2-3): 172-9.
63. Goubali A, Voukiklaris G, Kritsikis S, et al. Relation of hematocrit values to coronary heart disease, arterial hypertension, and respiratory impairment in occupational and population groups of the Athens area. *Angiology* 1995; 46(8): 719-25.

64. Greksa LP. Growth and development of Andean high altitude residents. *High Alt Med Biol* 2006; 7(2): 116-24.
65. Gretz JE and Duling BR. Measurement uncertainties associated with the use of bright-field and fluorescence microscopy in the microcirculation. *Microvasc Res* 1995; 49(1): 134-40.
66. Guyton AC and Richardson TQ. Effect of hematocrit on venous return. *Circ Res* 1961; 9: 157-64.
67. Harrison MJ, Pollock SS and Weisblatt E. Haematocrit and platelet aggregation. *Lancet* 1984; 2(8409): 991-2.
68. Hasegawa J, Wagner KF, Karp D, et al. Altered pulmonary vascular reactivity in mice with excessive erythrocytosis. *Am J Respir Crit Care Med* 2004; 169(7): 829-35.
69. He A, Azarov I and Kim-Shapiro DB. The role of nitric oxide in regulation of red blood cell deformability. in *Fourth International Conference on Biology, Chemistry and Therapeutic Applications of Nitric Oxide*. 2006. Monterey, CA.
70. Heinicke K, Baum O, Ogunshola OO, et al. Excessive erythrocytosis in adult mice overexpressing erythropoietin leads to hepatic, renal, neuronal, and muscular degeneration. *Am J Physiol Regul Integr Comp Physiol* 2006; 291(4): R947-56.
71. Henry CB and Duling BR. Permeation of the luminal capillary glycocalyx is determined by hyaluronan. *Am J Physiol* 1999; 277(2 Pt 2): H508-14.
72. Henry CB and Duling BR. TNF-alpha increases entry of macromolecules into luminal endothelial cell glycocalyx. *Am J Physiol Heart Circ Physiol* 2000; 279(6): H2815-23.
73. Ho V, Acquaviva A, Duh E, et al. Use of a marked erythropoietin gene for investigation of its cis-acting elements. *J Biol Chem* 1995; 270(17): 10084-90.
74. Hofer T, Wenger H and Gassmann M. Oxygen sensing, HIF-1alpha stabilization and potential therapeutic strategies. *Pflugers Arch* 2002; 443(4): 503-7.
75. Hu X and Weinbaum S. A new view of Starling's hypothesis at the microstructural level. *Microvasc Res* 1999; 58(3): 281-304.
76. Irace C, Ciamei M, Crivaro A, et al. Hematocrit is associated with carotid atherosclerosis in men but not in women. *Coron Artery Dis* 2003; 14(4): 279-84.
77. Jaillard AS, Hommel M and Mazetti P. Prevalence of stroke at high altitude (3380 m) in Cuzco, a town of Peru. A population-based study. *Stroke* 1995; 26(4): 562-8.
78. Jefferson JA, Escudero E, Hurtado ME, et al. Excessive erythrocytosis, chronic mountain sickness, and serum cobalt levels. *Lancet* 2002; 359(9304): 407-8.
79. Jelkmann W. Molecular biology of erythropoietin. *Intern Med* 2004; 43(8): 649-59.
80. Jha SK, Anand AC, Sharma V, et al. Stroke at high altitude: Indian experience. *High Alt Med Biol* 2002; 3(1): 21-7.
81. Juvonen E, Ikkala E, Fyhrquist F, et al. Autosomal dominant erythrocytosis caused by increased sensitivity to erythropoietin. *Blood* 1991; 78(11): 3066-9.
82. Kameneva MV, Antaki JF, Borovetz HS, et al. Mechanisms of red blood cell trauma in assisted circulation. Rheologic similarities of red blood cell transformations due to natural aging and mechanical stress. *Asaio J* 1995; 41(3): M457-60.
83. Karino T and Goldsmith HL. Role of blood cell-wall interactions in thrombogenesis and atherogenesis: a microrheological study. *Biorheology* 1984; 21(4): 587-601.
84. Kiani MF, Cokelet GR and Sarelius IH. Effect of diameter variability along a microvessel segment on pressure drop. *Microvasc Res* 1993; 45(3): 219-32.
85. Kim S, Kong RL, Popel AS, et al. Temporal and spatial variations of cell-free layer width in arterioles. *Am J Physiol Heart Circ Physiol* 2007; 293(3): H1526-35.
86. Kitani K, Osawa T and Yokozawa T. The effects of tetrahydrocurcumin and green tea polyphenol on the survival of male C57BL/6 mice. *Biogerontology* 2007; 8(5): 567-73.

87. Kiyohara Y, Ueda K, Hasuo Y, et al. Hematocrit as a risk factor of cerebral infarction: long-term prospective population survey in a Japanese rural community. *Stroke* 1986; 17(4): 687-92.
88. Klitzman B and Duling BR. Microvascular hematocrit and red cell flow in resting and contracting striated muscle. *Am J Physiol* 1979; 237(4): H481-90.
89. Kober F, Iltis I, Cozzone PJ, et al. Myocardial blood flow mapping in mice using high-resolution spin labeling magnetic resonance imaging: influence of ketamine/xylazine and isoflurane anesthesia. *Magn Reson Med* 2005; 53(3): 601-6.
90. Köhler A. Ein neues Belichtungsverfahren für mikrographische Zwecke. *Zeitschrift für wissenschaftliche Mikroskopie und für mikroskopische Technik* 1893; 10(4): 433-440.
91. Leon-Velarde F, Maggiorini M, Reeves JT, et al. Consensus statement on chronic and subacute high altitude diseases. *High Alt Med Biol* 2005; 6(2): 147-57.
92. Lipowsky HH, Kovalcheck S and Zweifach BW. The distribution of blood rheological parameters in the microvasculature of cat mesentery. *Circ Res* 1978; 43(5): 738-49.
93. Lipowsky HH, Usami S and Chien S. In vivo measurements of "apparent viscosity" and microvessel hematocrit in the mesentery of the cat. *Microvasc Res* 1980; 19(3): 297-319.
94. Lipowsky HH and Firrell JC. Microvascular hemodynamics during systemic hemodilution and hemoconcentration. *Am J Physiol* 1986; 250(6 Pt 2): H908-22.
95. Lipowsky HH, Cram LE, Justice W, et al. Effect of erythrocyte deformability on in vivo red cell transit time and hematocrit and their correlation with in vitro filterability. *Microvasc Res* 1993; 46(1): 43-64.
96. Long DS, Smith ML, Pries AR, et al. Microviscometry reveals reduced blood viscosity and altered shear rate and shear stress profiles in microvessels after hemodilution. *Proc Natl Acad Sci U S A* 2004; 101(27): 10060-5.
97. Lowe GD and Forbes CD. Platelet aggregation, haematocrit, and fibrinogen. *Lancet* 1985; 1(8425): 395-6.
98. Lowe GD, Lee AJ, Rumley A, et al. Blood viscosity and risk of cardiovascular events: the Edinburgh Artery Study. *Br J Haematol* 1997; 96(1): 168-73.
99. Maeda N, Suzuki Y, Tanaka J, et al. Erythrocyte flow and elasticity of microvessels evaluated by marginal cell-free layer and flow resistance. *Am J Physiol* 1996; 271(6 Pt 2): H2454-61.
100. Martini J, Carpentier B, Negrete AC, et al. Paradoxical hypotension following increased hematocrit and blood viscosity. *Am J Physiol Heart Circ Physiol* 2005; 289(5): H2136-43.
101. Martini J, Tsai AG, Cabrales P, et al. Increased cardiac output and microvascular blood flow during mild hemoconcentration in hamster window model. *Am J Physiol Heart Circ Physiol* 2006; 291(1): H310-7.
102. Martini P, Pierach A and Schreyer E. Die Strömung des Blutes in engen Gefäßen. Eine Abweichung vom Poiseuille'schen Gesetz. *Dt Arch Klin Med* 1930; 169: 212-222.
103. Maurer MH, Frietsch T, Waschke KF, et al. Cerebral transcriptome analysis of transgenic mice overexpressing erythropoietin. *Neurosci Lett* 2002; 327(3): 181-4.
104. Megens RTA, Reitsma S, Schiffers PHM, et al. Two-Photon Microscopy of Vital Murine Elastic and Muscular Arteries. *J Vasc Res* 2007; 44: 87-98.
105. Moore LG, Curran-Everett L, Droma TS, et al. Are Tibetans better adapted? *Int J Sports Med* 1992; 13 Suppl 1: S86-8.
106. Moore LG. Human genetic adaptation to high altitude. *High Alt Med Biol* 2001; 2(2): 257-79.
107. Mulivor AW and Lipowsky HH. Inflammation- and ischemia-induced shedding of venular glycocalyx. *Am J Physiol Heart Circ Physiol* 2004; 286(5): H1672-80.

108. Neuhaus D, Fedde MR and Gaehtgens P. Changes in haemorheology in the racing greyhound as related to oxygen delivery. *Eur J Appl Physiol Occup Physiol* 1992; 65(3): 278-85.
109. Neunteufl T, Heher S, Stefenelli T, et al. Endothelial dysfunction in patients with polycythaemia vera. *Br J Haematol* 2001; 115(2): 354-9.
110. Nieuwdorp M, van Haeften TW, Gouverneur MC, et al. Loss of endothelial glycocalyx during acute hyperglycemia coincides with endothelial dysfunction and coagulation activation in vivo. *Diabetes* 2006; 55(2): 480-6.
111. Nishikido N, Kobayashi T and Kashiwazaki H. Hematocrit correlates with blood pressure in young male office workers. *Ind Health* 1999; 37(1): 76-81.
112. Ogunshola OO, Djonov V, Staudt R, et al. Chronic excessive erythrocytosis induces endothelial activation and damage in mouse brain. *Am J Physiol Regul Integr Comp Physiol* 2006; 290(3): R678-84.
113. Osterloh K, Ewert U and Pries AR. Interaction of albumin with the endothelial cell surface. *Am J Physiol Heart Circ Physiol* 2002; 283(1): H398-405.
114. Penalzoza D and Arias-Stella J. The heart and pulmonary circulation at high altitudes: healthy highlanders and chronic mountain sickness. *Circulation* 2007; 115(9): 1132-46.
115. Pereira AA and Sarnak MJ. Anemia as a risk factor for cardiovascular disease. *Kidney Int Suppl* 2003(87): S32-9.
116. Platts SH, Linden J and Duling BR. Rapid modification of the glycocalyx caused by ischemia-reperfusion is inhibited by adenosine A2A receptor activation. *Am J Physiol Heart Circ Physiol* 2003; 284(6): H2360-7.
117. Potter DR and Damiano ER. The hydrodynamically relevant endothelial cell glycocalyx observed in vivo is absent in vitro. *Circ Res* 2008; 102(7): 770-6.
118. Prchal JT, Crist WM, Goldwasser E, et al. Autosomal dominant polycythemia. *Blood* 1985; 66(5): 1208-14.
119. Pries AR, Ley K and Gaehtgens P. Generalization of the Fahraeus principle for microvessel networks. *Am J Physiol* 1986; 251(6 Pt 2): H1324-32.
120. Pries AR, Ley K, Claassen M, et al. Red cell distribution at microvascular bifurcations. *Microvasc Res* 1989; 38(1): 81-101.
121. Pries AR, Secomb TW, Gaehtgens P, et al. Blood flow in microvascular networks. Experiments and simulation. *Circ Res* 1990; 67(4): 826-34.
122. Pries AR, Fritzsche A, Ley K, et al. Redistribution of red blood cell flow in microcirculatory networks by hemodilution. *Circ Res* 1992; 70(6): 1113-21.
123. Pries AR, Neuhaus D and Gaehtgens P. Blood viscosity in tube flow: dependence on diameter and hematocrit. *Am J Physiol* 1992; 263(6 Pt 2): H1770-8.
124. Pries AR, Secomb TW, Gessner T, et al. Resistance to blood flow in microvessels in vivo. *Circ Res* 1994; 75(5): 904-15.
125. Pries AR, Secomb TW and Gaehtgens P. Relationship between structural and hemodynamic heterogeneity in microvascular networks. *Am J Physiol* 1996; 270(2 Pt 2): H545-53.
126. Pries AR, Secomb TW and Gaehtgens P. Biophysical aspects of blood flow in the microvasculature. *Cardiovasc Res* 1996; 32(4): 654-67.
127. Pries AR, Schonfeld D, Gaehtgens P, et al. Diameter variability and microvascular flow resistance. *Am J Physiol* 1997; 272(6 Pt 2): H2716-25.
128. Pries AR, Secomb TW, Jacobs H, et al. Microvascular blood flow resistance: role of endothelial surface layer. *Am J Physiol* 1997; 273(5 Pt 2): H2272-9.
129. Pries AR, Secomb TW, Sperandio M, et al. Blood flow resistance during hemodilution: effect of plasma composition. *Cardiovasc Res* 1998; 37(1): 225-35.
130. Pries AR, Secomb TW and Gaehtgens P. The endothelial surface layer. *Pflugers Arch* 2000; 440(5): 653-66.

131. Pries AR and Secomb TW. Rheology of the microcirculation. *Clin Hemorheol Microcirc* 2003; 29(3-4): 143-8.
132. Pries AR and Secomb TW. Microvascular blood viscosity in vivo and the endothelial surface layer. *Am J Physiol Heart Circ Physiol* 2005; 289(6): H2657-64.
133. Quaschnig T, Ruschitzka F, Stallmach T, et al. Erythropoietin-induced excessive erythrocytosis activates the tissue endothelin system in mice. *Faseb J* 2003; 17(2): 259-61.
134. Rampling MW. Hyperviscosity as a complication in a variety of disorders. *Semin Thromb Hemost* 2003; 29(5): 459-65.
135. Reinhart WH, Boulanger CM, Luscher TF, et al. Influence of endothelial surface on flow velocity in vitro. *Am J Physiol* 1993; 265(2 Pt 2): H523-9.
136. Reinke W, Johnson PC and Gaetgens P. Effect of shear rate variation on apparent viscosity of human blood in tubes of 29 to 94 microns diameter. *Circ Res* 1986; 59(2): 124-32.
137. Reitsma S, Slaaf DW, Vink H, et al. The endothelial glycocalyx: composition, functions, and visualization. *Pflugers Arch* 2007; 454(3): 345-59.
138. Richardson TQ and Guyton AC. Effects of polycythemia and anemia on cardiac output and other circulatory factors. *Am J Physiol* 1959; 197(6): 1167-1170.
139. Robertson SA. Oxygenation and ventilation. In: Green SA (ed.) *Veterinary anesthesia and pain management secrets*, Philadelphia: Hanley & Belfus Inc., (2002): 15-19.
140. Rubio-Gayosso I, Platts SH and Duling BR. Reactive oxygen species mediate modification of glycocalyx during ischemia-reperfusion injury. *Am J Physiol Heart Circ Physiol* 2006; 290(6): H2247-56.
141. Ruschitzka FT, Wenger RH, Stallmach T, et al. Nitric oxide prevents cardiovascular disease and determines survival in polyglobulic mice overexpressing erythropoietin. *Proc Natl Acad Sci U S A* 2000; 97(21): 11609-13.
142. Sacco S, Marini C, Olivieri L, et al. Contribution of hematocrit to early mortality after ischemic stroke. *Eur Neurol* 2007; 58(4): 233-8.
143. Sarkar S and Rosenkrantz TS. Neonatal polycythemia and hyperviscosity. *Semin Fetal Neonatal Med* 2008; 13(4): 248-55.
144. Schneeberger EE and Hamelin M. Interaction of serum proteins with lung endothelial glycocalyx: its effect on endothelial permeability. *Am J Physiol* 1984; 247(2 Pt 2): H206-17.
145. Schuler B, Arras M, Keller S, et al. Optimal hematocrit for maximal exercise performance in acute and chronic erythropoietin-treated mice. *Proc Natl Acad Sci U S A* 2010; 107(1): 419-23.
146. Schunkert H, Koenig W, Brockel U, et al. Haematocrit profoundly affects left ventricular diastolic filling as assessed by Doppler echocardiography. *J Hypertens* 2000; 18(10): 1483-9.
147. Schunkert H and Hense HW. A heart price to pay for anaemia. *Nephrol Dial Transplant* 2001; 16(3): 445-8.
148. Seaman GV and Swank RL. The influence of electrokinetic charge and deformability of the red blood cell on the flow properties of its suspensions. *Biorheology* 1967; 4(2): 47-59.
149. Secomb TW, Hsu R and Pries AR. A model for red blood cell motion in glycocalyx-lined capillaries. *Am J Physiol* 1998; 274(3 Pt 2): H1016-22.
150. Secomb TW, Hsu R and Pries AR. Effect of the endothelial surface layer on transmission of fluid shear stress to endothelial cells. *Biorheology* 2001; 38(2-3): 143-50.

151. Secomb TW, Hsu R and Pries AR. Motion of red blood cells in a capillary with an endothelial surface layer: effect of flow velocity. *Am J Physiol Heart Circ Physiol* 2001; 281(2): H629-36.
152. Secomb TW, Hsu R and Pries AR. Blood flow and red blood cell deformation in nonuniform capillaries: effects of the endothelial surface layer. *Microcirculation* 2002; 9(3): 189-96.
153. Semenza GL. HIF-1, O(2), and the 3 PHDs: how animal cells signal hypoxia to the nucleus. *Cell* 2001; 107(1): 1-3.
154. Sharan M and Popel AS. A two-phase model for flow of blood in narrow tubes with increased effective viscosity near the wall. *Biorheology* 2001; 38(5-6): 415-28.
155. Shibata J, Hasegawa J, Siemens HJ, et al. Hemostasis and coagulation at a hematocrit level of 0.85: functional consequences of erythrocytosis. *Blood* 2003; 101(11): 4416-22.
156. Shiga T, Sekiya M, Maeda N, et al. Cell age-dependent changes in deformability and calcium accumulation of human erythrocytes. *Biochim Biophys Acta* 1985; 814(2): 289-99.
157. Shiga T, Maeda N and Kon K. Erythrocyte rheology. *Crit Rev Oncol Hematol* 1990; 10(1): 9-48.
158. Silberberg A. Polyelectrolytes at the endothelial cell surface. *Biophys Chem* 1991; 41(1): 9-13.
159. Silva M, Grillot D, Benito A, et al. Erythropoietin can promote erythroid progenitor survival by repressing apoptosis through Bcl-XL and Bcl-2. *Blood* 1996; 88(5): 1576-82.
160. Silva M, Benito A, Sanz C, et al. Erythropoietin can induce the expression of bcl-x(L) through Stat5 in erythropoietin-dependent progenitor cell lines. *J Biol Chem* 1999; 274(32): 22165-9.
161. Simchon S, Jan KM and Chien S. Influence of reduced red cell deformability on regional blood flow. *Am J Physiol* 1987; 253(4 Pt 2): H898-903.
162. Sims DE, Westfall JA, Kiorpes AL, et al. Preservation of tracheal mucus by nonaqueous fixative. *Biotech Histochem* 1991; 66(4): 173-80.
163. Slowinski T, Schulz N, Ruschitzka FT, et al. Pattern of prepro-endothelin-1 expression revealed by reporter-gene activity in kidneys of erythropoietin-overexpressing mice. *Clin Sci (Lond)* 2002; 103 Suppl 48: 44S-47S.
164. Smith ML, Long DS, Damiano ER, et al. Near-wall micro-PIV reveals a hydrodynamically relevant endothelial surface layer in venules in vivo. *Biophys J* 2003; 85(1): 637-45.
165. Smith WC, Lowe GD, Lee AJ, et al. Rheological determinants of blood pressure in a Scottish adult population. *J Hypertens* 1992; 10(5): 467-72.
166. Sorlie PD, Garcia-Palmieri MR, Costas R, Jr., et al. Hematocrit and risk of coronary heart disease: the Puerto Rico Health Program. *Am Heart J* 1981; 101(4): 456-61.
167. Soutani M, Suzuki Y, Tateishi N, et al. Quantitative evaluation of flow dynamics of erythrocytes in microvessels: influence of erythrocyte aggregation. *Am J Physiol* 1995; 268(5 Pt 2): H1959-65.
168. Spencer CG, Felmeden DC, Blann AD, et al. Haemorheological, platelet and endothelial indices in relation to global measures of cardiovascular risk in hypertensive patients: a substudy of the Anglo-Scandinavian Cardiac Outcomes Trial. *J Intern Med* 2007; 261(1): 82-90.
169. Spiess BD, Ley C, Body SC, et al. Hematocrit value on intensive care unit entry influences the frequency of Q-wave myocardial infarction after coronary artery bypass grafting. The Institutions of the Multicenter Study of Perioperative Ischemia (McSPI) Research Group. *J Thorac Cardiovasc Surg* 1998; 116(3): 460-7.

170. Spivak JL. Polycythemia vera: myths, mechanisms, and management. *Blood* 2002; 100(13): 4272-90.
171. Squire JM, Chew M, Nneji G, et al. Quasi-periodic substructure in the microvessel endothelial glycocalyx: a possible explanation for molecular filtering? *J Struct Biol* 2001; 136(3): 239-55.
172. Stace TM and Damiano ER. An electrochemical model of the transport of charged molecules through the capillary glycocalyx. *Biophys J* 2001; 80(4): 1670-90.
173. Starzyk D, Korbut R and Gryglewski RJ. Effects of nitric oxide and prostacyclin on deformability and aggregability of red blood cells of rats ex vivo and in vitro. *J Physiol Pharmacol* 1999; 50(4): 629-37.
174. Stobdan T, Karar J and Pasha MA. High altitude adaptation: genetic perspectives. *High Alt Med Biol* 2008; 9(2): 140-7.
175. Suzuki Y, Tateishi N, Soutani M, et al. Deformation of erythrocytes in microvessels and glass capillaries: effects of erythrocyte deformability. *Microcirculation* 1996; 3(1): 49-57.
176. Swetnam SM, Yabek SM and Alverson DC. Hemodynamic consequences of neonatal polycythemia. *J Pediatr* 1987; 110(3): 443-7.
177. Tangelder GJ, Slaaf DW, Muijtjens AM, et al. Velocity profiles of blood platelets and red blood cells flowing in arterioles of the rabbit mesentery. *Circ Res* 1986; 59(5): 505-14.
178. Tangelder GJ, Slaaf DW, Arts T, et al. Wall shear rate in arterioles in vivo: least estimates from platelet velocity profiles. *Am J Physiol* 1988; 254(6 Pt 2): H1059-64.
179. Tateishi N, Suzuki Y, Soutani M, et al. Flow dynamics of erythrocytes in microvessels of isolated rabbit mesentery: cell-free layer and flow resistance. *J Biomech* 1994; 27(9): 1119-25.
180. Tateishi N, Suzuki Y, Cicha I, et al. O₂ release from erythrocytes flowing in a narrow O₂-permeable tube: effects of erythrocyte aggregation. *Am J Physiol Heart Circ Physiol* 2001; 281(1): H448-56.
181. van den Berg BM, Vink H and Spaan JA. The endothelial glycocalyx protects against myocardial edema. *Circ Res* 2003; 92(6): 592-4.
182. van den Berg BM, Spaan JA, Rolf TM, et al. Atherogenic region and diet diminish glycocalyx dimension and increase intima-to-media ratios at murine carotid artery bifurcation. *Am J Physiol Heart Circ Physiol* 2006; 290(2): H915-20.
183. van Haaren PM, VanBavel E, Vink H, et al. Localization of the permeability barrier to solutes in isolated arteries by confocal microscopy. *Am J Physiol Heart Circ Physiol* 2003; 285(6): H2848-56.
184. Vargas E and Spielvogel H. Chronic mountain sickness, optimal hemoglobin, and heart disease. *High Alt Med Biol* 2006; 7(2): 138-49.
185. Vasquez R and Villena M. Normal hematological values for healthy persons living at 4000 meters in Bolivia. *High Alt Med Biol* 2001; 2(3): 361-7.
186. Vink H and Duling BR. Identification of distinct luminal domains for macromolecules, erythrocytes, and leukocytes within mammalian capillaries. *Circ Res* 1996; 79(3): 581-9.
187. Vink H, Constantinescu AA and Spaan JA. Oxidized lipoproteins degrade the endothelial surface layer : implications for platelet-endothelial cell adhesion. *Circulation* 2000; 101(13): 1500-2.
188. Vink H and Duling BR. Capillary endothelial surface layer selectively reduces plasma solute distribution volume. *Am J Physiol Heart Circ Physiol* 2000; 278(1): H285-9.
189. Vogel J, Sperandio M, Pries AR, et al. Influence of the endothelial glycocalyx on cerebral blood flow in mice. *J Cereb Blood Flow Metab* 2000; 20(11): 1571-8.

190. Vogel J, Kiessling I, Heinicke K, et al. Transgenic mice overexpressing erythropoietin adapt to excessive erythrocytosis by regulating blood viscosity. *Blood* 2003; 102(6): 2278-84.
191. Wagner KF, Katschinski DM, Hasegawa J, et al. Chronic inborn erythrocytosis leads to cardiac dysfunction and premature death in mice overexpressing erythropoietin. *Blood* 2001; 97(2): 536-42.
192. Wannamethee G, Perry IJ and Shaper AG. Haematocrit, hypertension and risk of stroke. *J Intern Med* 1994; 235(2): 163-8.
193. Wannamethee G, Shaper AG and Whincup PH. Ischaemic heart disease: association with haematocrit in the British Regional Heart Study. *J Epidemiol Community Health* 1994; 48(2): 112-8.
194. Warnke KC and Skalak TC. Leukocyte plugging in vivo in skeletal muscle arteriolar trees. *Am J Physiol* 1992; 262(4 Pt 2): H1149-55.
195. Weinbaum S, Zhang X, Han Y, et al. Mechanotransduction and flow across the endothelial glycocalyx. *Proc Natl Acad Sci U S A* 2003; 100(13): 7988-95.
196. Whitmore RL. *Rheology of the circulation*. 1st ed. Oxford, England: Pergamon Press Ltd., 1968.
197. Wiessner C, Allegrini PR, Ekatodramis D, et al. Increased cerebral infarct volumes in polyglobulic mice overexpressing erythropoietin. *J Cereb Blood Flow Metab* 2001; 21(7): 857-64.
198. Woodward M, Rumley A, Tunstall-Pedoe H, et al. Does sticky blood predict a sticky end? Associations of blood viscosity, haematocrit and fibrinogen with mortality in the West of Scotland. *Br J Haematol* 2003; 122(4): 645-50.
199. Wu Q, Andreopoulos Y and Weinbaum S. From red cells to snowboarding: a new concept for a train track. *Phys Rev Lett* 2004; 93(19): 194501.
200. Wu T and Kayser B. High altitude adaptation in Tibetans. *High Alt Med Biol* 2006; 7(3): 193-208.
201. Zhang J, Johnson PC and Popel AS. Effects of erythrocyte deformability and aggregation on the cell free layer and apparent viscosity of microscopic blood flows. *Microvasc Res* 2009; 77(3): 265-72.
202. Zhao Y, Chien S and Weinbaum S. Dynamic contact forces on leukocyte microvilli and their penetration of the endothelial glycocalyx. *Biophys J* 2001; 80(3): 1124-40.

7.2. Figures

- Figure 1. Relative apparent viscosity (normalized to plasma viscosity) as a function of tube diameter for flow of a rbc suspension with a discharge (or feed) hematocrit of 0.45; the red curve corresponds to best fit to data compiled from several *in vitro* studies [64]; insets show photomicrographs of red blood cells (discharge, or feed hematocrit 0.45) flowing through glass tubes of 3, 7 and 17 μm in diameter..... 3
- Figure 2. Tube hematocrit, H_T , normalized with respect to discharge hematocrit, H_D , as a function of tube diameter (*Fåhræus effect*) for different levels of H_D [68]. 5
- Figure 3. Relative apparent viscosity as a function of discharge hematocrit for distinct tube diameters *in vitro* [64]. 6
- Figure 4. Relative effective viscosity as a function of vessel diameter for different levels of discharge hematocrit, H_D , as calculated with a parametric equation, known as the *in vivo* viscosity law [61]. Symbols represent data derived from *in vivo* measurements of intravascular pressure drop [73,74]. 7
- Figure 5. Model image of capillary blood flow *in vivo* in the presence of a thick, gel-like layer. (adopted from Pries et al. [87]) 8
- Figure 6. Schematic image of the composition of the ESL including a thin layer of membrane-bound molecules (glycocalyx) and a thick layer of transiently attached soluble plasma components. (Based on Pries *et al.* [88]) 10
- Figure 7. Predictions of relative effective viscosity as a function of diameter *in vivo* (heavy lines) for distinct levels of discharge hematocrit, H_D , involving the effect of a possibly diameter-dependent ESL thickness [76]; by comparison, respective *in vitro* viscosity data [61,64] is delineated (thin lines). 11
- Figure 8. Fåhræus effect *in vivo* (heavy lines) [76] and *in vitro* (thin lines) [68] for distinct levels of discharge hematocrit, H_D 11
- Figure 9. Experimental protocol and analytical procedure; values on the time-scale are given in minutes. IVM, intravital microscopy. 17
- Figure 10. Schematic illustration of the division of experimental groups, with the subscript indicating mean systemic hematocrit; N, number of animals; n, number of vessels; HES, hydroxyethyl starch; plasma, rat plasma. 19
- Figure 11. Experimental set-up for intravital microscopic observation; dash-dotted lines indicate the course of epi-illumination and trans-illumination, respectively; some details related to the animal and the microscopic stage (e.g. cannulation, heating pad, substage condenser) are not shown for reasons of clarity. 22
- Figure 12. A, Schematic three-dimensional model of a vessel, including the vessel wall (1), the plane of focus (2), the vessel centerline (3), and the prevailing direction of flow (4). For reasons of clarity, the origin (O) of the coordinate system ($r;\theta;z$) is laterally displaced from the vessel centerline. B, Schematic two-dimensional image ($r;z$) of the microscopic field of view in the plane of focus ($\theta = 0$, yellow-colored scaffold). 23
- Figure 13. Typical bright field image of a 45.5- μm -diameter venule with a dual image of a microsphere (white dots). The white double arrow indicates the inner vessel wall. Detailed near-wall view (lower panel) reflects the common optical appearance of the luminal aspect of the vessel wall. 26
- Figure 14. Complete raw μ -PIV data set with velocity data plotted against their corresponding radial position. The dashed line (z -axis) corresponds to the vessel centerline (top). For the next step of analysis, data points from the left-hand side are reflected to the right-hand side (bottom). 27

- Figure 15. Monotonic filtering procedure selects relevant data points (red) from the raw data set (left plot), followed by the fitting of a curve (pink) to the filtered data points (right plot) 28
- Figure 16. Exemplary illustration of the data output arising from the microviscometric analysis of the monotonically filtered μ -PIV data shown in Fig. 15. The shaded area on the right-hand ordinate of each plot corresponds to the vessel-specific estimate in ESL thickness, t_{ESL} (see Fig. 17). 29
- Figure 17. Curve obtained by an iterative procedure, which minimizes the least-squares error, E^* , in the fit to the μ -PIV data set shown in Fig. 15. The local minimum of the curve is regarded as the best estimation of the actual thickness of the ESL. 31
- Figure 18. Schematic illustration of near-wall μ -PIV data and of the corresponding best velocity fit for different flow conditions, i.e. no-slip or pseudo-slip conditions, and finite or infinite hydraulic resistivity, K (dyns/cm⁴). The shaded grey bands along the velocity axis denote the resulting estimates of ESL thickness. r_b , radius of a microsphere; + symbol, corresponding fluid particle..... 33
- Figure 19. Upper panel: Course of mean arterial pressure in epo mice (dark) and wt mice (light grey) expressed as mean \pm SEM of the respective experimental period (P) with P₁ corresponding to the neck preparation, P₂ to the cremaster muscle preparation, P₃ to intravital microscopy (IVM) before hemodilution (HD), and P₄ corresponding to IVM after HD. Differences were tested for significance using paired t-test (P₁ vs P₂ and P₂ vs. P₃) or t-test (P₃ vs. P₄). Upper and lower bars correspond to dark and light grey symbols, respectively. 39
- Figure 20. Centerline velocity (upper panel) and average flow velocity (lower panel) in both epo mice (dark grey) and wt mice (light grey) before and after isovolemic hemodilution. Differences were tested for significance using paired t-test or Mann-Whitney U-test for paired and unpaired data samples, respectively. 40
- Figure 21. Upper panel: Volume flow rate in epo mice (dark grey) and wt mice (bright grey) before and after hemodilution. Differences were tested for significance using Wilcoxon Signed Rank test or Mann-Whitney U-test for paired and unpaired data samples, respectively. 42
- Figure 22. %-Change of volume flow rate in epo mice (dark grey) and wt mice (bright grey) upon hemodilution; columns denote mean \pm SEM; difference was tested for significance using Mann-Whitney U-test..... 43
- Figure 23. Assembly of all velocity profiles of each group. All data is normalized to the centerline velocity (v_{max}) and $r=R-t_{ESL}$, respectively..... 44
- Figure 24. Upper panel: Box-plot showing the ratio of centerline and average flow velocity (v_{max}/v_{mean}), which is a measure of the degree of bluntness of the velocity profiles, illustrated on Fig. 17. Differences were tested for significance using t-test. 45
- Figure 25. Upper panels: Dependence of the ratio v_{max}/v_{mean} on the corresponding vessel diameter in epo mice (left panel) and wt mice (right panel) both before (closed circles) and after (open circles) hemodilution; coefficient of correlation was not significant in any group as far as only data points corresponding to $\leq 60\mu\text{m}$ -diameter vessels were considered. 47
- Figure 26. Upper panel: Mean shear rate (i.e. shear rate averaged over the vessel cross-section) in epo mice and wt mice before and after hemodilution. 48
- Figure 27. Upper panel: Interfacial shear stress, $\tau(R-t_{ESL})$, in epo mice (dark grey) and wt-mice (light grey), before and after hemodilution. Large boxes denote experimental values, while small ones represent theoretical reference values according to Sharan *et al.* [160]. Experimental data of the epo_{0.85} group is not shown; instead, the estimated shear stress ($\tau_{epo0.85}^{\#}$) is presented. 49

- Figure 28. Relative apparent viscosity in epo mice (dark grey) and wt mice (bright grey), both before and after hemodilution. Differences were tested for significance using Wilcoxon Signed Rank Test and Mann-Whitney U-test for paired and unpaired data samples, respectively. Experimental data of the epo_{0.85} group is not shown due to methodical limitations (see discussion). *In vitro* viscosities, calculated with the *in vitro* viscosity law of Pries *et al.* [61], are denoted by the small boxes (median $\pm 1^{\text{st}}$ / 3^{rd} quartile). Note that these predictions are made on a vessel-specific basis rather than on group-averages with regard to the input data for the viscosity law, i.e. vessel diameter, species-specific mean corpuscular volume. 51
- Figure 29. %-Change of relative apparent viscosity (light grey) compared to that of systemic hematocrit (dark grey) upon isovolemic hemodilution. The change in viscosity in epo mice is based on the analytically predicted *in vitro* data shown in Fig. 28. Bars denote mean \pm SEM. 52
- Figure 30. Upper panel: Dependence of relative apparent viscosity (circles) on discharge hematocrit (H_D) for fixed tube diameter (40 μm) as obtained from glass tube experiments performed with human red cells (MCV 92 fl) [64]. Best non-linear fit to the experimental data is represented by the solid/dashed line, according to the *in vitro* viscosity law [61]. 53
- Figure 31. Ratio of H_T/H_D (Fåhræus effect) of the four experimental groups (large boxes). Small boxes represent predicted *in vitro* reference data according to Pries *et al.* [61]. Differences between the experimental groups were tested for significance with t-test, except for epo_{0.85} vs. wt_{0.46} (Mann-Whitney U-test). 54
- Figure 32. Relationship between H_T/H_D -ratio and systemic hematocrit. Each data point denotes a single vessel. Note, the abscissa is scaled inversely. 54
- Figure 33. Scatter plot of H_T/H_D -ratios as determined by microviscometric analysis (x) vs. those predicted by means of a linear multivariate analysis (y). The plot accommodates data of all vessels, irrespective of the experimental group. r^2 , coefficient of determination. 55
- Figure 34. Upper panel: Estimated ESL thickness in epo mice and wt mice both before and after hemodilution. Differences were tested for significance using the paired t-test or Mann-Whitney U-test, respectively. 56
- Figure 35. ESL thickness as a function of systemic hematocrit. Symbols represent mean values \pm SEM, while arrows indicate corresponding median values. 57
- Figure 36. Dependence of flow resistance in an experimental microvascular network on ESL thickness (I-III) and hematocrit (0.27, 0.46, 0.85). In addition, four other factors are considered. 64
- Figure 37. Influence of change in cell volume (45fl, dashed lines; 57fl, solid lines) on the dependence of relative apparent viscosity on tube diameter for high (black) and moderate (grey) levels of hematocrit *in vitro*. 66
- Figure 38. Functional capillary density (number of perfused capillaries, n, per unit area) in the extensor digitorum longus (EDL) muscle of epo mice and wt mice (unpublished data by O. Baum), values given as mean \pm SD; $p < 0.001$ (t-test). 70
- Figure 39. Pseudo-shear rate (equal to average flow velocity divided by vessel diameter) in epo mice and wt mice; columns represent mean \pm SEM. 71

7.3. Tables

Table 1. Systemic hematocrit in epo mice and wild-type mice before and after isovolemic hemodilution; values denote means \pm SD.	37
Table 2. Vessel diameter of the different experimental groups; values denote means \pm SD.	43
Table 3. Ratio v_{\max}/v_{mean} in epo mice and wt mice before and after isovolemic hemodilution; values denote means \pm SD.	46
Table 4. Relative apparent viscosity in epo mice and wt mice, before and after isovolemic hemodilution with HES or plasma. Values denote means \pm SD.	51
Table 5. Estimated ESL thickness in epo mice and wt mice before and after isovolemic hemodilution with HES or plasma; values denote means \pm SD.	57

8. Appendix

8.1. List of Materials

Drugs

Ketavet®, ketamine, 10mg/ml

Rompun®, xylazine, 1 mg/ml

Atropinsulfat, 0.02mg/ml

Narcoren®, Pentobarbital, 160 mg/ml

Heparine, Liquemin® N25000, 0.2%

RB 40.34 antibodies, 0.57µg/µl

FluoSpheres®, 0.5 µm diam, yellow-green, carboxylate-modified,
absorption/emission max 488/505 nm, excitation max 515 nm, Molecular Probes®

Hydroxyethylstarch, Voluven®, 6%, 130 kDa, 0.4 grade of substitution

Materials & Instruments

Stereo microscope, Carl-Zeiss, Jena, Germany

Scissor FST 14084-08, Modell „Bonn“

Microscissor FST, 15000-00, Spring Scissor straight

Mircoforcep FST, Extra Fine Graefe Forcep No.11152-10

Arterial clip, Gefäßclip nach Biemer, FD560 R, Aesculap®

Shaver Arco, Moser® Germany

Thermocauterizer, FST Small Vessel Cauterizer 18000-00

Harvard, Small Animal Respirator

Prolene 6-0

Frischhaltefolie, Quickpack Haushalts und Hygiene GmbH, Renningen Germany

Hettich Zentrifugen, Mod. Hettich Haematokrit Tuttlingen

Megafuge ® 1.0, Heraeus

Perfusor, Braun Perfusor

PE Microtube, Portex, Hythe, Kent, UK

Optical & Electronical Material/Devices

Intravital microscope, Leitz Wetzlar, Germany

Objective, Uapo/340, ×40/1.15W, ∞/0.13-0.25, Olympus

Ocular, Periplan GF ×12.5 M, Leitz Wetzlar, Germany

Objective sled, model 779, Leitz Wetzlar, Germany

Condensor , 0.60, L 11

Fiber Optic Video Sync Modul, Model 9630, Chadwick & Helmuth, El Monte, CA

Power Supply, Strobex, model 11360, Chadwick & Helmuth, El Monte, CA

Strobe generator, Model 273L, Chadwick & Helmuth, El Monte, CA

Green/Blue filter (I 213/513604)

Camera, CF 8/5 NIR, Kappa ®
 Camera, RCA® with Cosmicor tele-objective, 16 mm, 1:1.4
 Video tape, DV CAM 64, Sony®,
 Video recorder, DSR 20-P, Sony®
 Video monitor, PVM-122 CE, Sony®
 Video timer, VTG-33, FOR.A®

8.2. List of Abbreviations and Acronyms

bw	body weight
CVD	cardiovascular disease
ESL	endothelial surface layer
EPO/epo	erythropoietin [glycoprotein]/ synonymous with tg6 mouse strain
FE	Fåhraeus effect
FL (effect)	Fåhraeus-Lindqvist (effect)
Hct	hematocrit
H _D	discharge hematocrit
H _T	tube hematocrit
HD	hemodilution
HR	heart rate
iv	intravenous
IVM	intravital microscopy
K	hydraulic resistivity
MAP	mean arterial blood pressure
MCV	mean corpuscular volume
μ-PIV	micro-particle image velocimetry
NO	nitric oxide
NF	network Fåhraeus effect
RBC	red blood cell
ROS	reactive oxygene species
tg6	epo mouse transgenic mouse, see also epo
wt	wild-type (synonymous with C57Bl/6 mouse strain)

8.3. Acknowledgements

My special thanks go to Prof. Dr. Axel R. Pries, director of the Institute of Physiology, Campus Benjamin Franklin Charité Berlin, for supervising the present thesis and his support in completing it.

For their help in analyzing the experimental data, I want to thank Prof. Edward R. Damiano, Michele D. Savery and Bidhan Roy (Boston University, Biomedical Engineering, Boston, MA, USA).

My warmest thanks go to my dear parents for their encouragement and their great deal of patience with me.

8.4. Curriculum Vitae

“Mein Lebenslauf wird aus datenschutzrechtlichen Gründen in der elektronischen Version meiner Arbeit nicht veröffentlicht.”

8.5. Publications and presentations

- “Microrheology in skeletal muscle vessels upon increased erythropoietin (EPO) levels” (P4.33) by Richter V, Pries AR, Gassmann M, Damiano E.. in Biomedical Engineering Society 2007 Annual Fall Meeting, Los Angeles, CA.

- “Excessive erythrocytosis compromises the blood – endothelium interface in erythropoietin – overexpressing mice” (JPHYSIOL/2011/209262) by Richter V, Savery MD, Gassmann M, Baum O, Damiano ER, Pries AR.; revised manuscript has been resubmitted to The Journal of Physiology for final decision on publication.

8.6. Selbständigkeitserklärung

„Ich, Vincent Richter, erkläre, dass ich die vorgelegte Dissertation mit dem Thema: ‘Microrheology in skeletal muscle vessels of erythrocytic mice’ selbst verfasst und keine anderen als die angegebenen Quellen und Hilfsmittel benutzt, ohne die (unzulässige) Hilfe Dritter verfasst und auch in Teilen keine Kopien anderer Arbeiten dargestellt habe.“

Berlin, 09.06.2011

.....

(Vincent Richter)